Channel Modelling of Blood Capillary-based Molecular Communication

Yue Sun
Supervised by: Professor Kun Yang

A thesis submitted for the degree of PhD
School of Computer Science and Electronic Engineering
University of Essex
Date of Submission: Friday 6th July, 2018

Abstract

Molecular communication (MC) is a new and promising interdisciplinary bio-inspired communication paradigm, which uses molecules as information carriers. Differing from traditional communication, MC is proposed as a feasible solution for nano-scale communication with the help of biological scenarios to overcome the communication limitations. Meanwhile, it is inspired by intracellular and intercellular communication, which involves exchange of information through the transmission, propagation, and reception of molecules. Blood capillaries, extensively distributed in the human body and mutually connected with tissues, are potentially applied to MC, which is the major motivation of this thesis.

The focus of this PhD thesis is on the channel modelling of blood capillaries or blood vessels. The objectives of the research are to provide solutions to the modelling of blood capillary-based MC from a communication engineering and information theory perspective. The relationship of the biological scenario in blood capillaries to a communication system is studied. After demonstrating the mapping from biological phenomenon to emission, propagation and reception processes, system models are established. There are three models of blood capillaries behind different biological scenarios.

Firstly, the thesis establishes a basic model of vesicle release, vesicle diffusion through blood capillary and ligand reception processes within the endocrine phenomenon. Moreover, differing from previous research in macroscopic Fick's diffusion, this work involves microscopic Langevin diffusion to

describe the propagation process with a frequency domain method being proposed to calculate the information-theoretical performance channel capacity. Secondly, a much more realistic blood capillary model with blood flow drift which matches a laminar flow regime is presented, where a generalised Langevin equation is used to model the drift force exerted by blood flow. Finally, the thesis establishes a single input and multiple output MC model with hierarchical levels of Y-shaped bifurcation of blood capillaries, then BER, SNR, and channel capacity performance are analysed.

Acknowledgements

Firstly, I would like to express my sincere gratitude to my supervisor Prof.Kun Yang for the continuous support of my Ph.D. study and related research, and for his patience, motivation, and immense knowledge. His guidance helped me at all times of the research and writing of this thesis. I could not have imagined having a better advisor and mentor for my Ph.D. study.

Besides my advisor, I would also like to thank the rest of my board meeting committee: Prof. Anthony Vickers, Prof. Stuart Walker, and Dr.Luca Citi, for their insightful comments and encouragement, but also for the hard questions which inspired me to widen my research from various perspectives.

I thank my fellow lab mates for the stimulating discussions, for the sleepless nights we were working together before deadlines, and for all the fun we have had in the last four years.

Last but not the least, I would like to thank my family. To my father, for his faith in my capabilities, his life lessons, and his encouragement of me. To my mother, for her endless care and love for her family, and for her continuous support over my many weaknesses, where she exercised great and endless patience.

Contents

List of Figures

List of Tables

Abbreviations

Adenosine diphosphate	(ADP)
Adenosine triphosphate	(ATP)
Acyl homoserine lactone	(AHL)
Additive white Gaussian noise	(AWGN)
Bit error rate	(BER)
Cumulative distribution function	(CDF)
Carbon nano-tube	(CNT)
Cyclic adenosine monophosphate	(cAMP)
Equal-Gain combiner	(EGC)
Excitatory postsynaptic potential	(EPSP)
Endoplasmic Reticulum	(ER)
Molecular communication	(MC)
Inter Symbol Interference	(ISI)
Inverse Gaussian	(IG)
Green fluorescent protein	(GFP)
Generalised inverse Gaussian	(GIG)
Multiple input single output	(MISO)
Messenger RNA	(mRNA)
Maximum-Ratio combining	(MRC)
On-Off Keying	(OOK)

Probability density function	(PDF)
Power Spectral Density	(PSD)
Red blood cells	(RBCs)
Release-ready pool	(RRP)
Soluble CD40 ligand	(sCD40L)
Single input and single output	(SISO)
Single input and multiple outputs	(SIMO)
Signal to noise ratio	(SNR)
Synchronization and Threshold Detection	(STD)
Vascular cell adhesion molecules-1	(VCAM-1)

Symbol and meaning

Symbol	Meaning
m	Mass
D	Diffusion coefficient
t	Time
x	Displacement
J	Diffusion flux
d	Distance
T	Temperature
k_B	Boltzmann constant
η	Dynamic viscosity
τ_D	Constant refill time
$\lambda(t)$	Firing rate regarding time
$G_{xx}(\omega)$	Spectrum density of the random variable regarding the displacement x
$G_{vv}(\omega)$	Spectrum density of the random variable regarding the velocity v
γ	Dissipation coefficient
N	Number of vesicles
k_a	Constant rate for a free vesicle binding to a free binding site
k_d	Constant rate for a vesicle dissociating from its binding site
k_{int}	Internalised constant rate
C	Channel capacity
H	Entropy
$I(X;Y)$	Mutual information
$\mathcal{H}$	Enthalpy

$\overline{P}_{\mathcal{H}}$	Average thermodynamic power
p	Pressure
$\triangle p$	pressure differential along the vessels
L	Length of blood vessel
k_1	Constant binding rate
k_{-1}	Constant release rate
p_e	Probability of error
φ	Decision threshold
B	Bandwidth

Chapter 1

Introduction

The rising popularity of molecular communication (MC) has been accompanied by the development of nanotechnology. The concept of nanotechnology can be traced back to the Nobel laureate physicist Richard Feynman in his famous lecture entitled, there is plenty of room at the bottom, in 1959 [11]. In this speech, Feynman indicated that the extreme minimisation of devices could be achieved. Nanotechnology enables this at scales ranging from 1 to 100 nanometers. Since Feynman proposed the concept of nanotechnology, these kinds of activities have slowly increased, and its development has remarkably accelerated since the 2000s. Enormous improvements in this field have enabled the realisation of powerful as well as tiny functional devices, namely, nano-machines.

Nano-machines are considered as the functional components required to perform computing, sensing and data memory tasks in nano-scales [3]. Nano-networks interconnect the distributed nano-machines to execute collaborative and comprehensive tasks. Traditional communication technology uses electromagnetic waves to transmit information which cannot be directly applied to nano-machines [3]. According to [3], traditional communication at nano-scales is restricted by the size and power consumption of the transceiver.

However, in the area of biology, it has been recognised that microor-

ganisms, including cells and bacteria, gain information from the external environment. Gathered chemical information is sent to their neighbouring cells or bacteria. Cell signalling [12] is well studied in biology, involving cells sending messages to one another and controlling each other's behaviour. Quorum sensing [6] is another example, in which bacteria send molecular messages to one another in order to estimate the local population of their species. A large number of cells and bacteria can be regarded as biological nano-machines existing in the natural world. Furthermore, enormous numbers of cells interconnect to form an efficient and steady nano-network inside the human body. With advantages of size, power efficiency and adaptability to the biological environment, bio-inspired MC is the most promising approach for nano-networks [3].

The biological research aspect of molecular signalling has a history of many decades; however, research on aspects of information and communication have introduced the concept of MC only in recent years. With more researchers working on theoretical and implementation research of MC recently, the formation of the IEEE P1906.1 (IEEE COM/Nanoscale and Molecular Communications) Working Group was announced on the 18th of May 2011. It is the first IEEE standard to be proposed in the area of nano-networks and MC, and included developing common terminology, recommended practices and standardised performance metrics.

1.1 Basic Concept of Molecular Communication

MC is defined as the use of molecules as information carriers between transmitters and receivers. An abstract communication architecture is presented in [3, 6, 13], to generalise MC processes. Figure 1.1 shows an architectural design for MC. It consists of basic functional components: information molecules that represent the information carrier to be transmitted,

transmitter bio-nanomachines that release the information molecules, bio-nanomachines which receive the detected information molecules, and the channel that information molecules propagate through from transmitters to receivers.

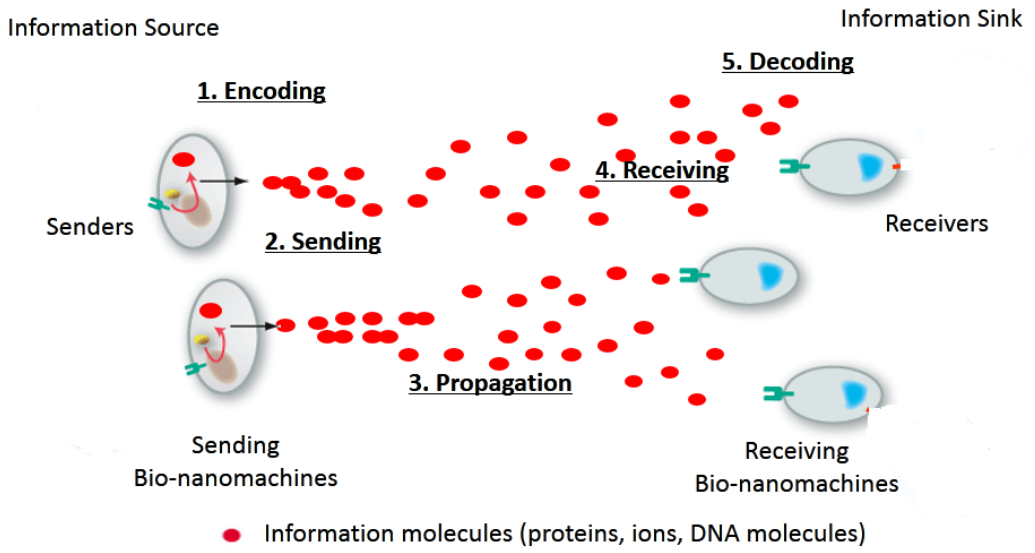

Figure 1.1: Illustration of molecular communication [1].

Figure 1.1 describes the communication processes in the MC system: encoding, sending, propagation, receiving and decoding. These communication processes are similar to traditional communication but with distinctly different characteristics.

Encoding is the process in which a sender or transmitter generates the information molecules, selecting the appropriate molecules and encoding the information onto it. Information may be encoded in various forms, such as molecules with three-dimensional structure [2], and information sequence of nucleotide molecules (DNA/RNA). Information could also be encoded in different concentrations of information molecules (numbers of information molecules per unit); for example, [14] illustrates an M-ary modula-

tion scheme, in which the information is encoded into the concentration of molecules emitted.

Sending is the process involving a sender bio-nanomachine releasing information molecules into the propagation environment. In the communication process between cells, a sender will release the molecules by opening a gap junction channel in the cell membrane [5].

Propagation is the phase which involves information molecules being transmitted from sender to receiver in various environments. The environment is vital to the channel of the MC system, while the channel for the MC includes the sender, receiver as well as the environment between sender and receiver. Information molecules may diffuse passively through the environment or propagate actively by binding to a motor molecule. Normally, the channel is divided into passive diffusion and active diffusion. The passive one involves free diffusion, diffusion with drift and reaction diffusion; while the active one is associated with molecular and bacteria, motor-based diffusion.

Receiving is the process in which the receiver detects and captures information molecules. A ligand-based reception mechanism, using a so-called ligand-receptor, exists in abundance within biological cells. Ligands bind to receptor sites on the cell's surface, detecting and capturing molecules' information in the environment. Figure 1.2 illustrates a ligand receptor on the cell membrane. Another option for capturing molecules without using receptors is the opening of chemically gated-channels (gap-junction channel) on the surface that allows molecular information exchange into the receiver [6, 5].

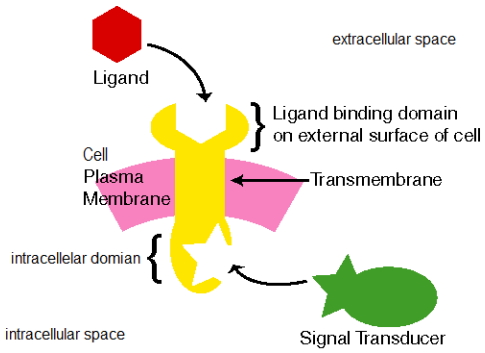

Figure 1.2: Illustration of Ligand receptor [2].

Decoding is the process involving the receiver decoding the received molecules' information into the original information with a chemical reaction. Chemical reactions for decoding may include the production of new molecules to perform a simple task [2, 15]. Recent research shows that receivers can also decode molecular information into digital signals or even binary text messages [16].

1.1.1 Cellular and Biological Nano-machines

Nano-machines with computing, sensing, data storage and communication ability are the basic component for MC and nano-communication. In [3], it proposed the architecture for an ideal nano-machine with the following architecture of functional components:

1. Control unit executes the instructions to control other components, aiming to perform the intended tasks.

2. Storage unit stores the data and information.

3. Communication unit consists of senders and receivers at nano-level.

4. Reproduction unit is used to produce each component of the nano-machine and then assemble them for recombination.

5. Power unit provides energy to all components in the nano-machine.

6. Sensors and actuators act as an interface between the environment and nano-machine.

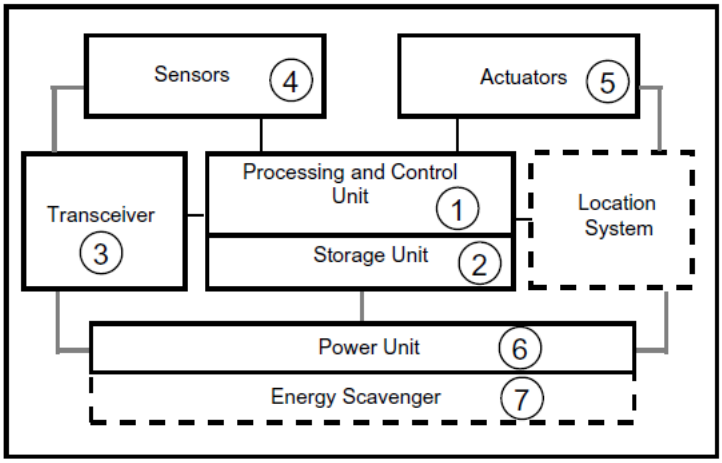

Figure 1.3: Architecture for nano-machine [3].

Currently such a complex man-made nano-machine could not be built using today's nanotechnology. However, existing biological systems are found in nature. Nature has evolved in various forms of biological nano-machines in small-scale and highly complex devices composed of chemically reacting biological molecules. Cells with similar architecture are regarded as an optimal approach to the nano-machines or more complex MC systems [3]. Figure 1.4 shows the generic architecture of a eukaryotic cell and the relationship with a nano-machine.

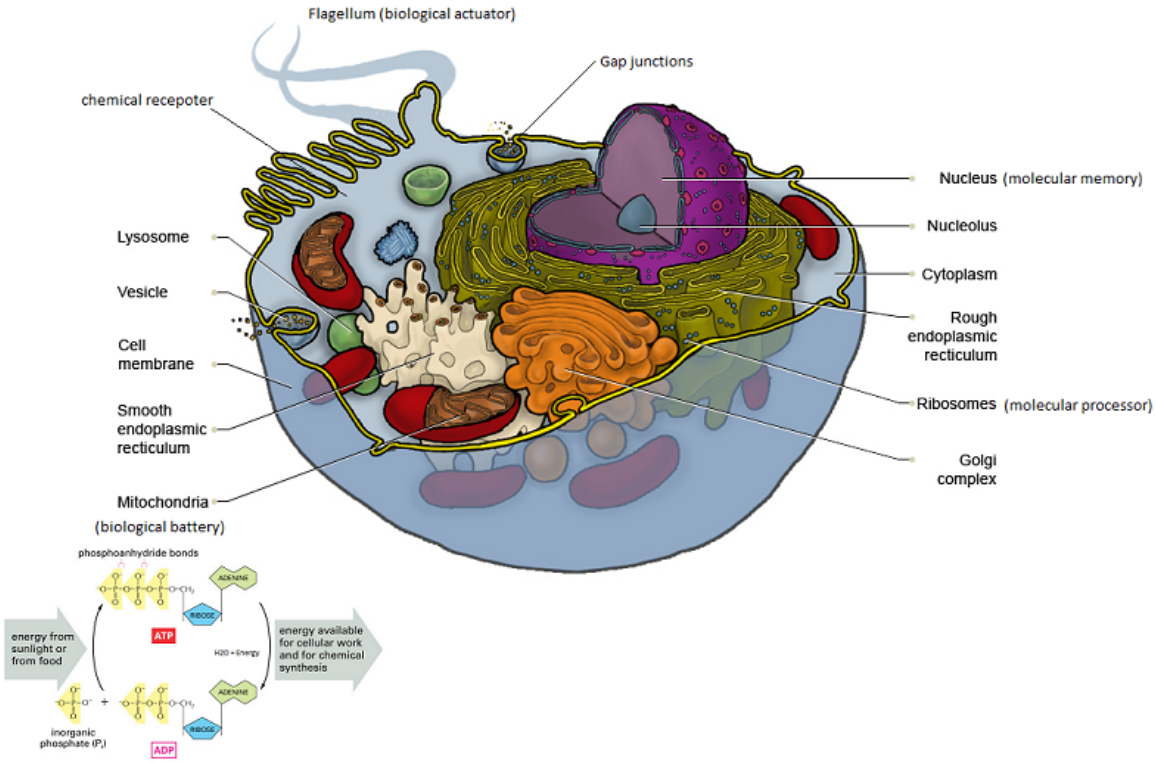

Figure 1.4: Cell as biological nano-machine.

The nucleus, which can be regarded as a control and storage unit, contains most of the cell's genetic material, organised as multiple long linear DNA molecules in a complex helix with a large variety of proteins. The function of the nucleus is to maintain genes and to control the activities of the cell by regulating gene expression. The nucleus is, therefore, the control centre of the cell. DNA functions as storage of genetic information and RNA is involved in decoding the genetic information to synthesise proteins [4].

The gap junction and receptors on the cell membrane act as senders and receivers, so these comprise the communication unit. Vesicles are small containers of molecules enclosed by a typically spherical lipid membrane [4]. In the cell, vesicles often function as the interface and container of molecules.

Vesicles encapsulate molecules, then with the help of motor proteins, vesicles and molecules are propagated from one place to another. More importantly, molecules transported in the vesicles can prevent noise interference from the environment [17].

The ribosome serves to convert the instructions found in messenger RNA (mRNA), which itself is produced from instructions in DNA into the chains of amino-acids that make up the relevant proteins [1]. The ribosome is responsible for the synthesis of proteins that play a role in the reproduction unit.

In the cell, power is generated by the chemical reaction of adenosine triphosphate (ATP). ATP hydrolysis detaches the phosphate from an ATP molecule to produce adenosine diphosphate (ADP), and at the same time releases a large amount of energy. ADP absorbs the energy from the external environment of the cell and is then synthesised to ATP- the recycling of ATP to ADP forms a power cycle [17].

1.1.2 Characteristics of Molecular Communication

In comparison with traditional communication technologies, the features or characteristics of MC are shown in Table 1.1:

Communication type	Molecular communication	Traditional communication
Information carrier	Molecule	Electromagnetic or acoustic wave
Signal type	Chemical or biological signal	Electrical or optical signal
Transmission medium	Liquid, fluid or gas	Cable or air space
Noise source	Medium particles or chemical reaction	Electromagnetic or other signal
Transmission speed	Slow (nm/s or μm/s)	Light speed (3×10^8m/s)
Transmission distance	nm-m	m-km
Energy consumption	low	high

Table 1.1: The difference between MC and traditional communication.

1.2 Application of Molecular Communication

MC has the potential to advance applications in biological engineering, medical and healthcare, industrial, environment, information and communication areas. Figure 1.5 shows its application in different areas.

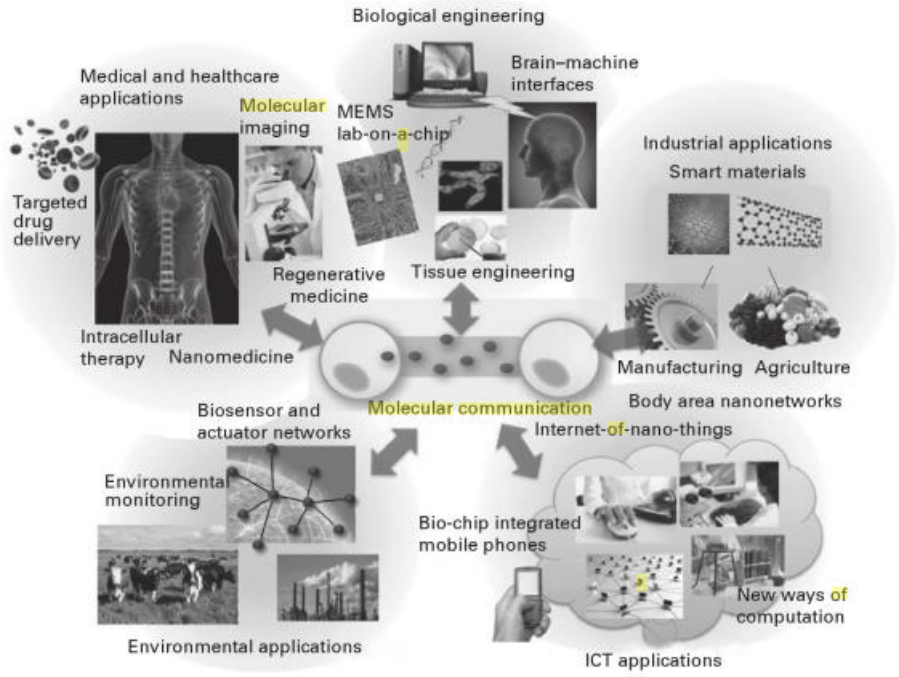

Figure 1.5: The application of molecular communication [4].

1.2.1 Biological engineering

MC will benefit the area of biological engineering to analyse biological materials, engineering of the biological system and interface biological systems [4]. Specific examples of relevant sub-areas are tissue engineering and brain-machine interfaces [4].

The purpose of tissue engineering is to restore the lost tissues of patient's bodies from biological cells [1]. MC may provide a mechanism to produce a spatial pattern of molecules and affect the growth or differentiation of cells in the specific tissue.

A brain-machine interface provides a direct channel between the human brain and electrical devices to restore lost functions [18]. Signals generated

from external devices may stimulate a specific part of the brain to treat a specific type of brain disease. Instead of using electrical stimulation, MC may provide a molecular means of interacting with the brain for brain-machine interfaces [4].

1.2.2 Medical and healthcare

MC may also apply to medical and healthcare system; for example, targeted drug delivery and molecular imaging.

Molecular imaging uses green fluorescent protein (GFP) as a reporter of gene expression to monitor cellular function and processes. MC may further improve coordination mechanisms for a group of bio-nanomachines carrying GFP to gather and aggregate the transmitted information to external devices.

In targeted drug delivery, in order to reach the targeted site (diseased cells or tumours) in a human body, the propagation process is performed by encapsulating drug molecules in drug delivery carriers. Delivering the carriers to the targeted site and releasing the drug molecules from carriers is targeted and controlled. MC may provide alternative techniques to improve the accuracy of reaching the target with the efficiency of the intended therapy [4]. Drug nano-particles can penetrate inside the body to deliver the therapy; it can, therefore, bypass all physiological barriers that inside the human body to protect it from foreign elements [19, 20].

1.3 Motivations and Research Objectives

The focus of this PhD thesis is on the channel modelling of blood capillary-based MC, where the molecules' information is exchanged for their ubiquitous distribution network in the human body. Blood capillaries are important channels for long-range communication [21], while they significantly differ from basic diffusion channels; the latter act as the fundamental type of MC among different types, and have been well investigated in recent years. Many

different types of MC have been studied so far, which involved either passive transport of molecules (diffusion-based architectures [22, 23, 24, 25]) or active transport: molecular motors [26] and bacteria motors [27]. However, blood capillary modelling, as a fundamental and promising area for future applications in MC, has not had sufficient research compared with basic diffusion channels. Furthermore, in the drug delivery system, drug particles propagate through blood vessels and capillaries with blood flow due to the pumping action of the heart [19, 20]. The modelling of blood capillaries is vital to drug delivery application in MC. The choice of this thesis in modelling a much more comprehensive blood capillary-based channel is motivated by this analysis, detailed in the literature of Chapter 2.

1.3.1 Methodology

As a consequence of the differences between the MC paradigm and traditional electromagnetic communication paradigms, the traditional communication engineering models and techniques are not directly applicable to this study and the design of blood capillary-based MC systems. While in the traditional communication systems antennas transmit and receive electromagnetic radiation; in biological cells, bio-signalling information is transmitted through the chemical synthesis of information molecules and received by chemical receptors through chemical reactions. Biological signalling systems inspire the blood capillary MC model in Chapter 4; for example, the system between the platelets (mobile transmitters) and endothelial cells (fixed receivers), based on the release of specific proteins (information molecules) known as CD40L. To establish a more realistic modelling of blood capillary to MC, the following research methodologies are being used.

The first step is to understand the biological communication mechanism, then to outline the mapping from biological scenarios of blood capillaries or blood vessels to an MC paradigm. First of all, the information molecules should be identified, as well as the mechanism to carry the information from

transmitters to receivers; their respective functions are clarified with respect to the coding, releasing, propagation, receiving and decoding processes as basic components in a communication system.

The second step is to demonstrate the propagation process through the blood capillary, which is vital to the model. Information molecules propagate through the blood vessels or capillaries according to the superposition of two most significant physical phenomena: namely, blood flow and diffusion. Blood flow is the transport of molecules suspended in a fluid due to the bulk motion of this fluid. Diffusion in a macro perspective is the spontaneous spread of molecules suspended in a fluid from a region with a higher concentration to another region with a lower concentration. While in a micro perspective, diffusion is the motion as a result of stochastic collisions from smaller particles. This thesis will use microscopic Langevin equation rather than macroscopic Fick's law for the diffusion process.

The third step is to implement the information theory and acceptable communication techniques to a blood capillary MC model. With the assistance of simulation models, we can analyse the performance and characterisation of blood capillary system; these have the potential to be an important step towards the understanding, diagnosis and treatment of cardiovascular diseases as well as MC application for drug delivery. In particular, Matlab is used to simulate the mathematical model we established and test the proposed hypothesis.

As a consequence, there is a need to build a complete understanding of the blood capillary-based MC system from the ground up. The research objectives addressed in this PhD thesis and the proposed solutions have been identified to target this need specifically, and they are summarised as follows.

1.3.2 Research Objectives

The first research objective is to develop a simple diffusion modelling of vesicles, as information interfaces, containing information molecules within them

and propagated through blood capillary. This model provides a mathematical frequency-domain characterisation of biological communication processes involved in the vesicle generating, releasing, propagating and receiving in order to exchange information between a transmitter and a receiver. To achieve this goal as the initial research of this thesis, we follow the most basic implementation of pure diffusion-based MC, which ignores the effect of blood flow. This model identifies the three biological processes of vesicle emission, diffusion and reception; In the emission process, the transmitter benefits from the classical three pools model and in the reception process, the chemical ligand receptors model is investigated. The previous diffusion model described in a macro perspective with Fick's Law illustrates the diffusion process in the relationship with molecular concentration. This model is intended to implement the Langevin equation as the diffusion motion in the micro perspective because it is limited by the small numbers of emitted vesicles that could be counted and the larger size of vesicles compared with molecules. Moreover, it is provided through an analytical expression of the Power Spectral Density (PSD) probability distribution of transmitted vesicles and the analytical closed-form expression that relates to the capacity performance of a diffusion-based MC blood capillary system, such as the diffusion coefficient, the temperature and the frequency of the transmitted signal.

As different from the first objective in a diffusion-based model, the second research objective is to develop a single input and single output (SISO) diffusion with blood flow drift system, which emphasises on the relationship between blood flow and the drift velocity. Moreover, since the information regarding time, such as delay and time duration between two symbols, is not directly presented in the frequency domain, this model is analysed in the time domain. This system implements a biological scenario within the blood vessels consisting of emission CD40 molecules from the platelets, and molecules propagating in the flow of blood vessels and received by the CD40L

in the endocrine cell. The second model is based on the assumption of the blood vessel being at a significant distance from the heart so that it is possible to model the laminar motion in the bloodstream without turbulence. A generalised Langevin equation is a statistical mechanics approach based on the decomposition of the molecule diffusion with blood flow drift into two main processes; namely, the diffusion and the laminar blood flow drift. The solution of its corresponding Fokker-Planck equation is presented with proper boundary conditions. The ligand-based receptor is considered in the receiving process. Upper bound to the capacity is derived to evaluate the information-theoretical performance of the SISO diffusion with a blood flow drift system.

The third research objective is the extension of a SISO model in the second objective to a single input and multiple outputs (SIMO) blood capillary system with hierarchy and levels of Y-shaped bifurcations. Proper distribution of blood flow within organs is essential for the matching of oxygen and nutrient supply to the tissue demand. This model is a further study on the foundation of the normal blood vessels model in the second objective. This model is divided into symmetric and non-symmetric models by the angles of the bifurcation. Given an information signal sent by a transmitter to receivers in a SIMO blood capillaries MC system, the interference may be due to distortions of the previous signals. The analysis of the interference is fundamental to the design of interference mitigation techniques and for increasing the performance of communication systems. The Inter Symbol Interference (ISI) and the additive noise at the receivers are jointly analysed for the SIMO blood capillaries system under the assumptions of having an additive Gaussian noise. The signals at each sub-channel are combined by two spatial diversity combining techniques Maximum-Ratio combining (MRC) and Equal-Gain combiner (EGC). Channel capacity performance of both symmetric and non-symmetric models are analysed within the implementation of the diversity combining techniques of EGC and MRC.

1.4 Thesis Outline

The remainder of this PhD thesis is organised as follows. A preliminary analysis of different types of MC options from the literature is described in Chapter 2, which also includes a survey of previous literature pertinent to the study of blood vessel or blood capillary- based MC. In Chapter 3, as my first research objective, results are obtained through mapping the biological scenario of vesicles diffused through blood vessels. Moreover, modelling of a diffusion blood capillary-based MC system is presented detailing the contributions of derivation for closed-form expression of channel capacity in the frequency domain. In Chapter 4, as my second research objective, a SISO diffusion with a flow drift model on a blood capillary system in the time domain is established. Firstly, methods from statistical mechanics and blood flow theory are used; then an information-theoretical approach is implemented. After that, the analytical expression of the channel capacity is derived and simulated. Chapter 5 presents my third research objective, with a SIMO blood capillary system with hierarchy and levels of Y-shaped bifurcations being established, where implementation-specific results regarding the time duration, ISI, noise effect, and information capacity are fully discussed. Finally, the conclusion with possible future directions for this research field is provided in Chapter 6.

Chapter 2

Literature Review

This chapter contains a review of the literature pertinent to the research on different types of MC and particular options regarding blood capillary. This review is organised as follows. In Section 2.1, different MC options from the literature are detailed on the basis of the types of short- and long-range MC. In Section 2.2, mathematical fundamentals of diffusion dynamics theory from the literature are detailed for the discussion of previous research on MC. In Section 2.3, the results from the literature focused on blood capillary-based MC are presented and analysed to motivate the research proposed in this thesis.

2.1 Biological Systems Applicable for Molecular Communications

In this section, we will discuss the biological systems in nature, which inspired MC. We will then discuss the great variety types of MC, particularly as it relates to the work of this thesis.

The first survey on general microscale MC was presented by Hiyama and Moritani in [28]. A more recent general survey was presented by Nakano et

al. in [2], which indicates the opportunities and challenges of MC research. In [29], a survey of MC based on microtubule and physical contact was presented, and [30] provided a guidepost for some of the experimental problems within MC. Additionally, a survey of MC from a layered communication network perspective was presented in [31] in 2015. Finally, a comprehensive survey on various aspects of MC focusing on recent advancements was presented in [32] in 2016, which also introduced the engineering of an experimental demonstration of MC by Farsad et al. [16]. In [16], a tabletop MC platform has been developed for transmitting short text messages across a room.

MC in different biological systems is widely found in nature, and thus should be tackled with respect to determining some of its rules. Based on the communication distance, in [3] MC systems are categorised into two types: short-range ($nm - mm$) and long-range ($mm - m$). In [27] medium range is added and MC channels are classified into three types: short-range ($nm - \mu m$), medium range ($\mu m - mm$) and long-range ($mm - m$). However, short- and medium-range communication exist in the same biological system, and it is difficult to classify them precisely. In this survey, similar to [3], it is divided into two types: short-range ($nm - mm$) and long-range ($mm - m$). On the basis of the transmission mechanism, MC in the biological system can also be divided into passive and active transport-based systems [6]. In this survey, these two categories will be discussed individually.

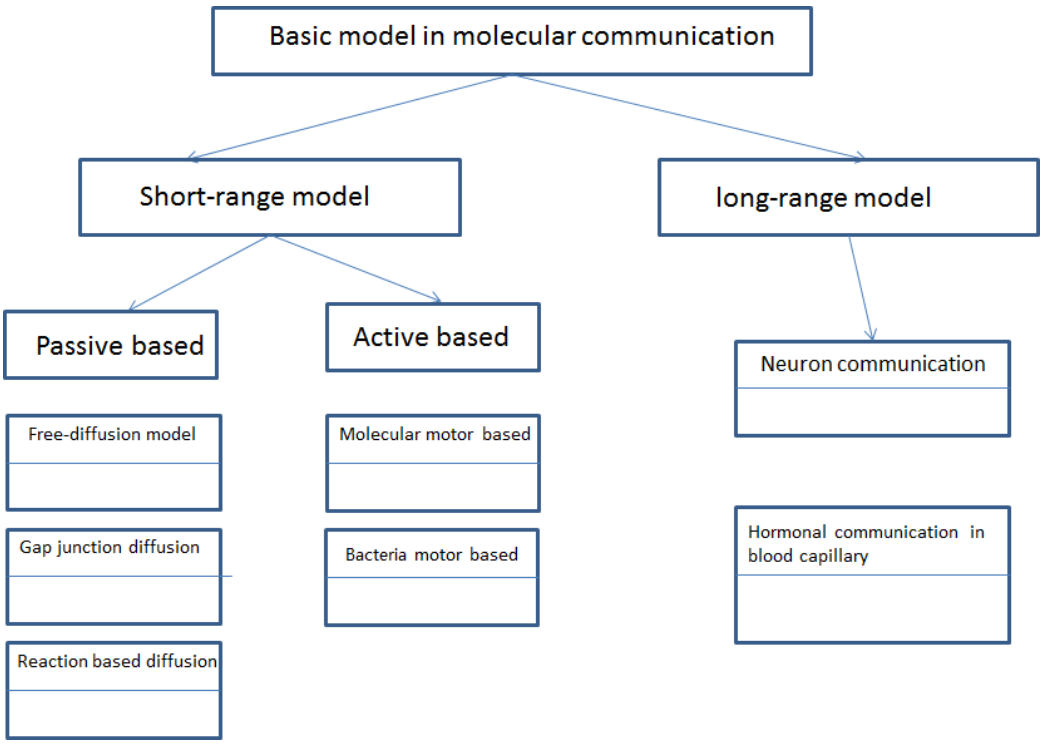

Figure 2.1: Basic channel models for molecular communication

2.1.1 Short-range Molecular Communication Mechanism

Various mechanisms of MC are found within and between cells or other biological systems. In the flowing survey, mechanisms in short-range communication are categorised based on how molecules are propagated; former type passive transport-based MC, and another type active transport-based MC.

2.1.1.1 Passive Transport-Based Molecular Communication in Short Range

In the passive transport-based model, molecules information diffuses in Brownian motion Molecules randomly diffuse in all available directions, which

makes its behaviour highly dynamic and unpredictable. Diffusion is the basic method for the passive transport-based mechanism. Passive transmission requires a large number of information molecules to reach a distant destination by random Brownian motion; thus, passive transmission is not suitable for the crowded or high-viscosity environment and long-range MC.

Three mechanisms for passive transported-based in short-range MC are described in the following: 1. free diffusion-based MC, 2. gap junction diffusion-based MC and 3. Reaction-diffusion based MC.

2.1.1.1.1 Free diffusion-based MC

Free diffusion-based MC is the most common model for the MC in the cell or between cells. In this mode, cells release information molecules into the extracellular environment, and neighbouring cells capture the information molecules with protein receptors, resulting in the activation of a chemical reaction (e.g., increased metabolism or transcription of cellular proteins).

An example of free diffusion-based MC is quorum sensing, a communication mechanism used by bacterial cells. In quorum sensing, bacterial cells release an auto inducer, acyl homoserine lactone (AHL), into the environment, then detect the concentration of AHL in the environment, to estimate the number of bacteria nearby. When the AHL concentration is sufficiently high, the bacteria interpret this as being indicative of the presence of a large number of bacteria in the environment, and thus, the bacteria start transcribing DNA to perform group functions [33].

2.1.1.1.2 Gap junction diffusion-based MC

In this model, diffusion of signal molecules can be guided through cell-to-cell communication channels called gap junction channels [34]. These are physical channels formed between two adjacent cells, connecting the cytoplasm of the two cells. Gap junction channels normally allow the small molecular

weight molecules ($< 1000Da$) to transmit through cells, enabling coordinated actions among adjacent cells [5]. These small molecules including, IP3, cyclic adenosine monophosphate (cAMP) and cytosolic Ca2+ are the most important information molecules in the biological system [35]. Figure 2.2 illustrates the design for gap junction communication system between cells [5].

Intercellular Ca2+ wave propagation, which plays an important role in the biological system, has many models for its diffusion of cytosolic Ca2+ signal between the cells. In the first model, Ca2+ itself diffuse through gap junction and causes Ca2+ release from other cells. In the second model, cells produce IP3, regarded as Ca2+ mobilizing molecules by chemical reaction then the IP3 diffuses through gap junction channel, Ca2+ store, and triggers Ca2+ release from the Ca2+stores to other cells. In the third model, stimulated cells produce ATP that diffuses through gap junction channels to the extracellular environment. These released ATP reacts with the receptors at each cell membrane, and each cell produces Ca2+ mobilising molecules, IP3, and triggering Ca2+ release from Ca2+ stores. As ATP diffuses into the extracellular environment, intercellular Ca2+ waves propagate. The second and third models combine the gap junction diffuse model and reaction-diffusion model. The Intercellular Ca2+ wave could represent the information of cell death and growth [36]. More complex information may be propagated by temporal and spatial modulation of cytosolic Ca2+, such as Ca2+ spikes [5].

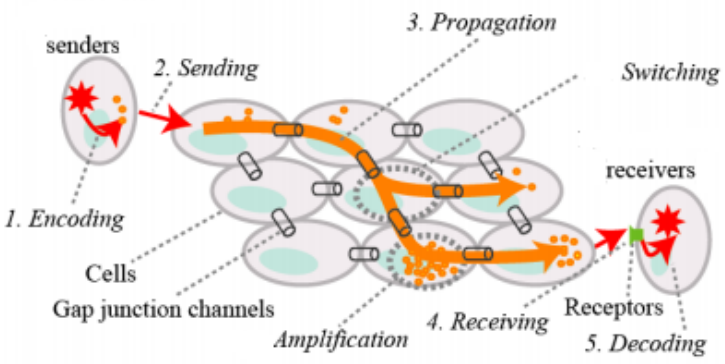

Figure 2.2: Gap junction communication between cells [5].

2.1.1.1.3 Reaction-diffusion-based MC

Diffusion of information molecules can involve biochemical reactions to achieve a different mode of communication that allows propagation of impulses. As a result of the rapid increase and decrease of information molecules in their concentrations, the information molecules propagating in the environment appear as an impulse. For instance, some glial cells produce impulses of calcium ions (Ca2+) for intercellular communication.

The endoplasmic reticulum (ER) in a cell gathers and stores calcium ions. It releases the stored calcium ions from the ER and the calcium diffuses to adjacent cells through cell-to-cell junction channels [1]. The diffused calcium, in turn, stimulates the adjacent cells, causing a chain reaction of calcium stimulation. Shortly after being stimulated, a cell pumps calcium within the cell back into the ER and suppresses further stimulation, thus creating a short impulse of calcium through the cell. Because the communication propagates in a short impulse of calcium concentration, cells can communicate with each other at a higher frequency [1].

2.1.1.2 Active Transport-Based Molecular Communication in Short Range

Active transport provides a communication mechanism to transport information molecules to specific locations directionally. Active transport can propagate signal molecules over longer distances as compared with diffusion-based passive transport. Large interface molecules or vesicles diffuse poorly in passive transport because of their size; on the other hand, active transport consumes chemical energy and generates sufficient force to transport large signal molecules directionally. Active transport provides a communication mechanism with a high degree of reliability even when the number of signal molecules to transport is small. Because the propagation of signal molecules is directional, the probability of signal molecules reaching the destination is higher than when using passive transport, and thus active transport requires fewer signal molecules to perform communication.

However, active transport often requires communication infrastructure to produce and maintain the transport, guide and interface molecules, e.g., molecular motors, microtubule filaments, and vesicles. Active transport of molecules also requires a regular supply of energy to overcome the chemical interactions between signal molecules and molecules in the environment. In the following, we describe two examples of active transport-based MC from biological systems, including, 1. Molecular motor-based MC and 2. Bacterial motor-based MC.

2.1.1.2.1 Molecular motor-based MC

This is found within a cell where molecular motors are used to transport information molecules. A molecular motor is a protein or a protein complex that converts chemical energy (e.g., ATP hydrolysis) into mechanical work at the molecular scale. Inside a cell, senders produce interface molecules, such as vesicles, to contain the information molecules and then bond to transport

motor. Molecular motors transport information molecules or vesicles that contain information molecules [37]. Molecular motors consume chemical energy to transport signal molecules or the vesicles along the pre-established guide molecules at the speed of $400mm/d$. Figure2.3 illustrates an example for the mode of molecular motor-based.

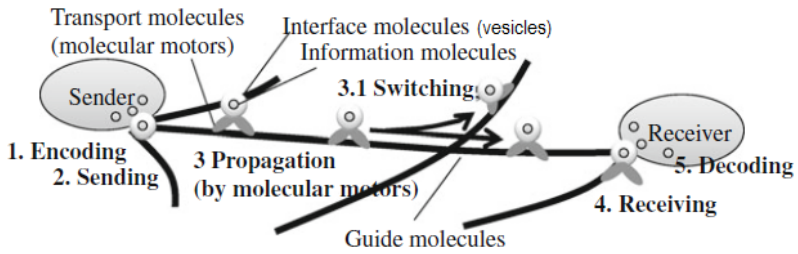

Figure 2.3: Illustration of motor-based molecular communication [6].

Existing research on engineering active transport, however, focuses on only a few types of molecular motors, such as kinesin [5]. Two examples of active transport using molecular motors introduced here are molecular motors walking on filaments and filaments propagating on a patterned surface coated with molecular motors.

In the first example, engineered active transport uses molecular motors and guide molecules e.g., microtubule filaments that self-organise into a network and molecular motors that actively transport information molecules along the guide molecules [26]. This first example uses components and processes similar to the active transport mechanisms in biological systems. In biological systems, a network of guide molecules e.g., actin or microtubule filaments, is created within a cell in a self-organizing manner through dynamic instability of guide molecules, and molecular motors transport information molecules to specific locations within the cell by walking along a network of guide molecules. Engineering of the self-organization of the filaments can produce simple patterns of filaments [37]. Through designing self-organization

processes of creating filament patterns and by selectively transporting on the designed filament pattern, molecular motors may be guided to desired locations.

In the second example of engineered active transport using molecular motors, the arrangement of microtubules and motors is inverted. A surface of the glass is coated with the molecular motor e.g., kinesin, and the motors, push the filaments along the surface. In this arrangement, transport molecules (i.e., the filament) load information molecules at a sender nano-machine and unload the information molecules onto a receiver [38]. The direction of filament movement is guided by adding walls (e.g., deposited proteins) onto the glass surface through lithographic techniques.

Various patterns may be generated that gather filaments toward a receiver nano-machine. For instance, an arrow-shaped wall pattern acts as a directional rectifier to ensure that filaments propagate in a single direction by rectifying filaments that are propagating opposite to the arrowhead direction [39]. The transmitter encodes information using information molecules and injects them into interface molecules. The transmitter then emits the interface molecules to molecular motors through a budding mechanism. The interface molecules are then attached to and loaded on molecular motors. The interface molecules are propagated by molecular motors that move along rail molecules. During propagation, molecular motors may switch guide molecules to reach destination receivers. When molecular motors approach the receiver, interface molecules containing information molecules are fused into the receiver. This allows receivers to receive information molecules and invoke reactions in response to information molecules.

2.1.1.2.2 Bacterial motor-based MC

In another type of engineered active transport, a transport molecule itself is a nano-machine using molecular motors to move toward a receiver nano-

machine along chemical gradients in the environment. This example uses components and processes similar to self-propulsion of single-cell organisms through an aqueous solution. In biological systems, a bacterium uses cilia or flagella, molecular motors that generate propeller-like forces to move the bacterium along chemical gradients toward favourable conditions and away from unfavourable conditions, e.g., harmful chemicals. With the engineered transport nano-machine with molecular motors, the receiver may generate guide molecules to indicate where the receiver is; this process is similar to a gradient of a food source or pheromone in the environment in the bacterium, which then influences the direction in which the transport nano-machine moves through the environment. The transport nano-machine does not require pre-established filament networks since guide molecules emitted by a receiver diffuse to form the chemical gradient around the receiver.

A good example of this is the pseudopodia of a cell, which can form complex shapes that links the entrance and exit of a maze [40]. The pseudopodia form the structure by growing towards a chemical gradient of food originating from both the entrance and the exit of the maze. Active transport using pseudopodia is robust since the pseudopodia adapt to match to the shape of the maze.

An example communication sequence based on this type of MC is illustrated in the Figure 2.4. In this type of MC, the sender and receiver contain information molecules therein (e.g., DNA or RNA molecules within cells), and the transport molecule is used to transport information molecules between them. The sender transports information molecules to the transport nano-machine via bacterial conjugation, while the receiver of communication emits guide molecules in the environment to attract the transport molecule.

The transport molecule propels closer to the receiver, indicating the propagation process. Once the transport molecule and receivers are physically touching, the information molecule is transported to the receiver which shows some response.

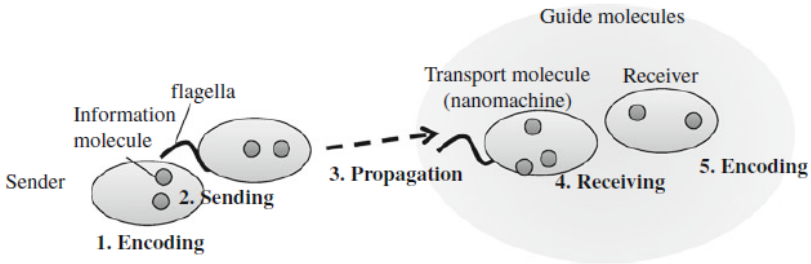

Figure 2.4: Illustration of bacterial motor-based molecular communication [6].

2.1.2 Long-Range Molecular Communication Mechanism

2.1.2.1 Neuron-Based Molecular Communication Mode

Neurons, electrically excitable nerve cells capable of generating, processing and transmitting information through chemical and electrical signalling mechanisms, are considered as transmitters and receivers of the nervous nanonetwork [7]. They receive signals from other neuronal cells, which changes the membrane electrical polarisation. The electrical potential is spread along the cell body and combined at the base of the axon, causing the generation of spikes or impulse signals, namely, action potentials. Spikes signals are then transmitted through the axon and arrive at its branches, where the neuron makes an interface with other neurons cell through synapses, and the conductive links between postsynaptic and presynaptic cells, where cell-to-cell signals occur, are produced [41]. Action potentials are used to carry information from one neuron to the other. Hence, we call the communication among neurons neuro-spike communication [42].

Performance of neuro-spike communication depends on the physical features of neurons, which affect the action potential transmission characteristics through such neurons. Although areas of the axon covered with a

myelin sheath cannot regenerate action potentials, they can rapidly conduct an electrical field to the next node by regenerating and transmitting the action potential along the axon to further nodes [43]. In [43], it indicates that another way to increase conduction velocity is to increase the diameter of an axon, through which axons with myelin sheaths can transmit action potentials extremely quickly.

There are two major types of synapses, electrical and chemical [44]. The former is a mechanical and electrically conductive link that is formed in a narrow gap between two neurons, such as the presynaptic and postsynaptic neurons. Despite causing amplitude loss in the signal transmitted, it conducts nerve impulses more rapidly compared to the chemical synapse. Mostly, the electrical impulses can be transmitted in either direction [44]. Different from electrical synapses, chemical synapses are specialised links through which signals are transmitted from neurons to other neurons. Chemical synapses allow neurons to form communication paths within the central nervous network, enabling the nervous nano-network to communicate with and control other networks within the body, and they are crucial to the biological computations that underlie perception and thought [7].

An arriving spike yields an influx of calcium ions through the voltage-dependent calcium ion channels. Ca2+ then bind to the proteins found within the membranes of the synaptic vesicles. The vesicles then release their contents, neurotransmitters, into the synaptic cleft [45]. The release of a neurotransmitter is triggered by the arrival of a nerve impulse, called an action potential, and then an unusually rapid process of cellular secretion occurs. Therefore, we consider the neuro-spike communication channel as a series of electrical and molecular channels and model it accordingly. The neuro-spike communication between the single presynaptic neuron and the single postsynaptic neuron includes the axonal, synaptic and spike generation phases [46]. Synaptic transmission is composed of vesicle release, diffusion, and generation and trial-to-trial variability of excitatory postsynaptic poten-

tial (EPSP). Also, there are two major sources of noise in neuro spike communication, axonal and synaptic. Hence, the overall model of SISO neuro spike communication channel for action potential generation and propagation phases between two neurons is illustrated in Figure 2.5.

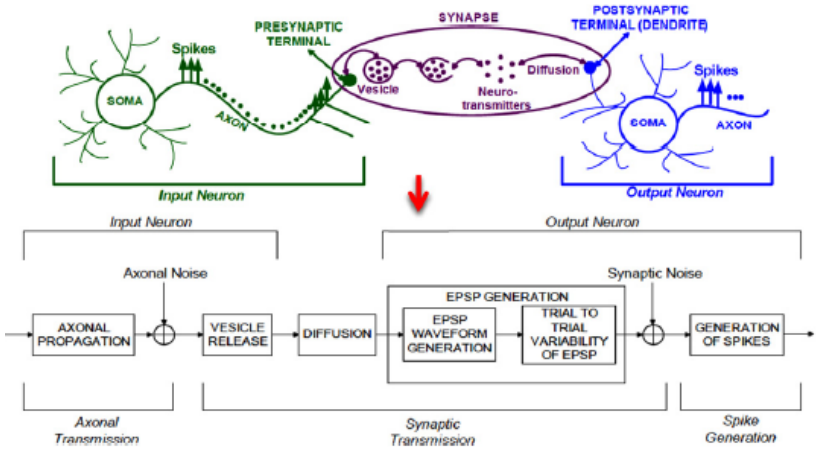

Figure 2.5: Illustration of neuron-based communication system [7]

As shown in Figure 2.5, the neuron-based MC model consists of different kinds of basic MC model: wired axon transmission for long-range in two neuron cells, the generation and receiving of spikes, the gap junction diffusion by vesicles between two neuronal cell, and the generation and transmission of the synapse.

In previous research [47, 46, 33, 48, 49, 50], neuro-spike communications are introduced to MC. Then, the channel capacity, inter-symbol interference and error probability performance are analytically investigated. In [47], it presents an analytical framework that incorporates the effect of mobility into the performance of electrochemical communication among nanomachines, which illustrates the scenario of neurospike transmission between nanomachines. In [46], the neuro-spike communication characteristics through developing a realistic physical channel model between two terminals are investigated. The neuro-spike communication channel is analysed based on the

probability of error in spike detection at the output, and the channel delay is characterised. In [33], synaptic Gaussian interference channel is investigated. Furthermore, the achievable rate region for the channel is characterised regarding power or firing rate. In [49], it provides the channel capacity of the neuro-spike communication system, which consists of axon propagation, vesicle release and neurotransmitter diffusion, while [48] focuses on the general multi-terminal channel model for neuro-spike communication, the multiple synaptic inputs single output (MISO) channel model and analysis of the inter-symbol interference and delays performance between the presynaptic input and output neurons. Eventually, [50] derives the error probability of the neuro-spike communication system. Moreover, it derives a closed-form description for the decision threshold to design an optimal spike detection receiver.

2.1.2.2 Blood Capillary-Based Hormonal Communication

The endocrine system provides communication mechanism among cells, senses the molecule concentration changes in tissues and secretes hormones for the regulation of body [7]. Moreover, the secreted hormone targets a specific tissue and instructs the tissue to produce a particular substance [51].

Hormones can be divided into two groups, lipid-soluble and lipid-insoluble; according to the ability to diffuse through the cell membrane of the target cell. Lipid-soluble hormones, are propagated through the blood vessels (see Figure 2.6) and can diffuse through the membrane and directly deliver the message. On the other hand, lipid-insoluble hormones cannot penetrate through the cell membrane by themselves and need extra messengers to translate the message to the cytoplasm of the target cell. Due to this reason, we consider lipid-soluble hormones in our blood capillary or blood vessel channel model. Lipid-soluble hormones can diffuse through the cell membrane and target the receptors in the cytoplasm.

The propagation of the hormones is due to diffusion with drift, the com-

bination movement of the blood flow that extends drift on the hormone diffusion. The reception process of the channel is selective due to the incompatible chemical structure of hormones to any other receptor type except for the receptors of target cells.

As shown in Figure 2.6, the overall hormonal molecular communication channel is constructed by considering endocrine glands as the transmitter, with the target cells acting as the receiver. The blood capillary is the communication channel between the transmitter and the receiver. In [7], it illustrates hormonal propagation through the blood vessel as the functional components within the human endocrine system, while detailed modelling was not presented.

Compared with the rich and detailed literature of neuron-spikes MC in the previous section, the literature of blood capillary-based molecular communication, discussed in Chapter2.3, is not well-studied. This provides a major motivation to investigate the biological mechanism of blood capillaries then establishes the appropriate model for this applicable and potential long-range MC. The rest of the literature regarding blood vessels or capillaries will be discussed individually in the last section of this chapter.

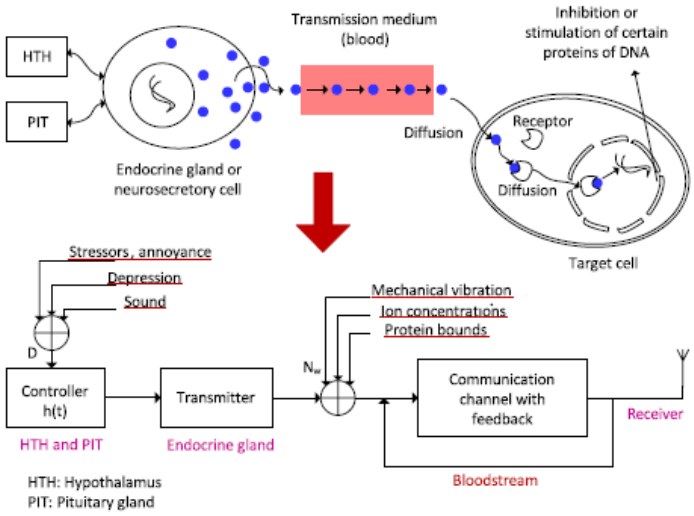

Figure 2.6: Long-range molecular communication applicable in blood capillary [7].

2.2 Mathematical Model for Molecular Communication

2.2.1 Diffusion and Brownian Motion

Diffusion, free molecules in a fluid propagating via Brownian motion, is the basic model for MC. Furthermore, the Brownian motion is a well-studied phenomenon, with a rich mathematical body of literature.

The free-diffusion model assumes that the transmitter and receiver are connected by a fluid medium, and are located a certain distance apart (compared with the range of the molecule). According to [52, 53], it matches the following assumptions:

1. The transmitter, located at the origin, is a fixed point source of molecules; moreover, it is the only source.

2. Molecules are immutable, and their motions are independent and i-

dentically distributed.

3. Once a molecule is released from the sender, the molecule does not interact with the sender in any way.

4. The medium is infinite in every direction.

5. The receiver is a surface surrounding a connected region of points.

The diffusion process or Brownian motion follows different mathematical models; the macroscopic approach with Fick's law, microscopic ones with the Einstein-Smoluchowski random walk equation and the Langevin equation [54, 55]. These degrees of freedom typically are macroscopic variables changing only slowly in comparison to the microscopic variables of the system. The microscopic variables are responsible for the stochastic nature of the Langevin equation [56].

In 1855, Fick published Fick's law to describe the diffusion process. Fick's first law of diffusion relates the diffusive flux to the molecular concentration [57]:

$$J = -D\nabla U(x,t) \tag{2.1}$$

Where J is the diffusion flux in mol/cm^2s, D is the diffusion coefficient in cm^2/s, U is the molecular concentration in mol/cm^3, and x and t are distance and time variables. It postulates that the flux goes from regions of high to low concentrations, with a magnitude that is proportional to the concentration gradient (spatial derivative). Fick's law describes the evolution of a dilute tracer substance in a medium. The left-hand side is the flux of this substance while the right-hand side is a multiple of the gradient of the density of this tracer substance [54].

Fick's second law of diffusion predicts how molecular concentration changes with time:

$$\frac{\partial U(x,t)}{\partial t} = D\nabla^2 U\left(x,t\right) + r\left(x,t\right) \tag{2.2}$$

Here $U(x,t)$ is the concentration of molecules at point x from the source and time t. $\nabla^2 U\left(x,t\right)$ is the spatial second derivatives of $U(x,t)$, D is the

diffusion coefficient of the medium, $r(x,t)$ is the molecule production rate at the source.

A typical example of the instantaneous emission concerns the emission of pheromones. In this kind of emission, the totality of a fixed amount of molecules is released into the medium in a minimal time, abruptly increasing the molecular concentration around the emitting nano-machine. Then, due to molecular diffusion, these molecules will travel through the medium dispersing them randomly.

The sudden release of a fixed amount of particles (instantaneous emission) is the most suitable modelling when molecular diversity is used to increase the molecules that can be emitted by a single nano-machine. In this case, we are not interested in variation in molecular concentration but in the type of emitted molecules. Thus, there is no need to continuously fill the medium with molecules, and the puff emission is the most suitable scenario.

Without any molecular interference, instantaneous emission of molecules is expressed by the impulse response of Fick's second law Eq.2.2. A method that delays the usage of the initial distribution is solving the equation using Green's functions. The idea behind this method is to solve the following equation [54]:

$$(\frac{\partial}{\partial t} - D\Delta)G(x,t) = \delta^d(x)\delta(t) \tag{2.3}$$

The Green's function that solves the above differential equation is given by [54]:

$$G(x,t) = \frac{e^{-\frac{x^2}{4Dt}}}{(4\pi Dt)^{d/2}} \tag{2.4}$$

Most of the previous literature apply this Green's function of Fick's diffusion. In [22, 24, 23, 58, 59, 60, 61, 46], they describe the diffusion process in the macroscopic aspect of Fick's law. That is to say, Fick's law does not focus on the movement of the single molecule, but on the variety of molecules concentration. In the MC system, Fick's law is suitable to describe the macroscopic aspect of diffusion process when the concentration of molecules

is regarded as information, such as the concentration of $Ca2+$, and $IP3$. While the literature[62, 63, 64] adopt another mathematical model for the diffusion process in a microscopic perspective, the Wiener process, focuses on the random walk or Brownian motion of molecules movement.

The Wiener process is an appropriate simple model for Brownian motion [53]. This process is defined in terms of Gaussian distribution, a continuous time random process with independent Gaussian-distributed increments, with location x having a probability density function (PDF) $f_X(x)$ given by:

$$f_X(x) = \frac{1}{\sqrt{2\pi\sigma^2}} \exp(-\frac{(x - m_x)^2}{2\sigma^2}) \tag{2.5}$$

Let $B(t)$ represent the position of a Brownian motion at time $t \geq 0$, where $B(0)$ represents the initial position. Then $B(t)$ is a one-dimensional wiener process if two criteria are satisfied:

1. For any times t_1 and t_2 (where $t_2 > t_1 \geq 0$), some constant σ^2,

$$B(t_2) - B(t_1) \sim N(0, \sigma^2(t_2 - t_1)) \tag{2.6}$$

2. For two intervals $[t_1, t_2]$ and $[t_3, t_4]$, the increments $B(t4) - B(t3)$ and $B(t2) - B(t1)$ are statistically independent if the intervals do not overlap. Intuitively, the Wiener process is a continuous-time random process with independent Gaussian-distributed increments. Then $B(k)$, the position at time k, is a Gaussian random variable with distribution.

$$B(k) \sim N(0, k\sigma^2) \tag{2.7}$$

Let the initial starts off at $B(0) = 0$, the increment between successive views of the process is

$$B(k) - B(k - 1) \sim N(0, x\sigma^2) \tag{2.8}$$

In Brownian motion, the variance parameter σ^2 is given by,

$$\sigma^2 = \alpha D \tag{2.9}$$

Where D is the free diffusion coefficient of molecules propagating in the given medium, and where $\alpha = 2, 4, 6$ if the system is $1-, 2-, 3-$ dimensional, respectively, the value of D is given by,

$$D = \frac{k_B T}{6\pi\eta R_H} \tag{2.10}$$

Where $k_B = 1.38 \times 10^{-23} J/k$ Boltzmann constant, T is absolutely temperature, η is the dynamic viscosity of the fluid, and R_H is the hydraulic radius of the molecule. According to [65], the values of D in the range $1 \sim 10 um^2/s$ were considered realistic for signalling molecules.

In [4], it considers the Wiener process with drift for long-range MC in a capillary. A sender released a signal molecule into the bloodstream; the propagation process would be biased in the direction of the blood flow. In a wiener process with drift, v is the drift velocity; the increment distribution is replaced with:

$$B(t_2) - B(t_1) \sim N\left(v(t_2 - t_1), \sigma^2 (t_2 - t_1)\right) \tag{2.11}$$

2.2.2 Model for Molecular Motors

A major disadvantage of drift-free Brownian motion is the potentially long and highly uncertain delay in the propagation of individual molecules. Moreover, adding drift is not always an available solution. In active-based molecular transmission, molecular or bacterial motors are applied to transport molecules actively. A simulation scheme for active transport was given in [66], which replaces the wiener process step equation with

$$xi = xi - 1 + \Delta r \cos\theta i \tag{2.12}$$

$$yi = yi - 1 + \Delta r \cos \theta i \tag{2.13}$$

where, given the microtubules average velocity V_{avg} and diffusion coefficient D, Δt is a Gaussian random variable with mean and variance

$$\mathrm{E}\left[\Delta r\right] = v_{avg}\Delta t \tag{2.14}$$

$$\mathrm{Var}\left[\Delta r\right] = 4\mathrm{D}\Delta t \tag{2.15}$$

$$\theta i = \theta i - 1 + \Delta\theta \tag{2.16}$$

given persistence length L_p,is $\Delta\theta$ also Gaussian random variable with mean and variance

$$\mathrm{E}\left[\Delta\theta\right] = 0 \tag{2.17}$$

$$\mathrm{Var}\left[\Delta\theta\right] = v_{avg}\frac{\Delta t}{L_p} \tag{2.18}$$

2.3 Literature for Blood Capillary

In this section, literature relevant to channel modelling of blood capillaries or blood vessels is classified into two types. The first type of prospective literature indicates that blood capillaries can be applied to MC. Although this literature does not present a practical mathematical model, it opens a gate to investigate the blood capillary system in the communication aspect.

In [21], the blood capillary system was proposed to long-range MC application for the first time. Meanwhile, it indicates the most suitable communication particles to be used the in blood capillaries system are the hormones. Hormonal communication channels through blood vessels, discussed in previous section 2.1.2.2, are classified as long-range MC, and our research follows this proposal.

After that in [7], it proposed a hormonal MC channel through the bloodstream within the human body, considering endocrine glands as the transmitter and the target cells as the receiver. The second model in Chapter 4

is also inspired by this phenomenon in the endocrine system.

The second type of literature considers the exact channel model of the blood capillary system. The most fundamental research of blood vessels is [67], and it analysed blood vessels as a Casson fluid and derived an explicit expression for the effective longitudinal diffusion. As a consequence, it indicates that both the rheology of blood and the permeability of the vessels may constitute a physiological barrier to the intravascular delivery of nano-particles.

Casson fluids models [68, 69, 70], the term for non-Newtonian fluids, are not considered in this thesis. In Casson fluids, the viscosity does not have a constant value, but depends on the shear rate. In [68], it presented a mathematical model for the peristaltic flow of rheologically complex physiological fluids, which is modelled by a non-Newtonian Casson fluid in a two-dimensional channel. Meanwhile, it is found that a Newtonian fluid is an important subclass of non-Newtonian fluids that may adequately represent some physiological phenomena. The blood capillary fluid, far from the heart, can be modelled by Newtonian fluids adequately. In [69], it is an improvement in the studies of the mathematical modelling of blood flow in narrow arteries with mild stenosis, while in [70], the artery is modelled as a circular tube. All these mathematical models in Casson fluids [68, 69, 70], are adequate to model the artery vessel, but are suitable for the smallest capillaries.

In the literature [71], it established a simple Synchronization and Threshold Detection (STD) module to describe nano-particle transmission in blood vessels. This STD module has two functions: 1. synchronizing the receiver with a new train of pulses, and 2. decoding the information through a decision threshold mechanism [71]. Moreover, this blood vessel MC system is inspired by a signalling phenomenon between the platelets and endothelial cells, based on the release of specific proteins known as CD40Ls, which can bind to the relevant receptors (CD40) available on the surface of the

receivers. Based on [71], Felicetti also published the following literature [72, 73, 74]. In [72], it presented a software platform, named BiNS2, able to simulate diffusion-based MC inside blood vessels. In [74], it presented a model which includes both a propagation model of blood vessel channel and the integration of the Markov chain in the receiver. In [73], it proposed tumour detection via tumour CD47 protein bio-markers on the cell surface, which is different from the method of CD40 propagation in previous research. However, tumours with bio-markers, regarded as the largest particles, have sizes similar to white blood cells, which are not suitable to be applied by advection-diffusion equation.

Both of the literature[72, 73, 74] apply the advection diffusion equation for the diffusion process in blood vessels, with the assumption of constant flow velocity. Moreover, the advection diffusion equation describes concentration variation with the relationship of flow velocity and diffusion coefficient, so that the information of the location and transmission distance is not provided. Differing from [72, 71, 73, 74], this thesis focuses on both the diffusion and blood flow in microscopic Langevin-based diffusion.

According to [32], other forms of mass diffusion assist the propagation of particles at macroscales. These include:

Advection-diffusion: Advection refers to transport with the bulk fluid flow [75]. For example, information particles released inside a duct with air flows, are moved by bulk air flows.

Convection-diffusion: In thermodynamics convection is the fluid flows generated because of differences in temperature [76]. For example, in a room, cold air, which is dense, moves downward while warm air moves upward. It must be noted that convection is also used to specify the combined advection-diffusion process in fluid mechanics.

As a consequence, advection-diffusion and convection-diffusion are not adequate for modelling the propagation process in blood vessels or capillaries.The propagation of particles in the communication environment of the

blood capillary is considered in terms of both blood flow and diffusion with the details as follows:

1. Particle diffusion, which is well-studied in the theory of Brownian motion [77, 53]; previous literature [58, 22], and in MC applied with respect to Fick's law. Furthermore, [78, 79, 74, 73]applied the advection diffusion equation to describe the diffusion process.

2. The blood flow model in blood capillary is divided into laminar and turbulent flows, which depends on the Reynolds number. The following literature [80, 81] discussed the difference between two blood flow models, laminar flow and turbulent flow.

3. Positive drift due to the pressure of the bloodstream, which depends on the position of the particle with respect to the axis of the blood flow. In the literature [82, 83, 84] of the mathematical modelling aspect, they introduce the generalised Langevin equation to model the diffusion with the drift process, the solution of which is the corresponding Fokker-plank equation.

In the literature [58, 85, 22, 86], basic diffusion channels are studied, and they all consider the simple diffusion channel match Brownian motions. Similarly, they describe Brownian motion in Fick's law. The paper [85] presents mathematical models of the fixed transmitter, channel and the fixed receiver. The authors evaluate the end-to-end gain and propagation delay as a function of some environmental parameters. Information is transferred by modulating the concentration of the particles emitted by the transmitter. In the same scenario, [58] models the noise sources affecting the diffusion-based MC, using a ligand-bind receptor at the receiver. All these works assume a transmission medium in which propagation is due to diffusion only, which does not apply to our scenario.

While there are a number of theoretical models applying all kinds of passively diffusion in MC, the literature of diffusion with drift model in MC is less. In [62], it shows that the additive inverse Gaussian noise channel is an appropriate model for MC in fluid media with drift. Differing from

the method used in[62], the Langevin equation is used to describe diffusion with drift in this thesis. Langevin equation is stochastic partial differential equations, and the stochastic term matches the Gaussian distribution.

The MC reception of nano-particles is also profoundly affected by the blood flow that interferes with the chemical interactions between ligands and receptors [87]. Also, the stochastic effects in the ligand-receptor binding kinetics and interference are modelled through the MC framework [88, 89]. However, in this literature [88, 89], the binding and unbinding process is only considered in the ligand-receptor model. The endocytosis process of vesicles is also significant in the vesicles reception by the ligand-receptor [8]. Different models of ligand-receptor are used in this thesis on the basis of reception mechanisms.

In particular, the study in [90] shows that the influence of the red blood cells within the blood capillary is dominant. The influence of red blood cells is complex and is not considered in this thesis.

Modelling of blood capillaries is a fundamental component when designing drug delivery systems. In the literature [19], it presents a drug delivery system in MC, where the transmitted message is the drug injection process, the channel is the cardiovascular system, and the received message is the drug reception process. Within this MC framework for drug delivery systems [19], analytical expressions of the noise and channel capacity are derived in [20].

2.4 Chapter Summary

This chapter provides a review of the literature for blood capillary-based MC with three subsections. The first section discuss great variety of biological systems applied in MC on the basis of communication range. Moreover, MC in short-range are categorised and discussed based on passive transport-based, and another type active transport-based. Three passive diffusion mechanisms in biological system is applied to MC, which including

free diffusion, Gap-junction based and reaction diffusion based, while active transport-based MC is divided to Molecular motor-based and Bacterial motor-based. Two long-range MC, neuron-Based and blood capillary-based hormonal communication, are discussed individually. Mathematical model in previous literature is discussed in section 2.2. The last section in this chapter discussed literature relevant to channel modelling of blood capillaries or blood vessels from initial proposal and latest research.

Chapter 3

Channel Modelling of Diffusion-based blood capillary in Frequency Domain

3.1 Biological System

Blood capillaries are considered as one of the long-range MC systems in our body [7]. Capillaries are the smallest blood vessels that make up the microcirculation. According to [91], the diameter of blood capillary ranges from a $5\mu m$ to $10\mu m$, while the diameter of the general vessel is about $30\mu m$. The length of a capillary could be compared to a neuron axon, from cm to m. Capillaries with the length of $67cm$ could be designed as testing units. In addition, several capillaries could be joined together to reach further nodes. The capillary channel in MC consists of encoding or emission processes, and propagation, reception or decoding processes. According to [7], the hormones or cytokines are suitable information molecules in the capillary channel.

The capillary wall performs an important function by allowing nutrients and waste substances to pass across it. Molecules larger than $3nm$, such as hormones and other large proteins, transport through transcellular carried

inside by vesicles, a process which requires them to go through the cells that form the wall. Molecules smaller than $3nm$ such as ions or gases cross the capillary wall through space between cells in a process known as paracellular transport [92].

The endocrine systems secrete specific hormones into the circulatory system and are carried towards distant target organs. Typically, cytokines are propagated by diffusion within the blood fenestrated capillaries. In paracrine function, hormones diffuse through the interstitial spaces to nearby target tissues. Additionally, hormones can bind to the specific receptor. Thus it plays a role as a selective filter[93, 27].

The biological scenario is in the endocrine systems, which consists of vesicle emission, transmission and reception by target cells. The endocrine cells release vesicles, which contain the hormones, from the release-ready pool (RRP) at the secretion site via exocytosis. Vesicles are emitted into the blood fluid medium by passing across the capillary wall. The information molecules represented by hormones are kept inside vesicles and flow through the blood capillary and reaches the reception. Vesicles can enter the target cells via receptor-mediated endocytosis first by binding to the cell-surface receptors, then internalising into the cell.

An example of this process is the endocrine cell of the adrenal medulla (the innermost part of the adrenal gland), which releases adrenaline into the blood [94]. The adrenal medullary hormones are kept in vesicles. Sympathetic nerve fiber impulses stimulate the release of adrenal medullary hormones. Hormonal effects can last up to ten times longer than those of neurotransmitters [94].

Figure 3.1 illustrates the basic mapping of the blood capillary communication system.

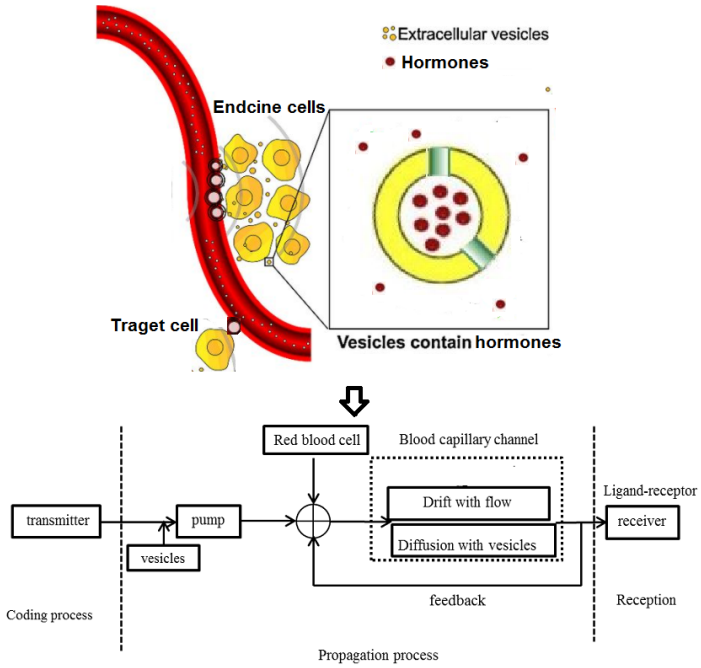

Figure 3.1: basic mapping of blood capillary-based channel model

According to [21], the encoding of the hormones in the blood capillary system is analogous to the pheromones emission. Instantaneous emission of pheromones is usual in nature when alarm situations occur. In this kind of emission, the totality of a fixed amount of pheromones is released into the medium in a minimal time, abruptly increasing the molecular concentration around the transmitter.

Two primary methods encode the information molecules transported in the fluid medium. Firstly, the molecular signal can be embedded to the particle concentration, modulating its amplitude or frequency according to the information to be transmitted. According to [6], $30,000$ molecules should be released to recover a signal peak consisting of five components correctly. Secondly, the utilisation of different particles could present short messages, assigning each particle type to each possible packet that can be transmitted.

This technique would be more efficient in a system with limited information to be transmitted.

Hormones have different types. They can be divided into two groups according to their ability to diffuse through the cell membrane of the receiver or receptor. Lipid-soluble hormones, steroids, can diffuse through the membrane and directly deliver the message. On the other hand, lipid-insoluble hormones cannot penetrate through the cell membrane by themselves and need extra messengers to translate the message to the cytoplasm of the target cell. Due to its outweighing number [3], we consider lipid-soluble hormones in the blood capillary channel model. Lipid-soluble hormones can diffuse through the cell membrane and target the receptors in the cytoplasm. Lipid-soluble hormones can easily gain access into vesicles by the endocytosis in the membrane.

The instantaneous emission of a fixed amount of molecules (hormones) is the most suitable coding mechanism for blood capillary. What we are interested in is the number of hormones released per unit time rather than variations in the types of emitted hormones.

In this chapter, we adopt On-Off keying (OOK), a simple coding mechanism, as the encoding mechanism. Namely, if there is an amount of hormones being released, it represents 1; in the converse situation, it represents 0.

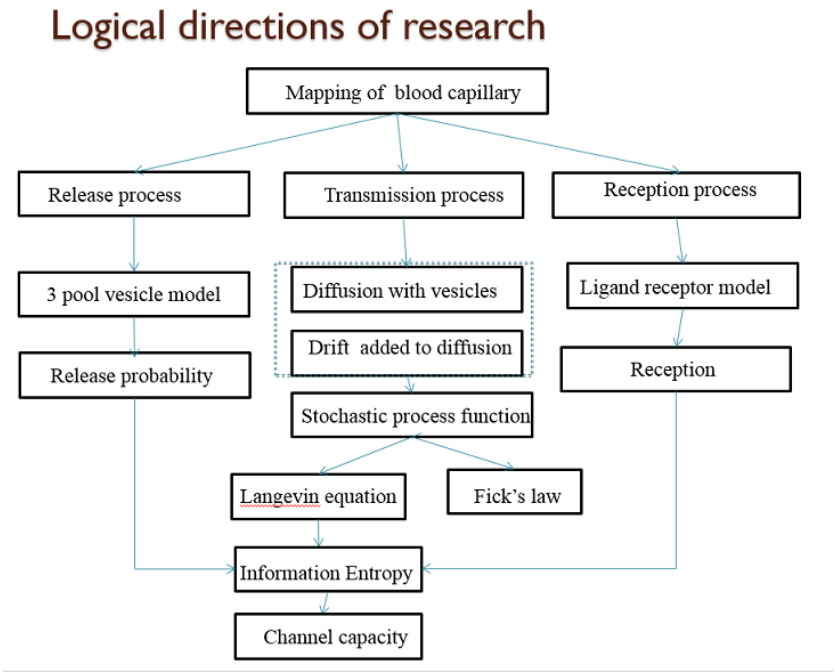

Figure 3.2: Logical flowchart to model vesicle transmission in blood capillary.

Figure 3.2 shows the flowchart of logical thinking to the model of vesicle transmission system in a blood capillary. Three basic processes -: vesicle release, vesicle propagation and vesicle reception will be investigated in the following section.

3.1.1 Vesicle Release Process

In this blood capillary model, vesicles are the transmission information containers or information interface. In the release model, the portability to release vesicle is closely related to the process. In a blood capillary, vesicles are docked at the membrane waiting to release their content upon the arrival of a trigger signal. Others are stored in the membrane pool, just above the docked vesicles, being more distant to the cell membrane. Vesicles in the blood capillary can be grouped into three sub-pools according to their

relative motilities: the release-ready pool (RRP), the recycling pool and the reserve pool [95, 96, 97].

The reserve pool makes up(approximately 80% to 90%) of the total pool, with the recycling pool being significantly smaller(approximately 10% to 15%).The release ready pool (RRP) consists of a few vesicles(approximately $\approx$ 1%) that are docked and primed for release [95]. Three kinetic components of release process (indicating release of three vesicle pools) coexist in the synaptic terminal on depolarization of goldfish bipolar cells. The vesicles in the release-ready pool are available to release, while vesicles in the reserve pool and recycling pool are unavailable to release. The number of vesicles in the release-ready pool maintains balance of the vesicles in the reserve pool refills into the release-ready pool by an endocytosis process [98, 95]. The reserve pool refills the available pool with a constant time τ_D [95]. Figure 3.3 shows the classic three-pool model.

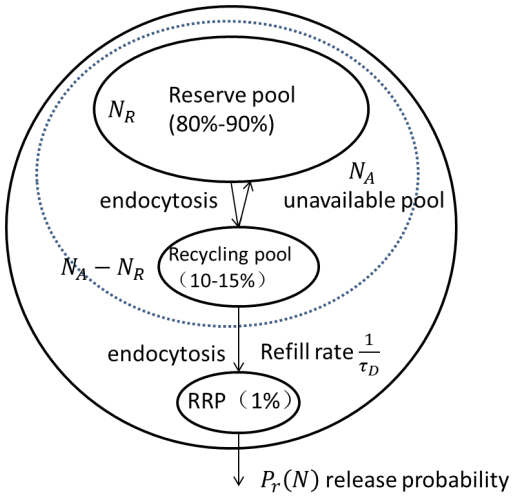

Figure 3.3: Three pools model of vesicle release

The number of vesicles in RRP, the recycling pool and the reserve pool, are doted as N, $N_A - N_R$, and N_R, respectively. N_A is the total vesicle size of the unavailable pool including the recycling pool and reserve pool.

The recycling pool is close to the cell membrane and tends to be cycled at moderate stimulation so that the rate of vesicle release is the same as the rate of vesicle formation. Once the RRP and the recycling pool are exhausted, the reserve pool is mobilised [97].

The vesicle release probability is the same as the release probability of the available pool, RRP, namely $p(N)$. Releasing a single vesicle upon arrival the signal is described by a Poisson process with firing rate $\lambda(t)$ [99]. According to [99], it indicates that the fusion rate at which the vesicles are expelled through exocytosis. The fusion rate for a single vesicle is shown below:

$$\alpha_{vk} = \int_0^{\Delta t_k} \lambda(t)dt \tag{3.1}$$

The integration is evaluated over the duration of k^{th} time window. In Eq.3.1, subscript k denotes the window index, and the integration is from the beginning of the release process then taken as the time origin until the end of k^{th} time window of the stimulus denoted as Δt_k. We assume that the time window duration is the same $\Delta t_1 = \Delta t_2 = \cdots = \Delta t_k$. In the calculation of α_{vk}, we divide Δt_k into windows of equal durations. According to [100], Δt_k is a linear function. We can easily find that α_{vk} is constant, set $\gamma_p = \alpha_{vk} = \int_0^{\Delta t_k} \lambda(t)dt$ The single vesicle release probability is:

$$p_{vk} = 1 - \exp\left(-\gamma_p\right) \tag{3.2}$$

Therefore the false probability of a single vesicle is$1 - p_{vk} = 1 - \exp\left(-\gamma_p\right)$. N_k is the number of vesicles in RRP at the k^{th} time window. The probability of none vesicles released at k^{th} time window is $\exp(-\gamma_p)^{N_k} = \exp(-\gamma_p N_k)$. Therefore, the vesicle release probability at the k^{th} time window means at least one vesicle is released, given by:

$$p_r(N_k) = 1 - \exp(-\gamma_p N_k) \tag{3.3}$$

The vesicle release probability is determined by γ_p and N_k. Similarly, in the next window $k+1^{th}$, the release probability shows as below :

$$p_r(N_{k+1}) = 1 - \exp(-\gamma_p N_{k+1}) \tag{3.4}$$

Importantly, the vesicles in the reserve pool will refill into the RRP within a constant time τ_D [97]. According to [95], the refill time of the vesicle pools is constant with $\tau_D = 14ms$ in blood capillary at the temperature $300K$, so that the number of the vesicles in the next window N_{k+1}, can be expressed as below:

$$N_{k+1} = N_k - W_k + N_{k+1}^{rf} = N_k - p_r\left(N_k\right) N_k + N_R P_{k+1}^{rf} \tag{3.5}$$

In Eq.3.5, W_k is the average number of vesicles released on k^{th} time window and N_{k+1}^{rf} is the number of vesicles in the release ready pool refilled by the reserve pool during the time between two consecutive windows.

$$P_{k+1}^{rf} = 1 - \exp(-\frac{\Delta t_k}{\tau_D}) \tag{3.6}$$

The average probability of all the windows is set to the vesicle release probability:

$$P_{release} = \overline{P_{vk}} = \frac{1}{N_k} \sum_{j=1}^{N_k} p_{vjk} \tag{3.7}$$

3.1.2 Vesicle Propagation Process

In general, the diffusion channel model is fundamental to MC. In blood capillary system, vesicles, act as transmission containers, capture and store the hormones. In this research, the information carriers are hormones. The numbers of hormones can be grouped and contained in vesicles. Small particles and vesicles follow different operational procedures, and thus need to be represented mathematically differently. As mentioned in the survey, the

ligand-receptor model extensively exists in the biological cell. Ligands bind to the receptor sites on the cell's surface, detect and capture the receiving vesicles in the environment of the reception area. Vesicles with the hormones are internalised into endocrine cells via endocytosis. Figure 3.4 illustrates the diffusion channel that vesicles are propagated through the blood capillary and received by the ligand-receptor.

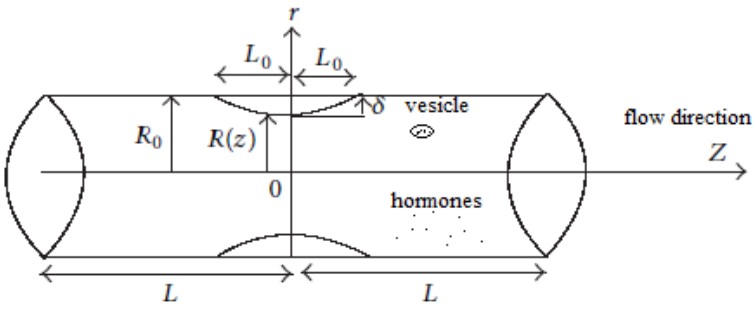

Figure 3.4: The illustration of diffusion model with vesicles

The diffusion is generally to be described by Fick's law, as shown by the Fick's First law $J = -D\nabla U(x,t)$ (Eq.2.1). It postulates that the flux goes from regions of high low concentration, with a magnitude that is proportional to the concentration gradient (spatial derivative). Fick's second law of diffusion predicts how molecular concentration changes with time (Eq.2.2).

Here $U(x,t)$ is the concentration of molecules at point x concerning the source location and time t. $\nabla^2 U(x,t)$is the sum of the n-dimension spatial second derivatives of $U(x,t)$, D is the diffusion coefficient of the medium, $r(x,t)$ is the molecule production rate at the transmitters.

When a large number of molecules are contained in vesicles, the concentration of vesicles becomes much less than that of particles. Furthermore, as the size of vesicles is larger than that of a particle the effect of collision cannot be ignored. However, Fick's law only focuses on the concentration

variation of information practices, which reflects the macroscopic aspect of the diffusion process, while ignoring some microscopic perspectives of the diffusion process such as object movement and collision. As such, a new model that is able to describe both molecules concentration and movement of collision from small particles shall be investigated. In this thesis, we propose to utilise the Langevin equation to describe this complex diffusion process in blood capillary. The Langevin equation is shown below:

$$m\frac{d^2x}{dt^2} = -\gamma\frac{dx}{dt} + f\left(t\right) \tag{3.8}$$

In Langevin equation here,x is the position of the particle and m denotes the particle's mass. The force acting on the particle is written as a sum of a viscous force proportional to the particle's velocity $v(\mathrm{t}) = \frac{dx}{dt}$, and a noise term $f(t)$ representing drift with the effect of the particles collisions with the molecules of the fluid. The force $f(t)$ has a Gaussian probability distribution with correlation function, as below:

$$\langle f_i(t_1)f_j(t_2)\rangle = 2\gamma k_B T\delta_{i,j}\delta(t_1 - t_2) \tag{3.9}$$

Where k_B is Boltzmanns constant and T is the temperature, and the Dirac delta function $\delta(t)$ form of the correlations in time means that the force at a time t is assumed to be completely uncorrelated with it at any other time.

The force $f(t)$ determines the drift velocity, according to [101, 56], and the noise term of Eq.3.9 has Gaussian distribution. Thus, it means the drift force variation with time matches the Gaussian distribution.

3.1.2.1 Transfer Function in Frequency Domain

To understand the strength of a signal distributed in the frequency domain, we have to go back to the spectral density of the transmitted signal. As it is not readily available in the literature, it is necessary to deduct the spectral density regarding vesicle velocity, or the transfer function of Langevin-based

diffusion process.

In the derivation, the Fourier transfer of the Langevin equation regarding velocity is the first step.

Firstly, we transfer the Langevin equation to a first order equation, and $v(\mathrm{t}) = \frac{dx}{dt}$ represents the velocity of vesicles, so we rewrite Eq.3.8 as below:

$$m\frac{dv(t)}{dt} + \gamma v(t) = f(t) \tag{3.10}$$

By applying the Fourier transform to Eq.3.10, we have an expression as below:

$$(j\omega) \cdot mv \cdot (j\omega) + \gamma v\,(j\omega) = F\,(j\omega)$$

$$v(j\omega) = \frac{F(j\omega)}{j\omega \cdot m + \gamma} \tag{3.11}$$

The relationship of the convolution of $G(t)$ and $f(t)$ in the fourier transfer is shown below:

$$v\,(t) = G_v\,(t) * f\,(t) \overset{fourier}{\Rightarrow} v\,(j\omega) = G_v(j\omega) \cdot F(j\omega)$$

$$\mathrm{G_v\,(j\omega)} = \frac{1}{j\omega \cdot m + \gamma} \tag{3.12}$$

$v_T\,(f)$, the spectral density of velocity at time T, $G_v(f)$, can be calculated by the Wiener-Khinchin theorem as below:

$$\phi\,(\omega) = \left| \frac{1}{\sqrt{2\pi}} \int_{-\infty}^{\infty} f(t) e^{-i\omega t} dt \right| = \frac{F(\omega)F*(\omega)}{2\pi} \tag{3.13}$$

while $G_{vv}(f)$ and $K_{vv}(t)$ are a Fourier transform pair, $G_{vv}\,(f) \Leftrightarrow K_{vv}\,(t)$.

$$F_1(j\omega) \cdot F_2^*(j\omega) = F(R_{12}(\tau)) \tag{3.14}$$

$$v_T(f) = \frac{F_T(f)}{2\pi jm + \gamma} = \frac{F_T(f) \cdot (-2\pi jm + \gamma)}{(2\pi jm)^2 + \gamma^2} \tag{3.15}$$

$$v_T^*(f) = \frac{F_T^*(f)}{2\pi jm + \gamma} = \frac{F_T^*(f) \cdot (2\pi jm + \gamma)}{(2\pi jm)^2 + \gamma^2} \tag{3.16}$$

$$G_{vv}(f) = v_T f \cdot v_T^* f = \frac{F_T(f) \cdot F_T^*(f)}{(2\pi fm)^2 + \gamma^2} = \frac{2k_B T\gamma}{(2\pi fm)^2 + \gamma^2} \tag{3.17}$$

So we rewrite as the $G_{vv}(\omega)$, spectrum density of the random variable regarding the velocity, has the relationship to the Langevin diffusion equation:

$$G_{vv}(\omega) = \frac{2k_B T\gamma}{(\omega m)^2 + \gamma^2} \tag{3.18}$$

The vesicle transmission in the blood capillary follows Langevin equation Eq.3.10, and Eq.3.18 is regarded as the transfer function of transmission process.

From Eq.3.18 we can also deduce $G_{xx}(\omega)$, the spectrum density of the random variable regarding the displacement x, which is proportional to $|x(\omega)|^2$, and it is given by,

$$G_{xx}(\omega) = \frac{2k_B T\gamma}{m^2} \frac{1}{(\omega)^4 + \gamma^2\omega^2} \tag{3.19}$$

Thus, we find the relationship between the spectral density regarding velocity $G_{vv}(\omega)$ and spectral density regarding displacement $G_{xx}(\omega)$ from Eq.3.18 and Eq.3.19,

$$G_{vv}(\omega) = \omega^2 G_{xx}(\omega) \tag{3.20}$$

3.1.2.2 Vesicle Velocity and Displacement

The dissipation coefficient γ is given by Stokes Law:

$$\gamma = 6\pi\eta \mathrm{a} \tag{3.21}$$

Where a is the radius of the vesicle, m is practical mass of the vesicle practical, which according to [98] approximately $10^{-14} \sim 10^{-15}$kg, and a is approximately 10nm $\sim$ 60nm. Also, according to [102], η, the viscosity of blood capillary, varies with temperature.

The random force $f(t)$ is a stochastic variable giving the effect of background noise due to the fluid on the Brownian particle. Due to this, the velocity of the Brownian particle is predicted to decay to zero at long times. Since we have extracted the average force $-\gamma v(t)$ in the Langevin equation Eq.3.10 the average of the fluctuating force must by definition be zero. $g = 2k_BT\gamma$ is a measure of the strength of the fluctuation force. In the conventional view of the fluctuation force, it is supposed to come from occasional impacts of the Brownian particle with molecules of the surrounding medium. The force during an impact is supposed to vary extremely rapidly over the time of any observation. The effect of the fluctuating force can be summarized by giving its first and second moments. We denote τ_B as below:

$$\tau_B = \frac{m}{\gamma} \tag{3.22}$$

We can obtain an explicit formal solution of Langevin equation Eq. 3.10 in time domain regarding velocity given by [103, 82],

$$v(t) = e^{-t/\tau_B} v(0) + \frac{1}{m} \int_0^t e^{-(t-s)} F(s) ds \tag{3.23}$$

and the autocorrelation function of velocity is given by,

$$C_{vv}(t) = \frac{k_BT}{m} e^{-\frac{t}{\tau_B}} \tag{3.24}$$

From Eq.3.23 we can also get an expression for the displacement of the particle.

$$x(t) = x_0 + v_0\tau_B(1 - e^{-t/\tau_B}) + \frac{\tau_B}{m} \int_0^t (1 - e^{-(t-s)/\tau_B}) ds \tag{3.25}$$

for the random force autocorrelation function regarding the displacement, we get, for any t:

$$C_{xx}(t) = \left\langle [x(t) - x(0)]^2 \right\rangle = 2Dt \tag{3.26}$$

3.1.3 Vesicle Reception Process

Vesicles can enter the cells via receptor-mediated endocytosis by first binding to the cell-surface receptors. Specific binding of the vesicle to the cell surface occurs when ligand-receptor interactions form between the vesicle and the cell surface. However, these interactions are not permanent and ligands can unbind from their receptors. This binding and unbinding keep a dynamic balance. Upon associating to a free binding site, vesicles can be internalised into the cell via endocytosis [104, 8].

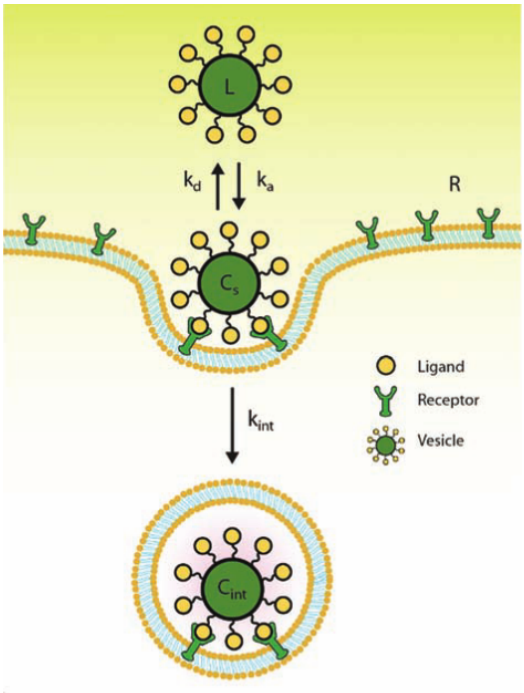

Figure 3.5: Illustration of the kinetic model for vesicle reception [8].

Kinetic vesicle reception model in this chapter is illustrated in Figure 3.5. Assuming that vesicle association to the cell surface is independent of other ongoing processes, the event can be described as below:

$$N + R_s \underset{k_d}{\overset{k_a}{\rightleftharpoons}} N_s \tag{3.27}$$

While the internalization process can be described as below:

$$N_s \xrightarrow{k_{\text{int}}} N_{\text{int}} \tag{3.28}$$

where N is the number of free vesicle reaching the reception area, R_s is the number of free binding sites, N_s is the number of vesicles bound to the cell surface, $k_a(M^{-1} \cdot s^{-1})$ is the association rate constant for a free vesicle binding to a free binding site, $k_d(s^{-1})$ is the dissociation rate constant for a vesicle dissociating from its binding site and $k_{\text{int}}(s^{-1})$ is the rate constant for a binding vesicle to be internalised. The balance on the number of bound vesicles yields the following expression, given by [8]:

$$\frac{dN_s}{dt} = k_a N R_s - (k_d + k_{\text{int}}) N_s \tag{3.29}$$

By solving the linear differential equation, we get the following equation, where K is an arbitrary constant:

$$N_s = K e^{-(k_d + k_{\text{int}})t} + \frac{k_a N R_s}{k_d + k_{\text{int}}} \tag{3.30}$$

Regardless of the physical nature of the binding site, this mathematical model assumes that the number of binding sites remains constant over time, as the cell is constantly regenerating and internalizing its membrane. Here it assumes that the constant K is equal to 0. Then the number of vesicles

bound to the receiver cell surface denoted by N_s, which can be given as:

$$N_s = \frac{k_a R_s}{k_d + k_{\text{int}}} N \tag{3.31}$$

Eq.3.29 expresses the ligand-based reception process as a function of time t. By applying the Fourier transfer to Eq.3.29, the expression as a function of frequency ω is as follows:

$$j\omega N_s(\omega) = k_a N(\omega) * R_s(\omega) - (k_d + k_{\text{int}}) N_s(\omega) \tag{3.32}$$

where $*$ is the convolution operator. As explained above, we assume a constant number of free binding sites R_s on the surface to the receiver cell. As a consequence, the expression of the transfer function of the ligand-receptor process $h_R(f)$ is as follows:

$$h_R(f) = \frac{k_a}{2\pi f + k_d + k_{\text{int}}} \tag{3.33}$$

where k_a, k_d and k_{int} are the ligand-receptor binding and release and internalise rates, respectively. The steady state approximations of the Ligand-Receptor Binding process to the constant values of reception probability, result from computing the transfer functions $h_R(f)$ for a value of the frequency $f = 0$, expressed as:

$$P_{receive} = \frac{k_a}{k_d + k_{\text{int}}} \tag{3.34}$$

Which correspond to the solution of Eq.3.29, when we set the first derivative $\frac{dR_s(t)}{d(t)} = 0$ in the number of free binding sites R_s to 0.

3.2 Channel Capacity in Frequency Domain

The capacity of a communication system in bits per second is defined as the maximum rate of transmission between transmitter and receiver. The general

expression Eq.3.35 from Shannon [105] defines that channel capacity is equal to the maximum mutual information $I(X;Y)$ between Input signal X and Output signal Y with respect to the probability density function $f_X(x)$ of all values of the transmitted signal.

$$\mathrm{C} = \max_{f_X(x)}\{\, I\,(X;Y) \tag{3.35}$$

The transmission process which is a cascade of three independent processes, vesicle release, vesicle propagation, described in the Langevin equation (see Figure 3.3), and vesicle reception. These processes follow the order input signal to output signal $X \to Y$. This is justified by the properties that are conditionally independent given, which is expressed as follows:

$$I(X;Y) = H\,(X) - H\,(X|Y) = H\,(Y) - (Y|X) \tag{3.36}$$

The closed-form expression for the mutual information $I(X;Y)$ in bits per second of the blood capillary system is computed by applying the Eq.3.36 .

where $H(X)$ is the marginal entropy per second of the transmitted signal and $H(X|Y)$ is the conditional entropy per second of the input signal X given by output signal Y, which is the consequence of the palpation process from the transmitter to receiver.

The entropy $H(X)$ per second of the transmitted signal is computed as the entropy measured in bits per symbol, multiplied by twice the bandwidth W, which corresponds here to the rate of the symbol transmission in symbols per second.

The transmitted signal, denoted by X, is here defined as the number of vesicles released into blood capillary as a function of the time t:

$$X = N_X(t), t > 0 \tag{3.37}$$

Given the communication system considered to release vesicles, the aver-

age power necessary for signal transmission corresponds to the energy necessary to emit the average number of vesicles $E(N_X)$ per time sample, divided by the duration of a time sample. In thermodynamics, this energy is defined as enthalpy.

According to[106], the enthalpy $\mathcal{H}$ is the energy necessary to emit N_x vesicles in the physical system and to heat these particles up to a temperature T when the system has the pressure P and the volume V, with the following expression:

$$\mathcal{H} = PV + \frac{3}{2}K_b T N_X \tag{3.38}$$

In [61, 22], they defines the average thermodynamic power $\overline{P}_{\mathcal{H}}$ the enthalpy variation $\Delta\mathcal{H}$ in a time sample divided by the time sample duration $1/2W$.

$$\overline{P}_{\mathcal{H}} = \frac{\Delta\mathcal{H}}{1/2W} = \frac{3}{2}K_b T E(N_X) 2W \tag{3.39}$$

We follow this definition in [61, 22], a constraint on the average thermodynamic power $\overline{P}_{\mathcal{H}}$ spent by the transmitter corresponds to a constraint in the average number of emitted vesicles $E(N_X)$ according to the following expression:

$$E(N_X) = \frac{\bar{P}_{\mathcal{H}}\overline{N_x}}{3W k_B T} \tag{3.40}$$

which is the continuous released numbers of vesicles which contains hormones information inside represents the input signal. The average number of vesicles at each time window is in the expression of $\overline{N_X} = p_{release} \cdot N$. Probability mass function is donated by $P(N_X)$.

The entropy $H(X)$ of input signal X is defined by the entropy of power of emitted vesicles $H(X_N)$in bits per sample multiplied by twice the bandwidth in samples per second.

$$\mathrm{H\,(X)} = 2WH(X_N) \tag{3.41}$$

The entropy of the number of emitted vesicles $H(X_N)$ per time sample with relationship of the average number, or expected value, is given by [107]

:

$$H(X_N) = 1 + \log_2(E(N_X)) \tag{3.42}$$

As proven in [105], we can express the conditional entropy $H(X|Y)$ of the transmitted signal given received signal as the entropy of the ensemble per degree of freedom in bits per sample multiplied by twice the bandwidth in samples per second. The entropy of the ensemble per degree of freedom corresponds to the entropy of a sample of the time-continuous signal.

$$H\left(X|Y\right) = -\frac{1}{W}\int_{-w}^{w} \log_2|P_{receive} \cdot G_{vv}\left(f\right)|^2 df \tag{3.43}$$

As we proved before, $G_{vv}(f)$ Eq.3.17 is the spectral density of Input signal propagation applying Langevin equationwhich is regarded as transfer function Fourier transform of propagation process. $P_{receive}$ Eq.3.34 is the steady state approximations of the ligand binding reception probability.

We deduct the close-form solution of $H(X|Y)$, by applying Eq.3.43 and Eq.3.17, as follows:

$$H(X|Y) = -\frac{2\gamma kT}{\ln 2}[\ln((2\pi fm)^2 + \gamma^2) + \frac{\gamma}{\pi m}\tan^{-1}(\frac{2\pi fm}{\gamma}) - 2\gamma] \tag{3.44}$$

Channel capacity is calculated by applying Eq.3.42 and Eq.3.44 into Eq.3.35, shown as follows:

$$\begin{aligned} C = \max_f\{2W(1 + \log_2(\frac{\bar{P}_H \cdot p_{release} \cdot N}{3Wk_BT}) \\ - \{-\frac{2\gamma kT}{\ln 2}[\ln((2\pi fm)^2 + \gamma^2) + \frac{\gamma}{\pi m}\tan^{-1}(\frac{2\pi fm}{\gamma}) - 2\gamma]\} \end{aligned} \tag{3.45}$$

3.3 Simulation Results and Parameters Setting

In this section, we present the numerical analysis on the capacity of vesicle transmission in blood capillary channel in Frequency domain. This analysis aims to determine the molecular channel characteristics involving vesicle releasing, propagating, receiving processes. PSD of transmission signals show channel characteristics in frequency domain. We also aim to observe the changes in these characteristics according to the MC physical and biological parameters in blood capillary such as Temperature T, the viscosity η , and the numbers of vesicles in RRP N. We perform the numerical analysis using Matlab.

3.3.1 Parameters Setting

The following table shows the parameters used in the simulation:

parameters	value	unit
a	2.0×10^{-9}	m
T	310	K
τ_D	$14 \times 10{-}3$	s
m	6.4×10^{-15}	kg
k_B	1.38×10^{-23}	J/K
η	$3 \sim 4 \times 10^{-3}$	$Pa.s(kg \cdot m^{-1}s^{-1})$
k_a	0.25	
k_d	0.20	
k_{int}	0.20	
$\overline{P}_{\mathcal{H}}$	1	$pW = 1 \times 10^{-12}W$

Table 3.1: Parameters in diffusion-based blood capillary model for simulation

Viscosity varies with different temperatures, as shown in the Table 3.2:

η viscosity of blood plasma $(Pa.s)$	Temperature (K)
5.2×10^{-3}	295
4.6×10^{-3}	305
4.0×10^{-3}	310
3.0×10^{-3}	315

Table 3.2: Viscosity varies with different temperatures

3.3.2 Analysis of Simulation Results

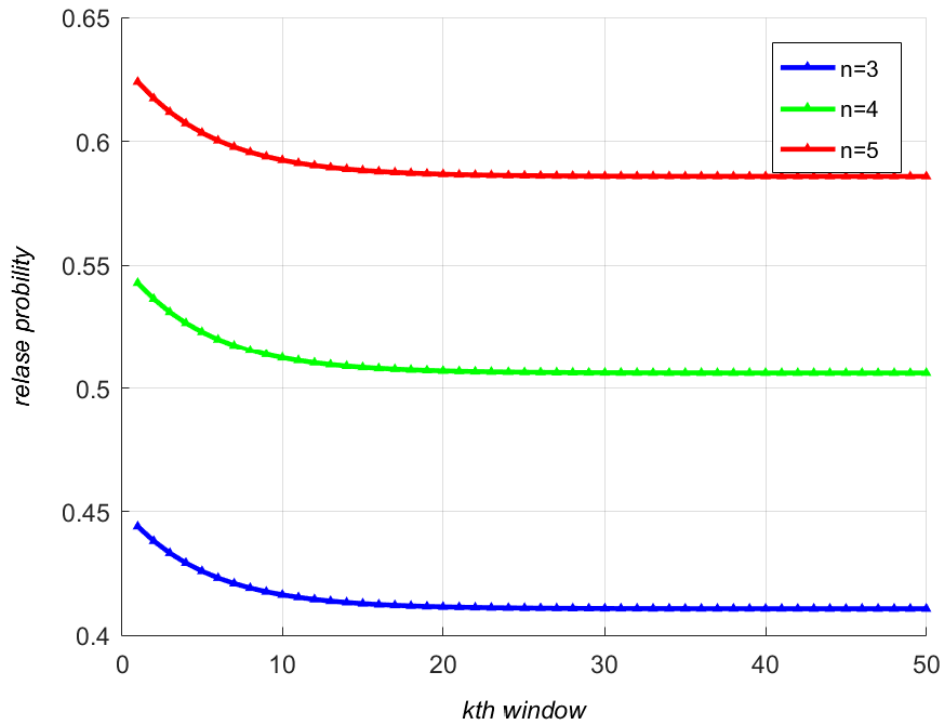

Figure 3.6: The release probability with different number of vesicles in RRP

In Figure 3.6, we can easily observe that the more vesicles in RRP, the release probability becomes larger. However, the maximum number of vesicles in

RPP is 5 [97]. The maximum average release probability is 0.5903 for that condition; there are 5 vesicles available in RRP. More important, at about 25 Kth windows, all the release probabilities are convergent to constant values. It means at that time; the refill process is finished. The number of vesicles in RRP keeps balance.

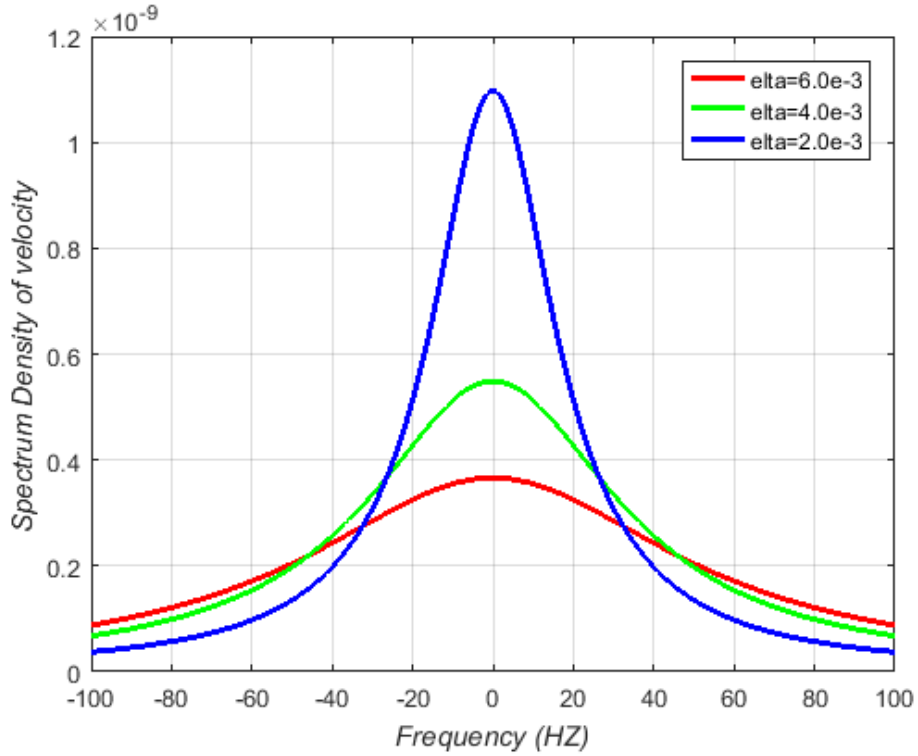

Figure 3.7: Spectral density regarding velocity $G_{vv}(f)$ varies with frequency in different viscosity coefficients η .

Figure 3.7 shows the spectral density varies with frequency in different viscosity coefficients. The spectral density of transmitted signal X, $G_{vv}(f)$, is regarded as the transfer function of the diffusion process. The stochastic force to the vesicles is completely determined by the dissipation coefficient γ and the temperature T, again a manifestation of the common origin of dissi-

pative and stochastic forces in smaller molecules collisions. The dissipation coefficient Eq.3.38 is proportional to the viscosity of blood capillary fluid. At the same temperature, as the viscosity increases, the spectral density distribution tends to concentrate at the y axis of $f = 0$ and reaches a higher peak value.

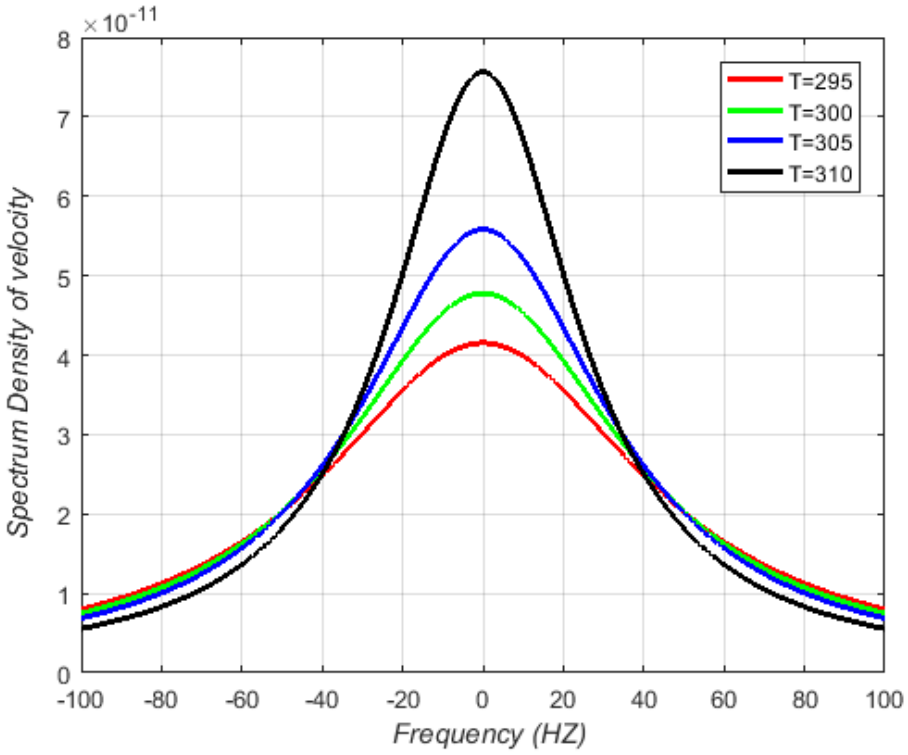

Figure 3.8: Spectral density regarding velocity $G_{vv}(f)$ varies with frequency in different temperatures T.

Figure 3.8 shows the spectral density varying with frequency at different temperatures. As we know from table 3.2, the viscosity of blood plasma decreases as the temperature increases from $295K$ to $315K$. In other words, in a higher temperature environment, particles collisions are more intense than in the lower temperature environment. At higher temperatures, spectral

density declines more quickly, as the frequency increases.

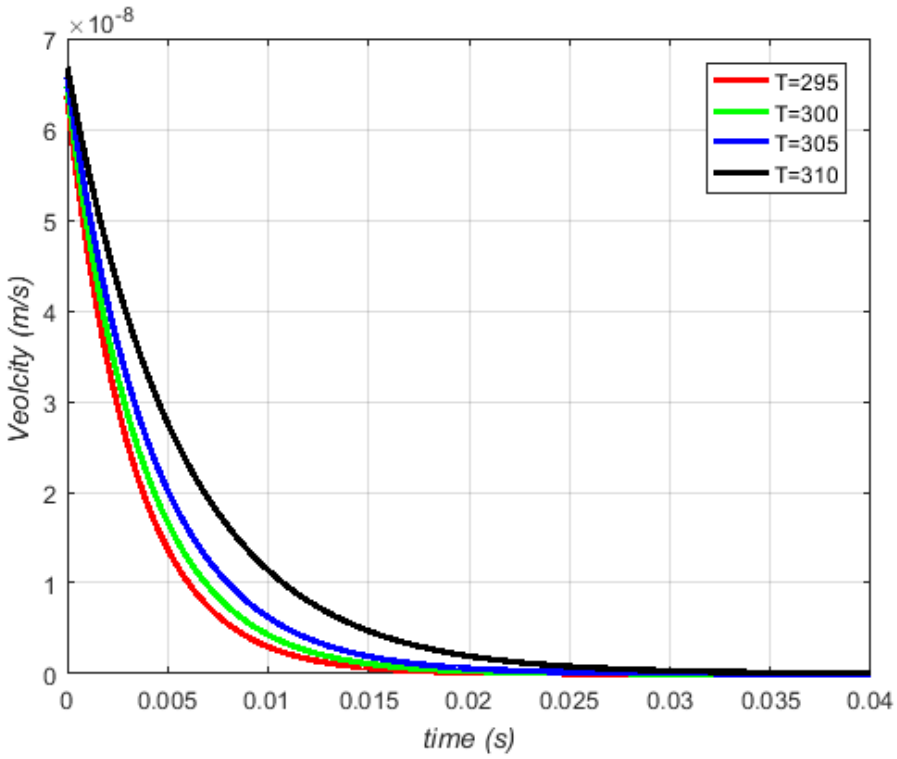

Figure 3.9: The illustration of the relationship between autocorrelation function regarding velocity and time.

Figure 3.9 illustrates the autocorrelation function regarding velocity varies with time, setting the initial velocity $v(0) = 0$. We are interested here in the dynamics of the velocity fluctuations of a particle in Langevin-based diffusion. During a long time, velocity fluctuations gradually decline and tend to zero, while the temperature T determines the rate of decline. As a consequence, in a lower temperature, the velocity declines more rapidly.

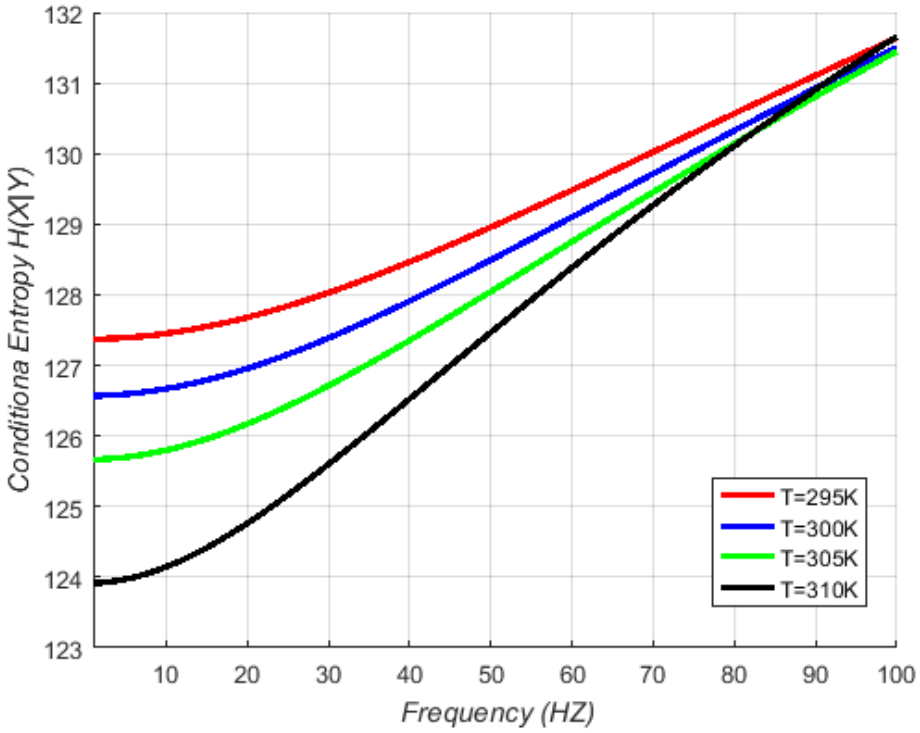

Figure 3.10: The conditional entropy $H(X|Y)$ varies with the frequency in different temperatures.

Figure 3.10 shows the conditional entropy $H(X|Y)$ varying with the frequency in different temperatures. As the frequency increases, the bandwidth of this communication system increases, and conditional entropy $H(X|Y)$ increase as well. Furthermore, the conditional entropy $H(X|Y)$ at a higher temperature, such as $T = 310K$, is lower than that at $T = 305K$. However, conditional entropy $H(X|Y)$ increases slightly more rapidly at a lower temperature, and two curves ($T = 305K$ and $T = 310K$) intersect at the point with a frequency of 80HZ.

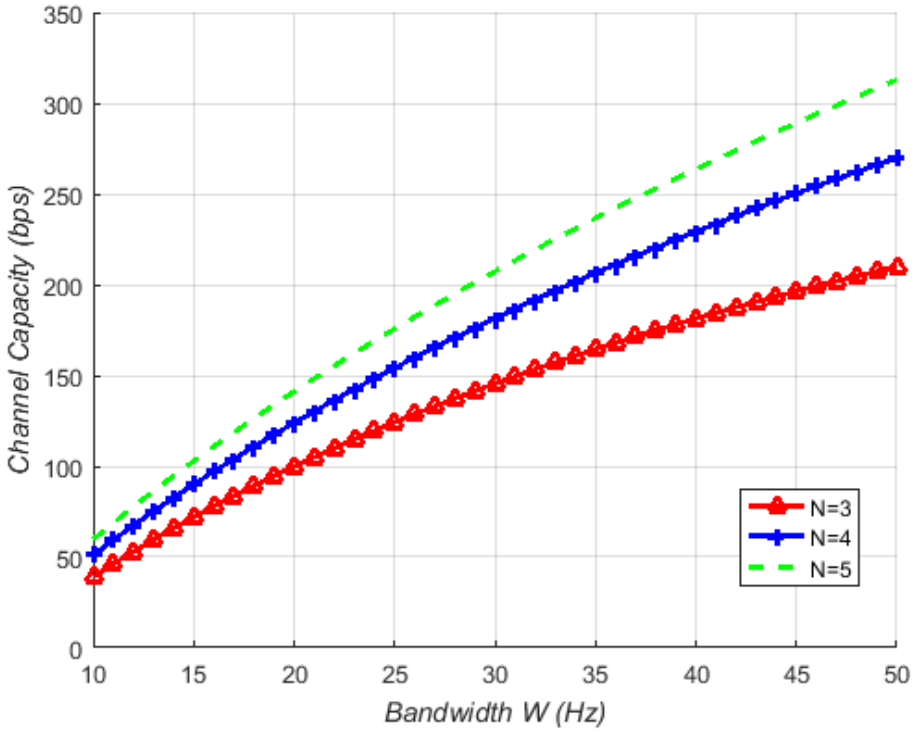

Figure 3.11: Channel capacity varies with bandwidth for different numbers of vesicles in RRP.

Figure 3.11 shows that channel capacity of blood capillary system dependent on the bandwidth W ranging from $10Hz$ to $50Hz$, and the number of vesicles N in RRP, setting the average thermodynamic power $\overline{P}_{\mathcal{H}} = 1pW$ and the temperature $T = 310K$. We can observe that the channel capacity has a positive correlation with the number of vesicles N in RRP, furthermore, the curves gradually become flat as bandwidth increases. According to Eq.3.3 the vesicle release probability is proportional to the number of vesicles in RRP, while the average release probability determines the input entropy $E(X)$. According to [95],the refill time of the vesicle pools is constant with $\tau_D = 14ms$ in the temperature of $310K$. It means at that time; the refill process is finished, and the number of vesicles in RRP keeps balance. We

must note that the up-bound limit value of bandwidth in blood capillary is determined by the transmission time. Compared with traditional communication, the frequency of molecular communication is extremely low. The main reason is the transmission time is extremely long by way of diffusion.

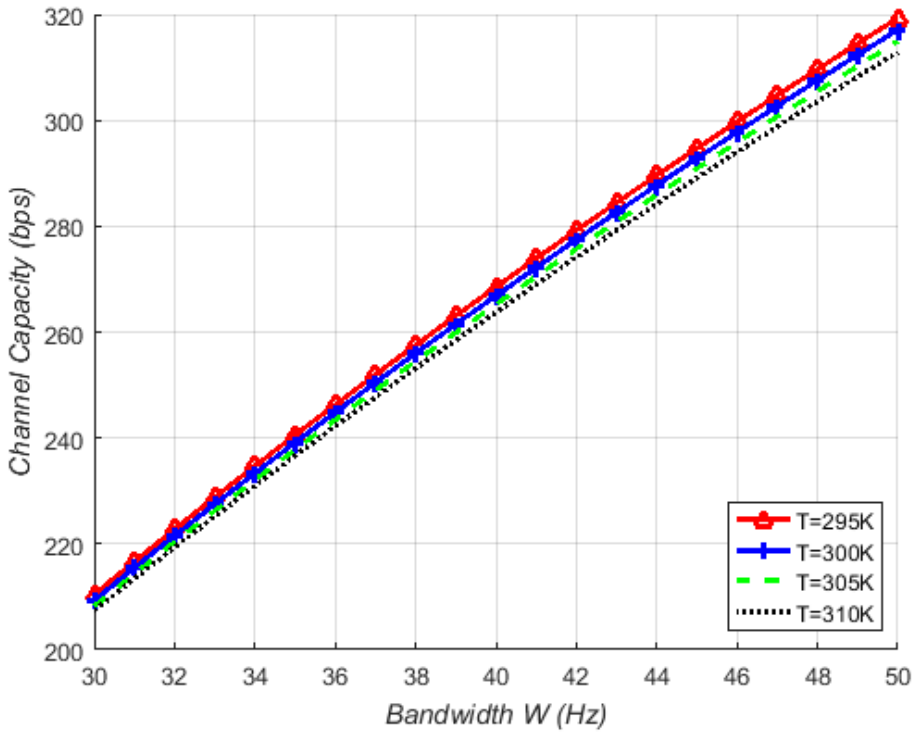

Figure 3.12: Channel capacity varies with bandwidth (Hz) in different temperatures.

Figure 3.12 shows that channel capacity dependent on the bandwidth W ranging from $30Hz$ to $50Hz$, bandwidth and the temperature T, setting the average thermodynamic power $\overline{P}_{\mathcal{H}} = 1pW$ and number of vesicles is $N = 5$ in RRP. Different curves refer to different system temperature T values, from $295K$ to $310K$. From Eq.3.41, we know that entropy of input $H(X)$ is proportional to the bandwidth W. As the bandwidth increase, entropy of input

increases and the channel capacity increases as well. Furthermore, channel capacity value is different for each temperature T value and it decreases as the temperature increases. However, the difference between different temperature T is tiny compared the varies of bandwidth, meanwhile, the difference of channel capacity C between two different temperature T increases as the bandwidth increases. Because Input entropy $H(X)$ of the channel capacity C in Eq.3.45 is greatly determined the bandwidth W. As the frequency of this communication system increases, the transmission time between the transmitter and the receiver decreases, so that we can not reach a higher bandwidth in blood capillary-based MC via diffusion.

3.4 Chapter Summary

This objective of this chapter is to provide a closed-form of channel capacity in blood capillary-based channel. Firstly, differing from the previous literature, this paper uses Langevin equation in a microscopic aspect instead of Fick's law in a macroscopic perspective to describe the diffusion of vesicles in blood capillary channel. Secondly, the closed form of channel capacity obtained here involves three processes; vesicle release, vesicle diffusion in blood capillary, and vesicle reception by ligand-receptors. Thirdly, we analyse the spectrum density regarding the velocity of vesicle in the frequency domain; then we analyse the velocity fluctuations regarding time and displacement correlation with time in the time domain. Finally, the numerical results show the relationship between channel capacity, temperature and bandwidth. From the simulation results, we can observe that pure diffusion is not suitable for a blood capillary model and figures in the frequency domain cannot show the transmission time, which is important to blood capillary-based MC thus Chapter 4 presents a diffusion with blood flow drift blood vessel model in the time domain.

Chapter 4

Channel Modelling of Blood Vessels with Blood Flow Drift in Time Domain

4.1 Biological Scenario for Blood Vessels

The biological scenario within the blood vessels consists of emission of information molecules from platelets, molecules propagation in the flow of blood vessels and receiving by endocrine cells. Soluble CD40 ligand (sCD40L) is contained in platelet granules, and thus its presence in the bloodstream is a marker of platelet activation [108]. Platelets are small anucleate cell fragments that circulate in blood playing a crucial role in managing vascular integrity and regulating hemostasis [109]. By interacting with CD40, which is found on endothelial and smooth muscle cells, sCD40L may trigger the release of inflammatory mediators [108]. The communication process from platelets and the endocrine cell plays a fundamental role during initial stages of atherogenesis [72, 73]. For this reason, the principal interest in this chapter is to establish a communication system through the blood vessel, which contributes to the understanding of the signalling process between the platelets

and the endothelium.

The components of the communication system within the blood vessels are platelets, endocrine cells and transmission information represented by cytokines. The transmitters, which are platelets, secrete and release cytokines, which are small cell signalling protein molecules, while the receivers, which are endocrine cells, are distributed in the blood vessels. These cytokines are propagated to the endocrine cells along the bloodstream with blood flow.

There are many types of cytokines, and each type has a matching kind of receptor on the cell surface. In [108, 73],the soluble CD40 ligand (sCD40L) is regarded as carriers with matching cytokines CD40 on the surface of endocrine cells. In this chapter, we still follow this specific biological phenomenon. Each endothelial cell has a number of CD40 receptors, and this number changes over time [73]. Decoding process in endothelial cells, which is known to express vascular cell adhesion molecules-1 (VCAM-1) produce the response to cytokines stimuli. The VCAM-1 is a member of the immunoglobulin superfamily and is a protein that functions as a cell adhesion molecule; that is, it facilitates binding of the cell with other cells or with other cellular material. For this reason, the number of VCAM-1 expressed on the surface of the cell is an important indicator, since it has a fundamental role in the development of atherothrombotic diseases.

Figure 4.1 illustrates the signal process from platelet to endocrine cell and mapping to relevant communication processes. This chapter lays more emphasis on the propagation process in blood vessels rather than the emission and decoding process. A generalised Langevin equation with colour-noise term models the emotion of constant blood flow drift and simultaneous diffusion. Moreover, the performance of delay and channel capacity in the simulation of this model will help to deeply understand this signalling process.

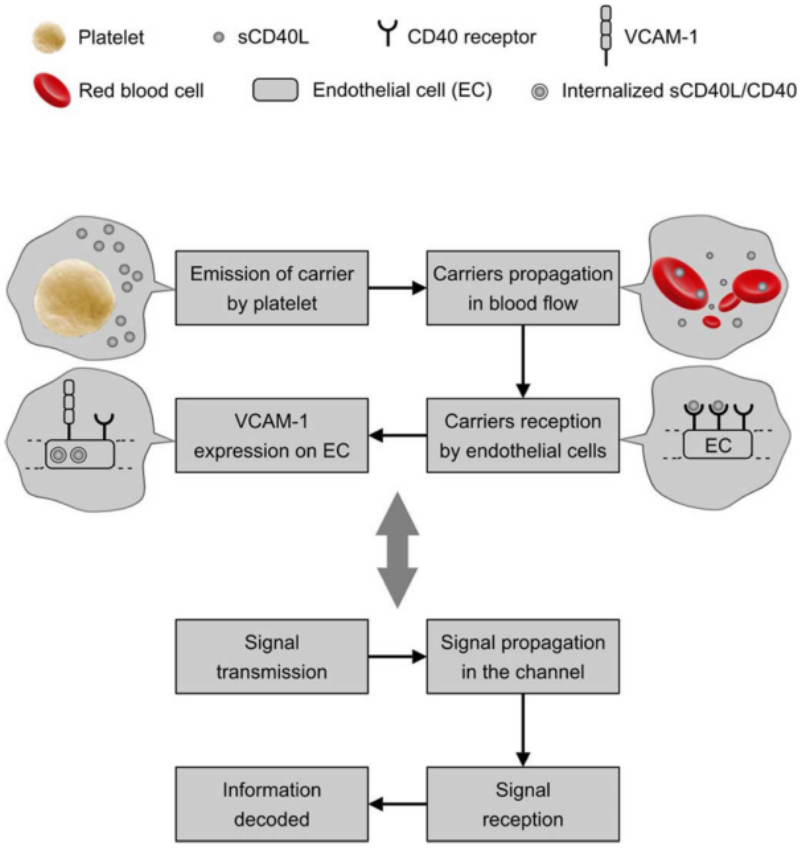

Figure 4.1: Signalling process and its relevant mapping of communication processes

4.2 Diffusion with Blood Flow Drift Model in Blood Vessels

In our analysis in the literature review, we assume that blood vessel is at a significant distance from the heart. In this assumption, we can model the bloodstream without turbulence. Consequently, the macroscopic flow properties, such as velocity and pressure in any site, can be assumed to be

constant over time and the resulting blood motion is laminar. In laminar flow (low Reynolds number), viscous forces are dominant, and the fluid motion is smooth and constant. In turbulent flow (high Reynolds number), the inertial forces dominate and tend to produce flow fluctuations. Reynolds number R_e in a tubular structure is defined as [21]:

$$R_e = \frac{\rho v r}{\eta} \tag{4.1}$$

Where ρ is the density of the fluid (kgm^{-3}), v is the velocity of the fluid (m/s), r is the radius of the vessels and η is the dynamic viscosity of the fluid ($Pa \cdot s$), or ($kg/(ms)$).

As a result of this assumption, the longitudinal shape of the vessel can be viewed as a set of concentric cylinders. The space between concentric cylinders is a lamina, and a laminar flow consists of fluid particles moving in longitudinal straight lines of each lamina [110].

The velocity profile of such laminar flow was shown to have a parabolic shape, modelled by the well-known Hagen-Poiseuille equation, derived from the Navier-Stokes equations [110, 111]:

$$vp(r) = \frac{1}{4\eta}\frac{\Delta p}{L}(R^2 - r^2) \tag{4.2}$$

where r is the distance from the longitudinal axis of the vessel, $vp(r)$ is the velocity profile with its position, R is the radius of the vessel, η is the fluid viscosity and Δp is the pressure differential along a vessel section of length L. Table 4.1 presents some known parameters for a blood vessel, used in our simulation.

We can use Eq.4.2 to compute the rate at which volume flows through the vessel. The technical term for volume flow rate is the volume flux per unit time through any cross section. It is given by the integral as below

$$V(a) = \int_0^a 2\pi r v p(r) dr \tag{4.3}$$

$$V(a) = \frac{-\pi p_x}{2\eta} \int_0^a r(a^2 - r^2) dr = \frac{-\pi \Delta p a^4}{8\eta L} \tag{4.4}$$

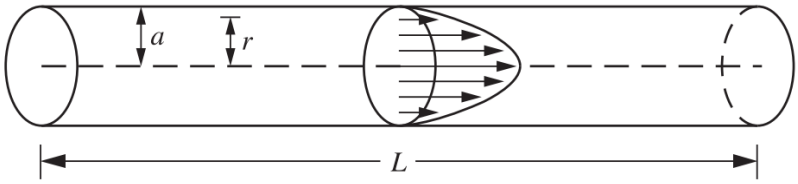

Figure 4.2: Illustration of blood flow in blood vessels

Figure 4.2 illustrates laminar flow in narrow blood vessel model. In laminar flow, the motion of the particles of the fluid is very orderly with particles close to a solid surface moving in straight lines parallel to that surface [110].

In consideration of large vessels, observations reveal that the velocity profile should be adopted by introducing a zero radial velocity gradient, as included in the Casson profile, non-Newtonian fluid [68, 112], while in straight narrow- blood behaves as a Newtonian fluid, especially in blood capillaries. This model generalises the motion model of particles in a fluid environment of the narrow and small blood vessels or blood capillaries.

The comparative sizes between the propagating molecule S_m and absolute the molecules of the fluid S_{fluid} affect the diffusion coefficient D [113]. Albert Einstein obtained the relationship between the macroscopic diffusion coefficient D and atomic properties of matter [53].For a given particle and fluid environment, D is given by

$$D = \frac{k_B T}{6\pi\eta R_a}, if S_m \gg S_{fluid}$$

$$D = \frac{k_B T}{4\pi\eta R_a}, if S_m \approx S_{fluid} \tag{4.5}$$

Where k_B is the Boltzmann's constant, T is the temperature, η is the dynamic viscosity of the fluid, and R_a is the hydraulic radius (also known as Stokes radius) of the information molecules. In the fluid of blood vessel, information molecules are Cd40 proteins, the size of which(about $2nm$) is much larger than the molecules of the blood fluid (about $0.4nm$) [73]. In this model of blood vessel the diffusion coefficient is determined as $D = \frac{k_B T}{6\pi\eta R}$.

The drag force of flow Fd is modelled by the Stokes law and can be applied to particles having a small Reynolds number, which matches the condition of laminar flow in a continuous viscous fluid;

$$Fd = 6\pi\eta avp \tag{4.6}$$

Where η is the dynamic viscosity of the fluid and vp is the relative velocity of the particle concerning the flow, given by Eq.4.2.

If we ignore the blood flow, that means the drag force of blood flow $Fd = 0$. This is exactly the same model as that used in Chapter 3 and particles are undergoing Brownian motion or free diffusion. We rewrite the basic one-dimensional Langevin equation Eq.3.8 for Brownian motion below:

$$m\frac{d^2x}{dt^2} + \gamma\frac{dx}{dt} = f(t) \tag{4.7}$$

In the Langevin equation here, x is the position of the particle, m denotes the mass of the particle ,and the friction or dissipation coefficient γ is given by Stokes Law $\gamma = 6\pi\eta a$. The diffusion force acting on the particle is written as a sum of a viscous force proportional to the particle's velocity. The force of diffusion $f(t)$ has a Gaussian probability distribution with correlation function as shown below:

$$\langle f_i(t_1) f_j(t_2) \rangle = 2\gamma k_B T \delta_{i,j}(t_1 - t_2) = 12\pi\eta a k_B T \delta_{i,j}(t_1 - t_2) \tag{4.8}$$

$$\langle f(t)\rangle = 0 \tag{4.9}$$

where k_B is Boltzmann's constant and T is the temperature, δ function means the correlations of the force that over a period of time t.

The force $f(t)$ determines the diffusion process, the noise term is white Gaussian noise. The average $\langle f(t)\rangle$ is an average with respect to the distribution of realisations of stochastic variable $f(t)$.

A generalised Langevin equation is used to deal with drift and diffusion. The generalised Langevin equation in one stochastic variable ξ has the form [82]:

$$\frac{\partial \xi(t)}{\partial t} = h[\xi(t), t] + g[\xi(t), t]F(t) \tag{4.10}$$

Stochastic force consists of drag force of blood flow drift and diffusion. The drag force of blood flow is expressed in Eq.4.6 and stochastic variable force in blood vessels model is rewritten as shown below:

$$\frac{\partial f_d(t)}{\partial t} = Fd(t) + f(t) = \gamma vp + 2\gamma k_B T \delta_{ij}(t_1 - t_2) \tag{4.11}$$

A generalised Langevin equation for the blood vessel model is rewritten as shown below:

$$m\frac{d^2x}{dt^2} + \gamma\frac{dx}{dt} = \gamma vp + 2\gamma k_B T \delta_{ij}(t_1 - t_2) \tag{4.12}$$

4.3 Stochastic Dynamical Theory of Coloured Noise

The stochastic dynamics leading to the Maxwell-Boltzmann distribution could be clearly explained by the variable Langevin equations [114]. Due to Brownian motion, a particle moves in a potential field, under the influence of a frictional force and in a white noise term [82]. The correlation strength of the noise, usually referred to as the diffusion coefficient, is a constant, associated with a friction coefficient γ by the fluctuation-dissipation theorem.

In this thesis, it is shown that this straightforward and elegant landscape would reappear when we are accounting for the microscopic dynamic origins to give rise to types of power-law distributions. We introduce the additive noise with inhomogeneous correlation strength to the Langevin equation. An energy-dependent relationship of diffusion to friction is determined by solving its corresponding stationary Fokker-Planck equation. Hence we derive a generalised fluctuation-dissipation theorem, one condition under which we could understand the microscopic dynamic origins giving rise to a type of power-law distributions.

The most general Langevin equation in stochastic variable ξ has the form as in Eq.4.10.

$$\dot{\xi}(t) = h[\xi(t), t] + g[\xi(t), t]F(t) \tag{4.10}$$

Comparing Eq.4.10 and Eq.4.11, we can find that $g[\xi(t), t] = 1$. If $g[\xi(t), t]$ is constant, and Eq.4.10 is called a Langevin equation with an additive noise term, while if $g[\xi(t), t]$ depends on ξ, Eq.4.10 is called a Langevin equation with a multiplicative noise term. We rewrite the langevin equation in the integral form:

$$\xi(t + \Delta t) - y = \int_{t}^{t+\Delta t} \{h[\xi(t'), t'] + g[\xi(t'), t']F(t')\}dt' \tag{4.13}$$

Now, expanding h and g as a Taylor series at the site $\xi = y$ and noting that the increment during the interval (t, t') is $\xi(t') - y$, we obtain:

$$h[\xi(t'), t'] = h(y, t') + [\xi(t') - y]\frac{\partial}{\partial y}h(y, t') + \cdots \tag{4.14}$$

$$g[\xi(t'), t'] = g(y, t') + [\xi(t') - y]\frac{\partial}{\partial y}g(y, t') + \cdots \tag{4.15}$$

According to [82], it proves that the Taylor series of $h[\xi(t'), t']$ and $g[\xi(t'), t']$ are truncated at $n = 2$. In this thesis, we follow this deduction, thus the

expression of $h[\xi(t'),t']$ and $g[\xi(t'),t']$ can be determined.

The relevant Fokker-Planck equation for the one-dimensional Langevin equation Eq.4.12 is shown as below:

$$\frac{\partial W}{\partial t} = -\frac{\partial [D^{(1)}W]}{\partial x} + \frac{\partial^2 [D^{(2)}W]}{\partial x^2} \tag{4.16}$$

$D^{(1)}$ is called the drift coefficient and $D^{(2)}$ the diffusion coefficient, which are calculated from the Langevin equation.

Referring to [82], $D^{(1)}$ is the drift coefficient and $D^{(2)}$ the diffusion coefficient, which are obtained by the following expression,

$$D^{(1)}(x,t) = \lim_{\Delta t \to 0} \frac{\overline{\xi(t+\Delta t) - y}}{\Delta t} = h + Dg\frac{\partial g}{\partial x} = v\gamma \tag{4.17}$$

similar for the diffusion coefficient $D^{(2)}$, we have

$$\overline{[\xi(t+\Delta t) - y]^2} = 2D \int_t^{t+\Delta t} \int_t^{t+\Delta t} g(\xi,t')g(\xi,t'')\delta(t'-t'')dt'dt'' \tag{4.18}$$

$$D^{(2)}(x,t) = \lim_{\Delta t \to 0} \overline{[\xi(t+\Delta t) - y]^2/(2\Delta t)} = Dg^2(x,t) = D \tag{4.19}$$

where $h(\xi,t)$ is the deterministic drift. Physically, the additive noise ($g(\xi,t)$ constant) may represent the heat bath acting on the particle of the system, and the multiplicative noise term, for variable $g(\xi,t)$, may represent a fluctuating barrier.

For $g = \sqrt{D}$ and $h(\xi,t) = 0$, Eq.4.12 describes the Wiener process and the corresponding probability distribution is described by a Gaussian function. In the case of $g(,t)$, some specific functions have been employed to study, for instance, in turbulent flows $g(x,t) \sim |x|^a t^b$ [115]. In our blood vessels model we consider a laminar flow model with constant $g(x,t)$.

So we rewrite the corresponding Fokker-Planck equation for its additive

noise term Langevin equation Eq.4.13 as below:

$$\frac{\partial W(x,t)}{\partial t} = -vp\gamma \frac{\partial W(x,t)}{\partial x} + D\frac{\partial^2 W(x,t)}{\partial x^2} \tag{4.20}$$

The solution of the corresponding Fokker-Planck equation is given by [82], and we have a PDF solution on the concentration of particles:

$$W(x,t) = \frac{C}{\sqrt{4\pi Dt}} e^{-\frac{(x-vpt)^2}{4Dt}} \tag{4.21}$$

This solution is based on these assumptions and boundary conditions for this communication system:

1) Initial Impulse, $W(x,0) = W_0 = C$, C is the contraction of released molecules at the transmitter at $t = 0$, and a pulse of concentration W_0 is emitted at the transmitter which is located at x distance away from the receiver;

2) Infinite Source : this condition states that an infinite source of molecules provide a continuous and finite flux of molecules, such that $W(0,t) = W_0 = C$;

3) No remission in the reception areas, the reception probability is based on ligand-recaptor model and non-received particles is not remitted to the channel;

4) Long-Term Capture and its boundary conditions, $W(x,\infty) = pW(x,t)$: if a molecule is captured, it cannot be remitted. Therefore, over a long time $(t{+}\infty)$, the receiver captures molecules with a probability p of ligand-receptor to an equilibrium state;

5) Diffusion only in x axis along with flow. So, we do not consider two-dimensional;

4.4 Channel Performance of Blood Vessel System

4.4.1 Reception Process

The reception process at the receiver side involves the capturing of molecules in the blood vessels by several ligand-based receptors sCD40L. However, this sCD40L ligand-receptor model is quite different from the one described in Chapter 3.1.3. Since no vesicles are considered in this model, molecules CD40 are received directly by sCD40L. Moreover, a vesicle internalisation process via endocytosis does not exist. We have simplified the model with respect to the ligand-receptor, thus, only binding and release rate are considered. When the sender emits one kind of molecule instantaneously, the receiver must receive the molecule with binding the molecule to the ligand on their surface. Generally, there are sufficient chemical receptors on the surface used to receive information coming from the diffusion process. The capture and release of molecules is modelled according to the chemical theory of the ligand-receptor binding process [116, 58]. The binding reaction occurs with a probability k_1 when the receptor was not previously bound to a molecule. The release reaction occurs with a probability constant k_2 when there is a complex formed by a molecule and the chemical receptor. Finally, the receiver decodes the message from the molecule concentration rate.

We consider a communication between only one transmitter and one receiver. When the platelets emit molecules into the blood stream and propagation to the receiver, the probability of molecules concentration at one site is expressed by Eq.4.22. When we consider the channel memory, the Inter Symbol Interference (ISI) could exist, i.e. the overlap in molecule concentration between the signal transmitted in the current time slot and the remaining signals transmitted in previous time slots. The probability that a molecule transmitted in slot $i \in 1, 2, \cdots, n$ arrives in slot m can be expressed

as [63]:

$$q_v = \int_{vT}^{(v+1)T} W(L,t) \int_t^{\infty} m_n(u) du dt \tag{4.22}$$

here,$v = n - i$. T is the length of a time slot. γ is the pdf of the molecule life expectancy (or the stability of the molecule in the environment) and is given as an exponential distribution function: $m_n(u) = \gamma e^{-\gamma u}$ with the mean of $1/\gamma$.

Assume that the distance between the transmitter and receiver is r, then the receiver binding rate is k_1 and release rate is k_{-1}, using the ligand-receptors binding model given in [116, 58], which can be given below:

$$B = \frac{k_1 N A}{k_{-1}} \tag{4.23}$$

Where k_1 and k_{-1} are the constant binding and release rate, respectively. k_{-1} is a constant which is affected by physical properties of the receptors on receiver and it does not change as long as the physical properties of the receptors on receiver do not change. Concentration of bond molecules of the receptors is denoted by B. A is the concentration of the molecules sent by the transmitter and N is the concentration of the ligand-based receptors on the receiver's surface.

We assume that k_1 is a constant which is only affected by the several environmental factors such as molecular diffusion coefficients, temperature, and distance between transmitter and receiver. In the literature, there are several realistic models for $k1$ that are experimentally tested for certain bio-chemicals. The expression of k_1 is given by [85]:

$$k_1 = \frac{4\pi D r_0 \beta}{1 - (1-\beta)\frac{r_0}{r_\infty}} \tag{4.24}$$

where r_0 is the radius of the receiver and r_∞ is the radius of the whole spherical shaped environment. β is the ratio of the radius of one molecule to the distance between transmitter and receiver, i.e. $\beta = r_0/r$. The coefficient

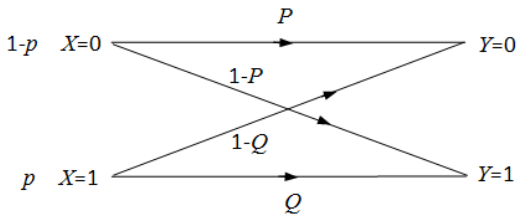

Figure 4.3: OOK mechanism illustration

of the A i.e. $\frac{k_1 N}{k_{-1}}$ could be treated as the probability of successfully reception of the receiver. Thus, considering the condition with ligand-based receptors, the probability that a molecule transmitted in slot i and arrives in slot n can be modified as:

$$Q_v = \frac{k_1 N}{k_{-1}} q_v = \frac{k_1 N}{k_{-1}} \int_{vT}^{(v+1)T} g_d(t) \int_t^{\infty} m_n(u) du dt \tag{4.25}$$

4.4.2 Channel Capacity of System

In this model, we assume that the transmitter adopts On-Off Keying OOK to transmit 1 or 0 signal. The basic binary communication model is shown in Figure 4.3. When the transmitter send 0 or 1, respectively, the probability of the receiver detecting correctly are P and Q. the signal of 1 or 0 is transmitted in different time slots. Here, we assume the transmitter and receiver are perfect synchronised in terms of time. We thus describe the probabilities of successful bit transmission as follows:

$$P[Y_n = 0 | X_n = 0] = P_n \tag{4.26}$$

$$P[Y_n = 1 | X_n = 1] = Q_n \tag{4.27}$$

Respectively, the false probability is $1 - P$ and $1 - Q$. For $n = 1$, $Q1 = q0$ and $P1 = 1$, i.e., it means communicating a 0 is always successful. For $n > 2$,

considering a recurrence relation for Q_n and P_n, we have:

$$Q_n = 1 - (1 - q_0) \prod_{i=1}^{n-1} (1 - pq_i) \tag{4.28}$$

$$P_n = \prod_{i=1}^{n-1} (1 - pq_i) \tag{4.29}$$

The information capacity of a communication system is expressed by the general formula from Shannon [105]. For a single-access channel, the general formula defines the information capacity as the maximum difference between the entropy $H(Y)$ of the signal x in input to the channel and the equivocation $H\,(Y|X)$:

$$C = \max\{I(X;Y)\} = \max\{H(Y) - H\,(Y|X)\} \tag{4.30}$$

For a discrete binary system, the single-access channel capacity equals the maximum mutual information, and can be obtained from slot 1 to n which is then expressed as:

$$C_{\mathrm{s}} = \frac{1}{T} \sum_{i=1}^{n} \frac{\max I(X_i;Y_i)}{n} \qquad bps \tag{4.31}$$

when n approaches ∞. Eq.4.31 represents the channel capacity. The critical problem is to find the $I(X;Y)$. For a discrete system, Shannon has given out the entropy in the case of two possibilities with probabilities ξ and $1-\xi$, namely

$$H = -\xi \log \xi - (1 - \xi) \log(1 - \xi) \tag{4.32}$$

Following Eq.4.30 and Eq.4.32, the mutual information in time slot n is represented as:

$$I(X_n;Y_n) = H(Y_n) - H(Y_n|X_n)$$

$$= \chi((1-p)P_n + p(1-Q_n))$$
$$- \{p\chi(Q_n) + (1-p)\chi(P_n)\} \tag{4.33}$$

Where $p = P[X_n = 1]$ and $\chi(\xi) = -\xi\log\xi - (1-\xi)\log(1-\xi)$ are assumed. The proof of Eq.4.17 is shown in [58].

For $n = 1$, there should be that $Q1 = q0$ and $P1 = 1$, substituting to Eq.4.17, we have:

$$I(X_1;Y_1) = \chi((1-p)P_1 + p(1-Q_1))$$
$$-\{p\chi(Q_1) + (1-p)\chi(P_1)$$
$$= \chi(1-pq_0) - p\chi(q_0)$$
$$= \log_2 \frac{(1-p)^{p(1-q_0)}}{p^{pq_0(1-pq_0)^{1-pq_0}}} \tag{4.34}$$

In the same way, for $n > 2$, substituting Eq.4.28 and Eq.4.29 to Eq.4.33, we have

$$I(X_n;Y_n) =$$
$$\chi((1-p)\prod_{i=1}^{n-1}(1-pq_i) + p(1-(1-(1-q_0)\prod_{i=1}^{n-1}(1-pq_i))))$$
$$-\{p\chi(1-(1-q_0)\prod_{i=1}^{n-1}(1-pq_i)) + (1-p)\chi(\prod_{i=1}^{n-1}(1-pq_i)) \tag{4.35}$$

Substituting Eq.4.25 to Eq.4.35, from $\frac{dI(X_n;Y_n)}{dp}\,|_{p=p_{\max}} = 0$, we can determine the value of p_{max}. The overall channel capacity of a single-access channel is finally derived as

$$C_s = \max_p \frac{1}{T}\sum_{i=1}^{n}\frac{I(X_i;Y_i)}{n} \qquad bps \tag{4.36}$$

By applying Eq.4.36, we can finally achieve the overall single-access channel capacity.

4.5 Simulation Results

In this section, we present the numerical analysis on the capacity of blood vessels with blood drift channel. This analysis aims to determine the molecular channel characteristics in the environment with both components. We also aim to observe the changes in these characteristics according to the M-C physical and biological parameters such as pressure differential Δp, blood flow velocity v, the priori probability p, diffusion coefficient D and the Length of blood vessels L. We perform the numerical analysis using Matlab.

4.5.1 Parameter Setting

Table 4.1: Symbol meaning and parameters of blood vessels with flow drift model

Parameters	Symbol	value
Diffusion coefficient	D	$10^{-5} - 3 \times 10^{-5} m^2/s$
Pressure differential [34]	Δp	$60 - 120 mmHg, mmHg = 133.3 N \cdot m^{-2}$
Viscosity	η	$5.3 \times 10^{-3} kg/(ms)$
Boltzmann constant	k_B	$1.38 \times 10^{-23} J \cdot K^{-1}$
Best sample time	t_{max}	
Length of vessel	L	$0.1 - 0.2m$
Radius of blood vessel	R	5×10^{-5}
Temperature	T	310K
Constant binding rate [116]	k_1	0.01
Constant release rate [116]	k_{-1}	0.008
Flow veolcity	v	$0.001 - 0.007 m \cdot s^{-1}$
Channel capacity	C	

4.5.2 Analysis of Simulation Results

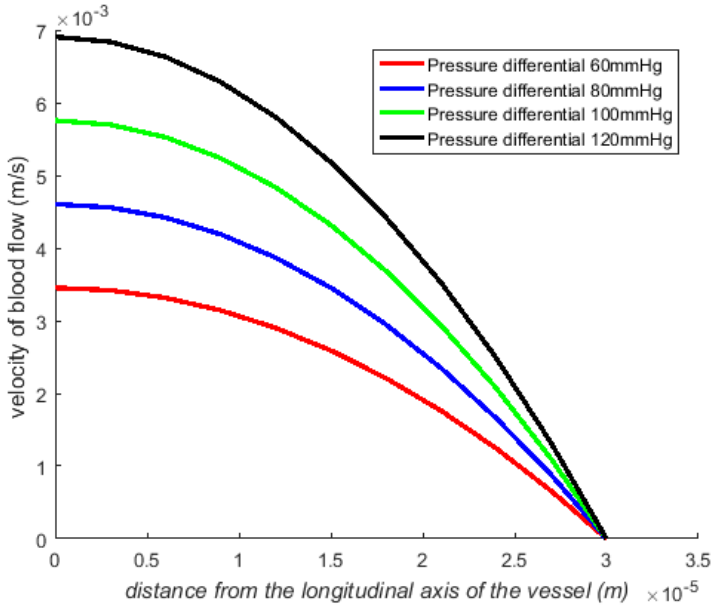

Figure 4.4: Velocity of blood flow in various pressure differential

Figure 4.4 illustrates the relationship of velocity of flow between the position in vessels and the blood pressure differential $\triangle p$. According to [34], the pressure differential of blood is divided into two types: Systolic and Diastolic. Systolic pressure measures the amount of pressure that blood exerts on arteries and vessels while the heart is beating. Systolic pressure relates to the maximum pressure exerted on the arteries ($90 \sim 140 mmHg$ for adults, average $100 mmHg$ for children from 6 to 9 years, $mmHg = 133 kg \cdot m^{-1} \cdot s^{-2}$). Diastolic pressure is the pressure that is exerted on the walls of the arteries around the body in between heartbeats when the heart is fully relaxed. Diastolic pressure represents the minimum pressure in the arteries ($60 \sim 90 mmHg$ for adults, average $65 mmHg$ for children from 6 to 9 years). In this simulation, we use the systolic pressure. As the pressure differential along the same distance of blood vessels increases, the velocity of blood flow increases as well

proportionally.

In the same condition of blood pressure differential, the velocity is higher when it is closer to the central axis of blood vessels; while at the central axis, the velocity has the maximum value. However, the velocity is extremely slow at the site which is close to the blood vessel's wall. Thus the molecules at that site will adhere to the endothelial cells.

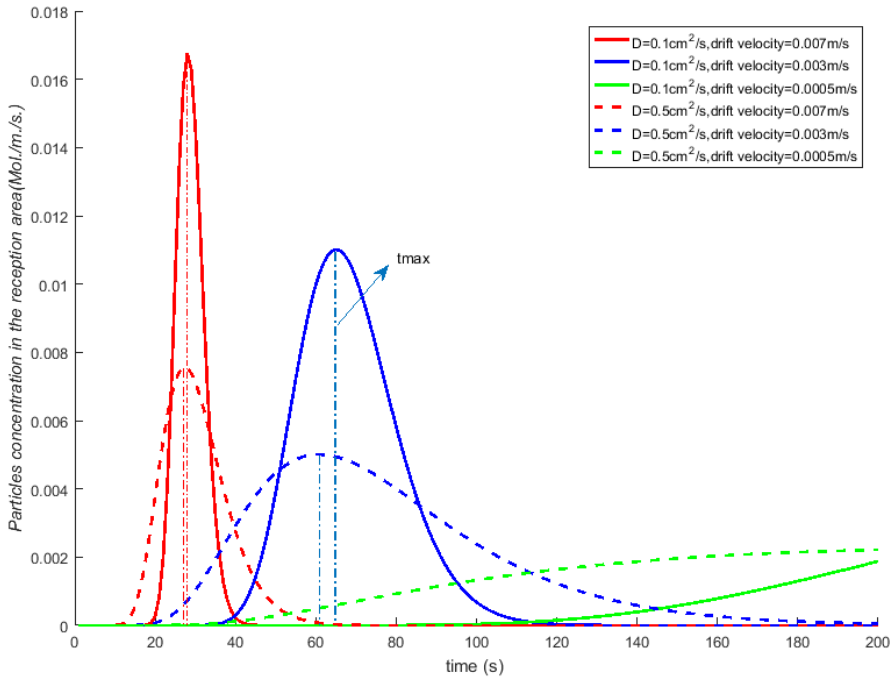

Figure 4.5: Concentration of particles in reception area

Figure 4.5 presents that the concentration of particles in the reception area varies with flow velocity v and diffusion coefficient D. With higher flow velocity, particles are propagated to the reception area in a shorter period of time. For smaller flow velocity v, with the same diffusion coefficient D, the peak becomes broader, and the curve is shifted to longer time apparently. For small diffusion coefficient D, with the same flow velocity v, the peak becomes

narrower and higher, and the curve is shifted to shorter time slightly.

The expected transmission delay is $50s$, $T = 2t_{\max}$ and $t_{\max} = 25s$, when flow velocity is $0.007m/s$ and the diffusion coefficient D is set to $0.1cm^2/s$. While in the same diffusion coefficient, the expected transmission delay is about $T = 2t_{\max} = 130s$ with the decreased flow velocity $0.003m/s$. In the same condition of flow velocity, the particle concentration in the reception area is higher, in an inverted relationship, when the diffusion coefficient of the blood vessels environment declines. Considering the two components: blood flow and diffusion motion; With the higher flow velocity, it has a significantly shorter transmission delay, however, the impact on diffusion motion in an inverted relationship.

We have to indicate that the transmission symbol is the Non-symmetric curve. As different from additive white Gaussian noise (AWGN) channel in traditional telecommunication, where the transmission symbol matches the symmetric Gaussian distribution, this Probability density function (PDF) of transmission symbol can be classified to generalised inverse Gaussian(GIG) distribution [117]. Time for the maximum concentration, $t_{\max}$, is obtained by solving the following operation for t:

$$\frac{\partial W(\mathrm{L},\mathrm{t})}{\partial t} = \frac{\partial(\frac{C}{\sqrt{4\pi Dt}}e^{-\frac{(L-vpt)^2}{4Dt}})}{\partial t} = 0 \tag{4.37}$$

As it shown in Figure 4.5, setting the expected transmission delay, regarded as time duration for one symbol, $T = 2t_{\max}$, will cause inter-symbol-interference (ISI). The impact of ISI will be discussed in detail in Chapter 5.

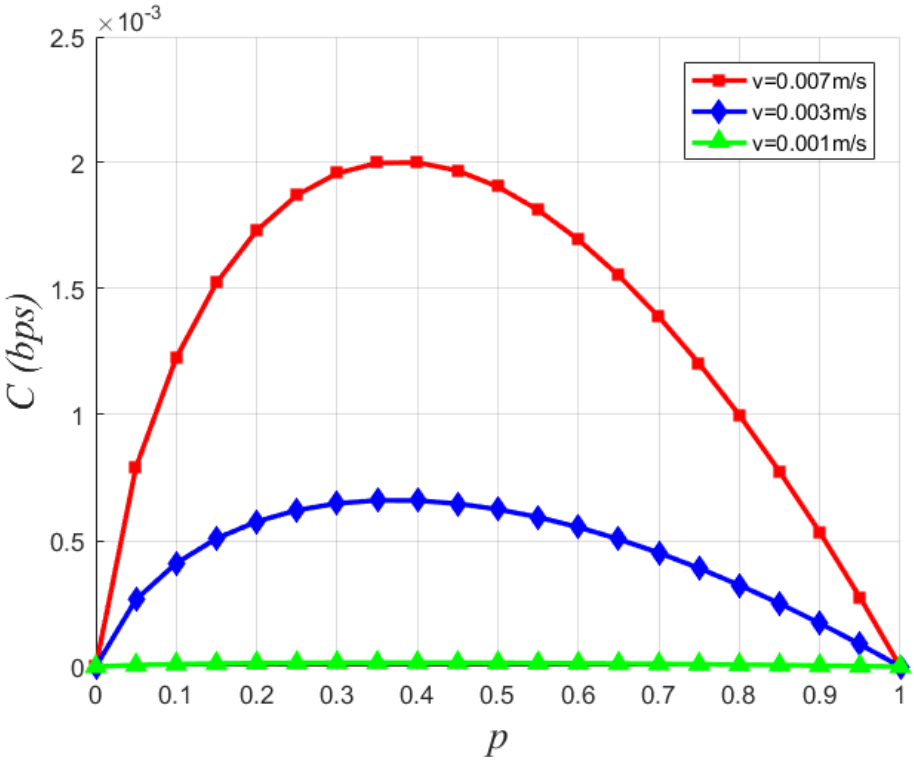

Figure 4.6: Channel capacity C varies with priori probability p for different blood flow velocity v, setting $L = 0.2m$, diffusion coefficient $D = 3e - 5$.

Figure 4.6 illustrates that the channel capacity varies with different blood flow velocity over a time period of $100s$. The channel capacity increases as the velocity increases. In the conditions that velocity largely reduced to $0.001m/s$, the channel capacity almost decreases to 0, as almost no particles are transmitted to the reception area and can be captured over a time period of 100s. In traditional communication, Shannon's theory [105] indicates that the channel capacity is the maximum with prior probability $P = 0.5$, while in the diffusion with flow channel model, capacity reaches the maximum when prior probability $p = 0.4$. In [58], it got the similar result and pointed that C does not always keep the maximum when prior probability $p = 0.5$, the part

of curve is lower than that of $p = 0.4$. The reason is that as the PDF curve, shown in Figure 4.6, is non-symmetric. Thus, channel capacity reaches the maximum when prior probability $p < 0.5$.

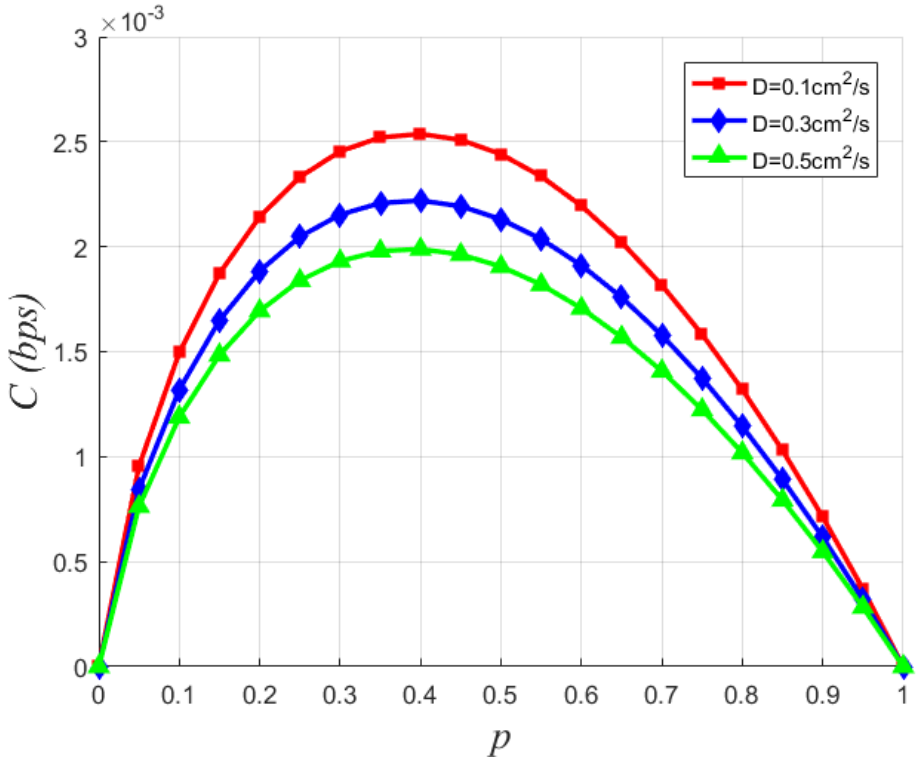

Figure 4.7: Channel capacity C varies with priori probability p for different diffusion coefficients D, setting flow velocity $v = 0.003m/s$, $L = 0.2m$.

Figure 4.7 shows the channel capacity varies with different diffusion coefficient values D in a time period of $100s$. The channel capacity increases as the diffusion coefficient D declines. Moreover, compared with the dominating flow velocity in the propagation process, diffusion coefficient has minor impact than that of flow velocity. Similarly to Figure 4.6, where capacity reaches the maximum when prior probability $p = 0.4$.

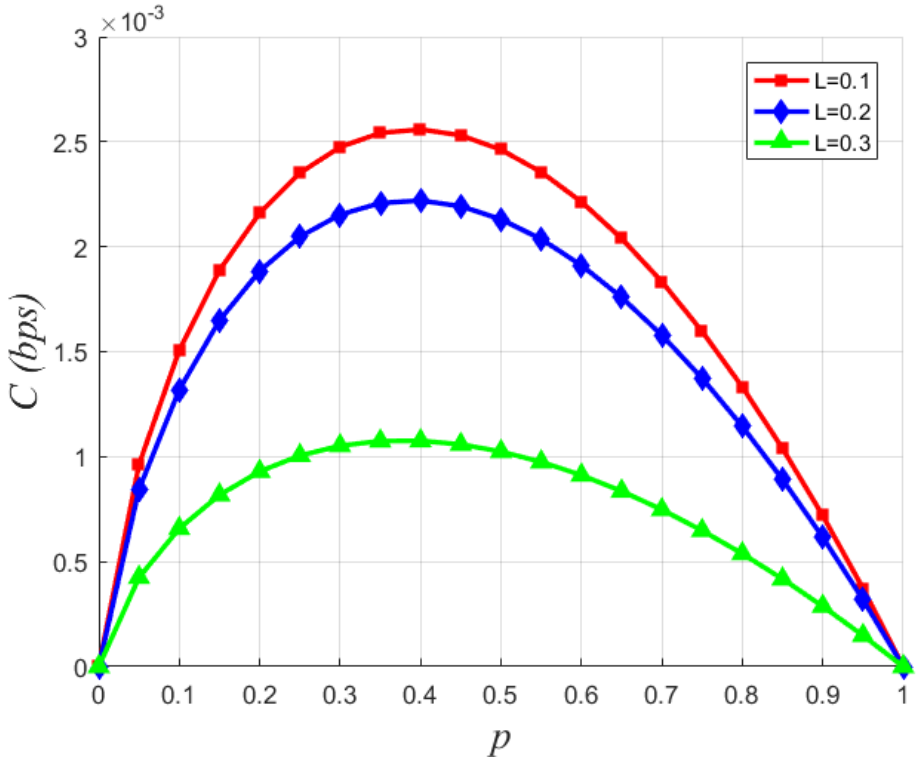

Figure 4.8: Channel capacity C varies with priori probability p for different length of blood vessels L, setting flow velocity $v = 0.003m/s$,diffusion coefficient $D = 3e - 5$.

In Figure 4.8, it shows that the channel capacity varies with the length of blood vessels in a time period of 100s. The channel capacity declines as the transmission length along blood vessel L increases, when other conditions are the same. In the same emitting model, it is clear that C decreases as L increases, i.e. closer to the transmitter, larger the capacity is. As L represents the distance between transmitter and receiver, the increase of L means that the distance increases between the transmitter and receiver resulting in the capacity decreasing. It predicts that, for good channel capacity performance, the length of blood vessels should not be longer than 0.3m.

4.6 Chapter Summary

This chapter involves consideration of two major components of the model: blood flow and the particles diffusion with blood flow drift. Based on these issues, we investigated the capacity of single input and single output (SISO) blood vessels MC channel. The ultimate objective of this chapter is to study the performance of channel capacity in these scenarios. Numerical results revealed that the capacity of this channel is related to some physical parameters of the blood vessels, the length of blood vessels L, the diffusion coefficient D and pressure differential along the vessels $\triangle p$. With this model of blood vessels, we can have a deeper insight towards mechanisms of blood vessels. This chapter provides a prediction for a significant application for future research of targeted delivery in blood vessels. we will develop my future research to blood capillaries, the smallest vessels, with multiple levels of bifurcation in Chapter 5. In the scenario of multiple receptors in branches of blood capillaries, we will establish a system of single input and multiple outputs(SIMO) channel for blood capillaries .

Chapter 5

SIMO System for Bifurcation of blood capillaries

5.1 Introduction and Motivation

Blood capillaries or blood vessels can be applied to long-range MC [21]. Moreover, blood capillaries, extensively distributed in the human body and mutually connected with tissues, are potentially applied to MC-based nano-networks. Nowhere is this truer than with applications of blood capillary-based MC to modern medicine, ranging from more reliable diagnostic techniques to improved drug delivery systems [118]. It is the intention of our work to investigate the application of this specific biological phenomenon to information communication. This chapter follows my previous research, modelling the transmission process in the blood vessels as the laminar blood flow and diffusion, then focus mainly on the Y-shaped bifurcation of blood capillary branches system, which forms multiple outputs in the communication scenario. The communication scenario in this chapter is SIMO, with the single input and multiple outputs. Firstly, we need to find out how blood capillaries system applies to SIMO communication, based on which its biological scenarios mapping to the communication procedure is investigated.

Secondly, based on the research in Chapter 4, the modelling of blood vessels considers both laminar flow and diffusion. Thirdly, multiple outputs are formed with multiple receivers in hierarchy Y-shaped branches of the blood capillary system. Finally, we can analyse the channel capacity of a SIMO blood capillary system by employing information theory.

From a biological point of view, the blood capillary system forms part of the vascular system. The vascular system is the collection of all arteries, veins, and capillaries that permit the flow of blood from the heart, around the body, and back to the heart again. Blood capillaries are the narrow vessels between arteries and veins which form a network that distributes oxygen-rich blood to all cells in the body, contributing to the blood vascular system. Blood flows from the heart through arteries, which branch and narrow into arterioles, and then branch further into capillaries. The capillaries then join and widen to become venules, which in turn widen and converge to become veins, which then return blood back to the heart through the great veins [9]. Blood flows through the circulatory system as a result of being pumped out by the heart. Blood flows out of the heart through the arteries with saturated oxygen.

The arteries break down into smaller and smaller branches to bring oxygen and other nutrients to the cells of the body's tissues and organs. As blood moves through the capillaries, the oxygen and other nutrients move out into the cells, and waste matter from the cells moves into the capillaries. As the blood leaves the capillaries, it moves through the veins, which become larger and larger to carry the blood back to the heart. A combination of fluid flow and diffusion brings every cell in a healthy body within reach of the nutrients and gases it needs. The combined length of all this plumbing is rather large: Indeed, in 1967 the mathematical biologist Robert Rosen [119] claimed that the total length of the vascular system in large mammals is of the order of 50,000 miles. Therefore, based on this proposal, the communication range of the blood capillary system is classified as long-range communication.

The basic purpose of this model is to describe the capillaries branches of a SIMO system in terms of understanding the biological nature of blood capillaries. To accomplish this, in the first step, we established modelling of transmission with diffusion along the blood flow in blood capillaries or normal vessels. This part of modelling works was e well-established in Chapter 3 and Chapter 4, which were published [120, 121]. We adopt diffusion with the blood flow model to do extension work. In the second step, we establish modelling Y-shaped capillaries bifurcation. In 1997, Kurz and Haymo [122] discussed the Wilhelm Roux's thesis of relationships among the angles and radius of bifurcating blood vessels, showing how they arise from some simple principles of optimality. Our objectives here are to rederive and further research Roux's results, to establish a mathematical model for blood capillary bifurcation. We present a sequence of increasingly faithful models of blood-vessel branching. Our modelling is also based on some other study on blood vessels bifurcation [123, 124, 125], referring to numerical results by Jafari [126], and in somewhat more details of modelling by [127].

In [123], it proposes a novel method to detect and classify the vascular bifurcation, branch and crossover points, and landmarks, based on vessel geometrical features. In [124], it presents a machine learning method for vascular structure segmentation with fully automatic detection of bifurcation points. This method is based on a machine learning technique called, AdaBoost, and it has over a 97% success rate for detecting bifurcation points. However, these two papers did not consider the features of velocity and blood rate. In [125], it presents a scale-space model from a computational perspective for the bifurcation evolution with increasing scale, which was combined with eigenvalue analysis to create a bifurcation-Ness filter. It is not appropriate to assume that vessel profile is diffusion and matches Gaussian distribution. In [126], it investigates the non-Newtonian fluid flow in a bifurcation model with a non-planar daughter branch by using a finite element method to solve the three-dimensional Navier-Stokes equations. Finally, [127] investigates red

blood cells (RBCs) flowing in a Y-shaped bifurcating micro-fluidic channel.

We will also discuss some assumptions including an initial focus on the nature of blood fluid flow. Newton modelled these kinds of fluids in an assumption that consist of thin layers that slide past one another, developing a resistance to the flow. An important factor of the ratio of drag linearly proportional to the velocity gradient perpendicular to the direction of flow is called viscosity, and these forces can be mathematically approximated to first order by a viscous stress tensor. A fluid with the property that the viscosity is independent of the forces applied to it, is called a Newtonian fluid. Naturally enough, if the viscosity does depend on the applied force, then the fluid is called non-Newtonian.

In the Casson fluid model, blood is regarded as a non-Newtonian fluid consisting of shear rate and shear stress. According to the literature [128, 80], during a normal flow in straight narrow blood behaves as a Newtonian fluid, especially in blood capillaries. So in this thesis, we model blood flow as a Newtonian fluid. In these narrow capillaries, it is not reasonable to think of layers of fluid sliding past each other, so our models do not apply. Furthermore, the pressure differential along the capillary system is assumed as constant. We also assume time-independence and a constant shape for the blood vessels. Furthermore, the Reynolds number in the scenario of blood capillaries is low and regarded as following a laminar flow model. In laminar flow (low Reynolds number), viscous forces are dominant, and the fluid motion is smooth and constant. In turbulent flow (high Reynolds number), the inertial forces dominate and tend to produce flow instabilities. In addition, the bifurcation of capillaries is all Y-shaped and hierarchical capillaries branches form a capillary network with input from a greater capillary and multiple outputs in smaller capillaries branches. Having acknowledged these assumptions and realities, we can present our SIMO communication model for a capillary system.

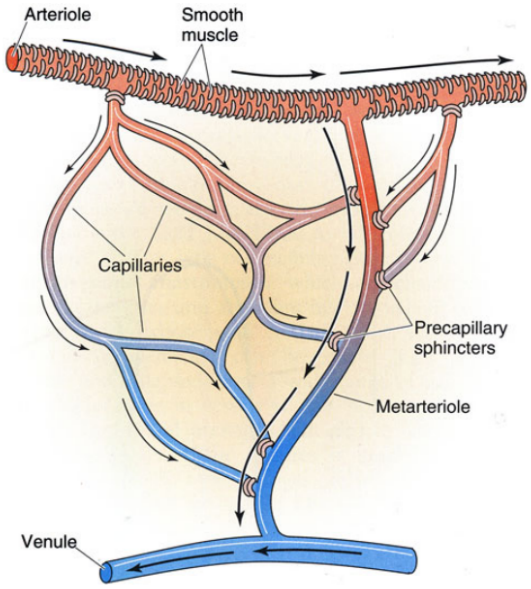

Figure 5.1: Idealised microcirculatory circuit with capillaries [9]

5.2 Biologic Scenario for Branches of Blood Capillaries

Blood flows from the heart through arteries, which branch into narrow arterioles, and then bifurcate into capillaries where nutrients and waste are exchanged. In the return process, the capillaries join to become wider venules, which in turn widen and converge to become veins, which then return blood to the heart through the great veins.

Capillaries do not function on their own, but instead in a capillary bed, an interweaving network of capillaries supplying organs and tissues. The more metabolically active a cell or environment is, the more capillaries are required to supply nutrients and carry away waste products.

Figure 5.1 from the book [9] illustrates the function of blood capillaries in the microcirculatory system between arterioles and venules. The general ar-

chitecture of the circulation is frequently explained with schematic drawings depicting precapillary sphincters and metarterioles in addition to arterioles, capillaries and venules.

There are three main types of blood capillary [10], shown in Figure 5.2:

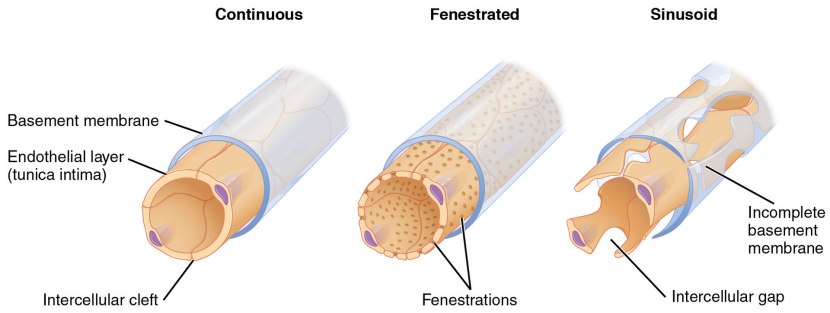

Figure 5.2: Major types of capillaries [10]

Continuous capillaries provides a continuous blood wall with an uninterrupted lining, and they only allow smaller molecules, such as water and ions to pass through their intercellular clefts [129]. However lipid-soluble molecules can passively diffuse through the endothelial cell membranes along concentration gradients. With numerous transport vesicles in endothelial cells, molecules can enter into blood capillaries via endocytosis.

Fenestrated capillaries have pores covered by diamonds of radially oriented fibers in endothelial cells ($60 - 80nm$ in diameter) and allow small molecules and limited amounts of protein to diffuse [130]. These types of blood vessels have continuous basal laminae and are primarily located in the endocrine glands, intestines, pancreas, and the glomeruli of the kidney [130].

Sinusoidal capillaries, also known as discontinuous capillaries, are a special type of open-pore capillary, that have larger openings ($30 - 40\mu m$ in diameter) in the endothelium [130]. These types of blood vessels aided by a discontinuous basal lamina, allow red and white blood cells ($7.5\mu m - 25\mu m$ diameter) and various proteins to pass. These capillaries lack pinocytotic

vesicles and therefore utilise the cell gap junctions to permit diffusion across the endothelial cell membrane.

Sinusoidal capillary is used in this model, so that hormones or cytokines can diffuse across the blood wall and into capillary. Vessels in the vascular system are classified as arterioles, capillaries and venules. Those vessels with a diameter in the dilated state of less than $8um$ are classified as capillaries [9]. Capillary networks form the connections between the arterial and venous systems. The complexity of each capillary network varies in response to the metabolic needs of the tissues served. Tissues with lower needs, such as the intestinal tract, have two or three capillary branches from each metarterioles [9]. In [127], it predicts that two branches is the majority in most capillaries and modelled the bifurcation as being Y-shaped. In this assumption, levels of Y-shaped branches of capillaries form a SIMO capillary network in this model.

The biologic scenario within the blood capillaries consists of emission of carriers from platelets, carriers propagation in the flow of blood vessels, and receiving by endocrine cells. Soluble CD40 ligand (sCD40L) is contained in platelet granules and thus its presence in the blood is a marker of platelet activation. By interacting with CD40, which is found on endothelial and smooth muscle cells, sCD40L may trigger the release of inflammatory mediators [108]. The communication process from platelets and the endocrine cell plays a fundamental role during initial stages of atherogenesis [131].

The components of the communication system within the blood vessels are platelets, endocrine cells and transmission information represented by cytokineses. The transmitters, which are platelets, secrete and release cytokineses, which are small cell-signalling protein molecules, while the receivers, are endocrine cells in the blood stream. These cytokineses are propagated to the endocrine cells across the bloodstream with blood flow. There are many types of cytokineses, with matching types of receptors on the cell surface. In [108, 73], the soluble CD40 ligand is regarded as a carrier with matching

recanters CD40 on the surface of the endocrine cell. In this chapter, we still follow this concept. Each cell has a number of CD40 receptors, and this number changes over time [73]. A decoding process functions in endothelial cells, which are known to express vascular cell adhesion molecules.

Nano-particles propagation in blood capillaries though the branches is modelled in the following subsections: Diffusion with blood flow for capillary channels, and bifurcations for blood capillary.

Earlier it was mentioned that endothelial cells have CD40 receptors that are a match for the cytokine sCD40L on the surface of the endocrine cell. The CD40 receptor is of the transmembrane type, meaning that it provides a pathway between the exterior and interior of a cell. Nano-particles, which are emitted by platelets, are propagated through branches of the capillaries system and received by multiple receptors which lies on the surface of endothelial cells in each branch of the blood capillaries. These emission, transmission and reception processes form a SIMO MC. Figure 5.3 illustrates the mapping from biological scenario to SIMO MC process.

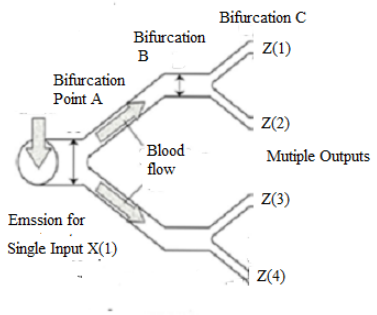

Figure 5.3: Mapping for Y-shaped bifurcation blood capillaries SIMO model

5.3 SIMO Model for Blood Capillaries

5.3.1 Diffusion with Blood Flow Drift in Blood Capillary

In Chapter 4, we have fully discussed that a generalised Langevin equation with additive noise term Eq.4.14 models particles propagating through the blood vessels with drift, and the corresponding Fokker-Planck equation is shown in Eq.4.20:

$$\frac{\partial W(x,t)}{\partial t} = -v\gamma \frac{\partial W(x,t)}{\partial x} + D\frac{\partial^2 W(x,t)}{\partial x^2} \tag{4.20}$$

With appropriate assumptions and boundary conditions, the solution of its corresponding Fokker-Planck equation is shown below, and we have a PDF of concentration of particles:

$$W(x,t) = \frac{C}{\sqrt{4\pi D t}} e^{-\frac{(x-vt)^2}{4Dt}} \tag{4.21}$$

We have some assumptions and boundary conditions for the for this communication system:

1) Initial Impulse, $W(x,0) = W_0 = C$, C is the contraction of released molecules at the transmitter at $t = 0$, with a pulse of concentration $W0$ being emitted at the transmitter which is located at x distance away from the receiver;

2) reception areas and their boundary conditions, if the transmitter is in the capture areas, are located at $x \ll R$ from the receiver, and anything emitted will be captured immediately. At any time $t > 0$, the concentration outside the zone is $W = 0$. so in most case this is the distance between transmitter and receiver $x \gg R$.

3) No remission occurs in the reception areas, and the reception probability is based on the ligand-receptor model and non-received particles are not remitted to the channel.

4) Long-term capture and its boundary conditions, $W(x,\infty) = pW(x,t)$: if a molecule is captured, it cannot be remitted. Therefore, over a long time ($t+\infty$), the receiver captures molecules with a probability p of ligand-receptor to an equilibrium state.

There are a number of alternative conditions used in previous models in literature, which are not suitable in for this blood capillary model:

1) Infinite Source [132]: this condition states that an infinite source of molecules provide a continuous and finite flux of molecules, such that $W(r,t) = W0$.

2) Infinite Environment [133, 134]: this condition states that the propagation environment is infinite. It is valid for an boundaryless communication system, but is not realistic for enclosed structural environments in blood vessel.

3) Fast Sensor Response [78]: that is to say the molecules at sensors are immediately converted to electrical charge and there is zero aggregated chemical interference from previous emissions. It is not realistic in blood capillary systems, information cytokineses have a response time.

Therefore, the cumulative captured number of molecules can be defined as the cumulative distribution function (CDF) of the concentration inside of the reception area to any given time t. The resulting number of molecules captured is a monotonically increasing function:

$$\theta(x,t) = \int_{L-R}^{L} W(x,t) = \int_{L-R}^{L} \frac{C}{\sqrt{4\pi Dt}} e^{-\frac{(x-vt)^2}{4Dt}} \tag{5.1}$$

The partial derivative of the cumulative function with respect to time yields the likelihood of capture between any particular time t and $t+\delta t$ for a $\delta t \to 0$:

$$g(x,v,t) = \frac{d\theta(x,t)}{dt} = C\frac{\xi}{\sqrt{4\pi Dt^3}} e^{-\frac{(\xi-vt)^2}{4Dt}} \tag{5.2}$$

Eq.5.2 gives the probability density function of the absorption time of a particle released in a fluid medium with diffusion constant D, at a distance

ξ from the transmitter, when the blood vessel has a constant drift velocity v. Eq.5.2 is the inverse Gaussian (IG) distribution [135], where

$$u = \frac{\xi}{v} \tag{5.3}$$

and

$$\text{Var} = \frac{\xi D}{v^3} \tag{5.4}$$

u and Var represent the mean and the variance of Inverse Gaussian distribution. Note that Eq.5.2 is valid only for positive drift velocities, thus the receiver is downstream with the blood flow from the transmitter.

5.3.2 Bifurcations for Blood Capillaries

The liquid motion equations for the circulatory system are very complicated. In order to obtain an analytical solution the following simplification has been assumed. The blood flow obeys a Newtonian fluid model consists of nanoparticles and blood plasma. In this model, we did not consider the non-Newtonian fluid model with the influence of red blood cells (RBCs). However, the yield shear stress refers to bulk blood flow and does not apply to RBCs flowing in narrow capillaries [91]. The assumption of constant blood viscosity and homogeneity in the whole vessels' tree is necessary to estimate blood flow through this trees. According to the literature [119] during a normal flow in straight arteries blood behaves as a near Newtonian fluid. In real blood vessels, the vessel walls are elastic and can change their diameters.

In this way, resistance of the blood capillary system is regulated. This process is known as autoregulation, and corrects nutrition of all cells in human body. Assumption of the vessel wall as a rigid pipe with constant diameter for given vessel segment is necessary to application of hydrodynamical equations and analytical calculation of modelled trees. Blood flow estimation assumes laminar flow for the entire fractal vessel tree.

In large arteries, systolic aberrations of laminar flow is a result of wave

propagation. Turbulent flow is also observed in pathological vessels. In small arteries, which are the subject to described research, an assumption of laminar flow is correct. Hydrodynamic equations for small arteries give the correct results in biological circulatory system [128].

In this model, we consider the optimal angle at both symmetric and non-symmetric bifurcation in blood vessels. By minimizing a cost function, we are able to determine the optimal radius of a blood vessel, given its length and the flow of blood through it. We then use this optimal radius to determine our minimum cost as a function of radius and length.

The lengths of the blood vessels, however, depend on where the bifurcation occurs. By finding the location of the optimal bifurcation which keeps the cost function minimised, we are able to write expressions for the bifurcation angles as a function of blood vessel radius. Furthermore, using conservation of mass, we are able to eliminate the need for knowing the radius of all three vessels. With this, we can determine the angle of bifurcation of a blood vessel without knowing its radius; instead, we just need to know the radius of the other two blood vessels.

Once the expressions are derived, we can then use them to study special cases. The exemplary special case examined here occurs when the radius of two secondary blood vessels are equal. In this case, the two blood vessels have the same bifurcation angle of 37.5°.

Throughout the human body, arteries from the heart bifurcate many times in order to become capillaries. We shall first consider a bifurcation for symmetric branches. The bifurcation occurs at the point $'O'$. To the left of $'O'$, some flow Q_0 of blood is entering the vessel $'AO'$ through $'A'$. To the right of $'O'$, Q_0 is divided between the two vessels $'OB'$ and $'OD'$, each now with flow Q_1 and Q_2, respectively. The goal now is to find a cost function which can be minimized in order to determine the bifurcation pattern of the blood vessels. Then, by varying the location of $'O'$, we will be able to determine the angle of bifurcation as a function of the radius of the blood

vessels.

The cost function proposed by Murray [136]and Rosen [119] is the sum of the rate at which work is done on the blood vessel bifurcation. The rate of energy is used up by the blood vessels by metabolism. The rate at which work is done on the blood is equal to $E = Q\Delta p$ [119], where Q is flow and Δp is the change in pressure along the vessel. The rate at which energy is used by metabolism is equal to $K\pi a^2 L$ where K is a proportionality constant. The cost function for blood vessels is then:

$$C(L) = Q\Delta p + K\pi a^2 L \tag{5.5}$$

Using Poiseuille's Law Eq.4.16, we can rewrite Δp and obtain

$$C(L) = \frac{8\mu L}{\pi a^4} Q^2 + K\pi a^2 L \tag{5.6}$$

To find the optimal radius a for a given length L and flow, the cost function is minimized with respect to a

$$\frac{\partial}{\partial a}(C(L)) = -\frac{32\mu L}{\pi} Q^2 a^{-5} + 2K\pi La = 0 \tag{5.7}$$

and is solved for the optimal a:

$$a = (\frac{16\mu}{\pi^2 K})^{-\frac{1}{6}} Q^{\frac{1}{3}} \tag{5.8}$$

At the optimal radius, the minimum cost function is equal to:

$$c(L)_{\min} = \frac{3\pi}{2} K L a^2 \tag{5.9}$$

5.3.2.1 Model A: Symmetric Branches

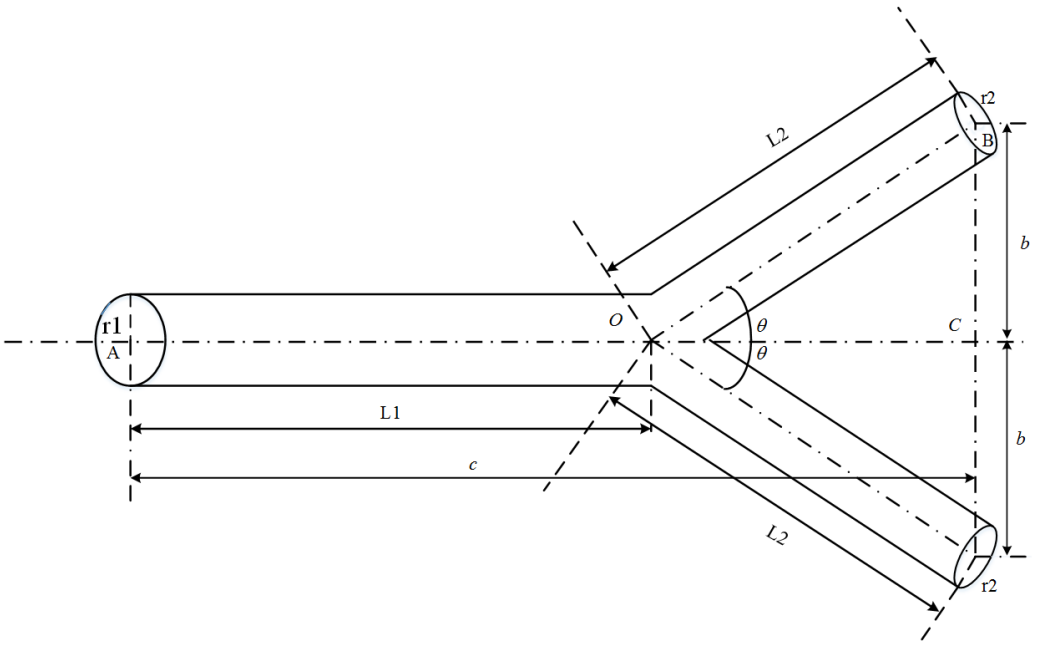

Figure 5.4: Schematic diagram of symmetric bifurcation

Model of a bifurcation Introduction to the problem Model of a bifurcation: Simplifying Assumptions for symmetric model:

1. The bifurcation is symmetric, so the flows in the two daughter vessels are identical ($Q1 = Q2$). The vessels are rigid, that is the walls do not deform.

2. The blood is incompressible, that is the density ρ of the blood (mass per unit volume) is constant, with no viscous forces. Steady, that is, it does not change with time, which means the transmission is a stationary process.

3. The velocities of blood flow v_0, v_1 and v_2 at the inlets and outlets are constant (rather than functions of the position), and axial, that is the direction of the velocity is along the tube and perpendicular to the surfaces.

These assumptions simplify the problem enormously, but they are only valid in some cases. Even so, there are cases in which the following analysis yields an answer close to reality.

According to [136], by the principle of the conservation of mass, the flow of blood in the vessel AO must be equal to the sum of the flow of blood through vessels BO and DO; namely,

$$Q_0 = Q_1 + Q_2 \tag{5.10}$$

If we solve our equation for optimal radius for flow, obtaining

$$Q = a^3(\frac{16\mu}{\pi^2 K})^{-\frac{1}{2}} \tag{5.11}$$

and substitute this into our conservation equation, we obtain Murray's law.

$$a_0^3 = a_1^3 + a_2^3 \tag{5.12}$$

In this symmetric bifurcation model, we consider the case in which the daughter blood vessels have the same radius with some angle. In this case, $a_1 = a_2$, and our expressions for θ and ϕ reduce to

$$\cos\theta = \frac{a_0^2}{2a_1^2} \tag{5.13}$$

$$\cos\phi = \frac{a_0^2}{2a_2^2} = \frac{a_0^2}{2a_1^2} \tag{5.14}$$

which are clearly equal. This means that, when the radii of the daughter blood vessels are equal, their bifurcation angles are also equal. Furthermore, we can determine exactly what the bifurcation angle is in this case. When the $a_1 = a_2$, Murray's law becomes

$$a_0^3 = 2a_1^3 \tag{5.15}$$

which can be rearranged as,

$$\frac{a_0}{a_1} = 2^{\frac{1}{3}} \tag{5.16}$$

Substituting this into reduced expression for $\cos, \theta$ results in

$$\cos\theta = \frac{1}{2}(2^{\frac{1}{3}})^2 \tag{5.17}$$

When we solve for θ , we find that the bifurcation angle is $\theta = 37.5°$.

Apply the Eq.4.2, we can calculate the velocity at the daughter capillaries.

$$v_1(r) = \frac{1}{4\eta}\frac{\Delta p_1}{L}({a_1}^2 - r^2) \tag{5.18}$$

$\overline{v_1(t)}$ is the average cross sectional velocity in the main blood vessels, defined as

$$\overline{v_1(t)} = \frac{2}{{r_1}^2}\int_0^{r_1} r v_1(r,t)dr \tag{5.19}$$

5.3.2.2 Model B: Non-Symmetric Branches

In this model, we consider the optimal angle at which non-symmetric bifurcation in blood vessels occurs-. By minimizing a cost function, we are able to determine the optimal radius of a blood vessel, given its length and the flow of blood through it. We then use this optimal radius to determine our minimum cost as a function of radius and length.

1. The branches do not have the same radius, then the larger branch makes a smaller angle with the original direction than does the smaller branch.

2. Branches that are so narrow that they do not significantly diminish the flow in the main stem branch off at large angles (typically between 70° and 90°).

The lengths of the blood vessels, however, depend on where the bifurcation occurs. By finding the location of the optimal bifurcation which keeps the cost function minimised, we are able to write expressions for the bifurcation angles as a function of blood vessel radius. Furthermore, using

conservation of mass, we are able to eliminate the need for knowing the radius of all three vessels. With this, we can determine the angle of bifurcation of a blood vessel without knowing its radius; instead, we just need to know the radius of the other two blood vessels.

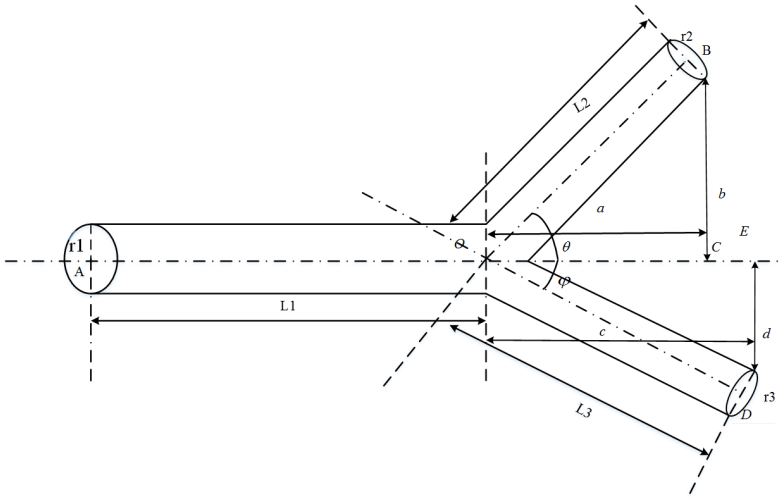

Figure 5.5: Schematic diagram of non-symmetric bifurcation

Suppose that the bifurcation point is moved to location O' in the direction of the AO blood vessel, as shown above. Then, the changes in the lengths of the vessels are $\delta L_0 = \delta$, $\delta L_1 = -\delta \cos\theta$, $\delta L_2 = -\delta \cos\phi$, and the change in the cost function is

$$\delta P = \frac{3\pi K}{2}\delta(a_0^2 - a_1^2 \cos\theta - a_2^2 \cos\phi) \tag{5.20}$$

In order for the cost function to remain unchanged, the following relationship must be true:

$$a_0^2 = a_1^2 \cos\theta + a_2^2 \cos\phi \tag{5.21}$$

Now suppose that the bifurcation point is moved along the direction of OB, as shown above. In this case, the changes in the lengths of the blood

vessels are $\delta L_0 = -\delta\cos\theta, \delta L_1 = \delta, \delta L_2 = \delta\cos(\theta+\phi)$ The change in the cost function is

$$\delta P = \frac{3\pi K}{2}\delta(-a_0^2\cos\theta + a_1^2 + a_2^2\cos(\theta+\phi)) \tag{5.22}$$

In order for the cost function to remain unchanged, the following relationship must be true:

$$-a_0^2\cos\theta + a_1^2 + a_2^2\cos(\theta+\phi) = 0 \tag{5.23}$$

Finally, suppose the bifurcation point is moved along the direction of OD, as shown above. In this case, the changes in the lengths of the blood vessels are $\delta L_0 = -\delta\cos\phi, \delta L_1 = \delta\cos(\theta+\phi), \delta L_2 = \delta$,

The change in the cost function is:

$$\delta P = \frac{3\pi K}{2}\delta(-a_0^2\cos\phi + a_1^2\cos(\theta+\phi) + a_2^2) \tag{5.24}$$

In order for the cost function to remain unchanged, the following relationship must be true:

$$a_0^2\cos\phi + a_1^2\cos(\theta+\phi) + a_2^2 = 0 \tag{5.25}$$

We now have three equations and three unknowns. The optimal conditions Eq.5.21, Eq.5.23, and Eq.5.25 that resulted from each of the shifts can be solved for $\cos\theta$, $\cos\phi$, and $\cos(\theta+\phi)$. The result is

$$\cos\theta = \frac{a_0^4 + a_1^4 - a_2^4}{2a_0^2a_1^2} \tag{5.26}$$

$$\cos\phi = \frac{a_0^4 - a_1^4 + a_2^4}{2a_0^2a_2^2} \tag{5.27}$$

$$\cos(\theta+\phi) = \frac{a_0^4 - a_1^4 - a_2^4}{2a_1^2a_2^2} \tag{5.28}$$

If we know the radius of each of the three vessels, we can now determine the angle of the bifurcation.

5.4 Channel Performance for SIMO Model

5.4.1 Channel Capacity in SISO Model

The reception process at receiver side involves capture or release of molecules from/into the blood vessels by several ligand-based receptors sCD40L. When the sender emits one kind of molecule instantaneously, the receiver must receive the molecule with binding the molecule to the ligand on their surface. The capture and release of molecules is modelled according to the chemical theory of the ligand-receptor binding process in [137, 93]. We consider a communication between only one transmitter and one receiver. When the platelets emits molecules into the blood stream which propagate to the receiver, the concentration of molecules in random point of space follows the generalised Langevin equation. Assume that the distance between the transfer and receiver is r, then the receiver binding rate is k_1 and release rate is k_{-1}, using the ligand-receptors binding model given in [137], then the concentration of by bond molecules of the receiver denoted by P_R can be given as:

$$P_R = \frac{k_1 N A}{k_{-1}} \tag{5.29}$$

Where k_1 and k_{-1} are the constant binding and release rates, respectively. In this chapter, we follow model for k_1 in the literature [137], which is a realistic model for k_1 that is experimentally tested for certain biochemical.

$$k_1 = \frac{4\pi D r_0 \beta}{1 - (1 - \beta)\frac{r_0}{r_\infty}} \tag{5.30}$$

Where r_0 is the radius of receiver and r_∞ is the radius of the whole spherical shaped environment. β is the ratio of the radius of one molecule to the distance between transmitter and receiver, i.e. $\beta = r0/r$. A is the concentration of the molecules sent by the transmitter. N is the concentration of the ligand-based receptors on the receiver's surface. Thus, considering the condition with ligand-based receptors, the probability that a molecule transmitted

in slot i arrives in slot n can be modified as:

$$Z = \frac{k_1 N}{k_{-1}} q_v \cdot X + I = \frac{k_1 N}{k_{-1}} \int_{iT}^{(i+1)T} g_d(t)dt \cdot X + I \tag{5.31}$$

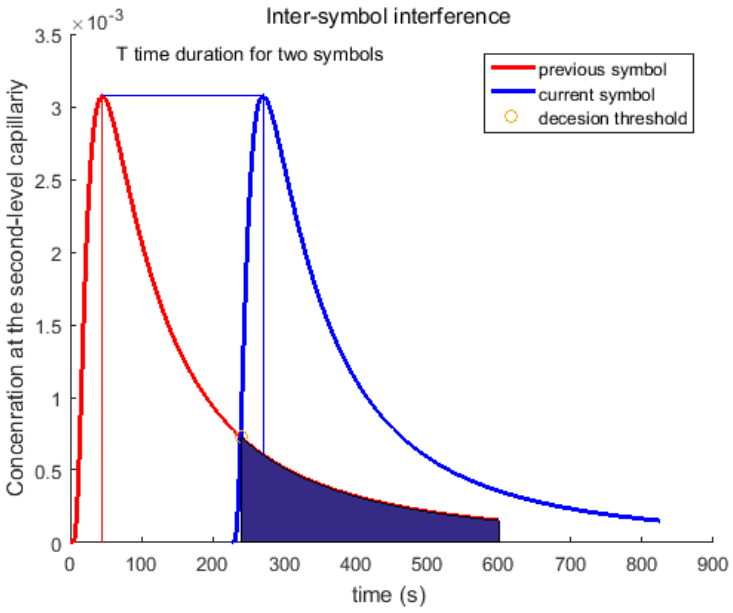

Figure 5.6: An illustration of Inter-symbol Interference and optimal detection threshold.

Differing from traditional communications, the non-received molecules from previously transmitted symbols becomes a dominating source of error, thus the ISI of a channel is a major consideration. The ISI is comprised of aggregated molecules from previous symbols, which has been received in error. According to illustration in Figure 5.6, ISI is major components for the error. After a time duration T, a flux of molecules will be released as a new symbol. Time duration T is calculated by two sample times between the previous symbol and the current symbol, and the highest probability of concentration is at a sample time t_{max}. The cross point of previous and cur-

rent symbols is the decision threshold value φ of the concentration of arrived molecules at the reception area. In this chapter, we lay our emphasis on the effect of ISI. At first, we should consider the maximum error probability of ISI in this system. The upper bound on symbol error probability is given by [62].

$$P_e < \sum_{i=1}^{T-1} p_i(1 - FN(t_{i+1} - t_i)) \tag{5.32}$$

FN is the CDF of $g(x, v, t)$ given by [135]:

$$FN(t_{i+1} - t_i) = \int_{t_i}^{t_{i+1}} C\frac{\xi}{\sqrt{4\pi D t^3}} e^{-\frac{(\xi - vt)^2}{4Dt}} dt \tag{5.33}$$

The value of the received concentration of molecules given in Eq.5.33 represents the outputs in the main capillary. We consider two forms of errors in the system, one from the previously mentioned ISI and the other from additive Gaussian noise N at the receiver. In order to obtain the optimal detection threshold, we have following expression:

$$u_{Z^0} = E[Z\,|X = 0] = u_I + u_N \tag{5.34}$$

$$u_{Z^1} = E[Z\,|X = 1] = u_I + u_N + Z_{\max} \tag{5.35}$$

$$\sigma_Z^2 = \sigma_I^2 + \sigma_N^2 \tag{5.36}$$

$$\sigma_I^2 = \frac{\mu_I}{V_R} = Var[Z\,|X = 0] = Var[Z\,|X = 1] \tag{5.37}$$

The distribution of ISI is given by the PDF of the capture concentration with u_I and σ_I. The distribution of the AWGN follows a normal distribution $N(u_N, \sigma_N^2)$.The optimal decision threshold can be obtained by minimizing the probability of error. The probability of error, denoted by p_e, is expressed as,

$$p_e = p(1 - Q(\frac{\varphi - u_{Z^1}}{\sigma_I})) + (1 - p)(Q(\frac{\varphi - u_{Z^o}}{\sigma_I})) \tag{5.38}$$

By solving $\frac{\partial P_e}{\partial \varphi} = 0$ (under the condition that $\varphi \geq 0$ which is a realistic one), the optimal threshold is derived as follows,

$$\varphi = \sqrt{u_{Z^0} u_{Z^1} [1 + \frac{1}{V_R(u_{Z^1} - u_{Z^0})} \ln(\frac{(1-p)^2 u_{Z^1}}{p^2 u_{Z^0}})]} \tag{5.39}$$

The minimum error probability is discussed in digital communication [138] with the decision threshold φ in a criterion of a standard symmetric detection framework. As previously mentioned, the transmission system is an OOK modulation scheme with p_i probability of transmitting a 1. Note that the probability of error given a 1 is transmitted is equal to the probability of error given a 0 is transmitted. Therefore, with prior probability $p = 0.5$, the system is a binary symmetric channel. Replace with the prior probability value $p = 0.5$ to the Eq.5.39, we obtain the following optimal decision threshold for symmetric channel. Correspondingly, we get the lower bound of the symbol error probability p_e as below.

$$Z \begin{matrix} > 1 \\ < 0 \end{matrix} \frac{\sigma_Z^2}{u_{Z^1} - u_{Z^0}} \ln(\frac{1-p}{p}) + \frac{1}{2}(u_{Z^1} + u_{Z^0}) = \varphi \tag{5.40}$$

$$\frac{1}{2}(u_{Z^1} + u_{Z^0}) = \varphi \tag{5.41}$$

$$P_e = Q(\frac{u_{Z^1} - u_{Z^0}}{2\sqrt{{\sigma_I}^2 + {\sigma_N}^2}}) \tag{5.42}$$

We evaluate the bit error rate of the blood capillary channel with respect the power of a signal and power noise ratio including ISI, with SNR defined as [133]:

$$\gamma = \frac{P_z}{P_N + P_I} = \frac{\int_0^T |h_z(t)|^2 dt}{\sigma_N^2 + \sigma_I^2} = \frac{\left(\frac{k_1 NC}{k_{-1}}\right)^2 \int_0^T |g(Z_n(t))|^2 dt}{\sigma_N^2 + \sigma_I^2} \tag{5.43}$$

where P_Z is the signal power at the receiver, the term P_N is noise power, and

P_I is power of ISI.

5.4.2 Diversity Combining for SIMO

We next consider the case where the information sink has access to N physically separated reception nodes, while there is only one transmission node, SIMO configuration. An illustration is provided in Figure 5.7. We assume that each reception node is separated from one another by a large enough distance such that transmission and reception probability at each receptors in each capillary is statistically independent.

Given a modulated number of emitted molecules at the transmitter, according to Eq.5.2, $g(L1, v1, t)$ is the concentration of molecules at the first order bifurcation node A at the location of the main blood capillary.

$$g(L1, v1, t) = C\frac{L1}{\sqrt{4\pi Dt^3}}e^{-\frac{(L1-v1t)^2}{4Dt}} \tag{5.44}$$

The arrival probability of a molecule at the second-level bifurcation node is computed through the convolution integral with the $g(L1, v1, t)$ and the propagation process at the first-order daughter blood capillaries.

$$\mathrm{g(y_n(t))= g(L1, v1, t)*g(L2, v2, t)} \tag{5.45}$$

Similarly, Z_n is the molecules concentration at the reception location of the end of second-level daughter blood capillaries,

$$\mathrm{g(Z_n(t)) =g(L1, v1, t) * g(L2, v2, t) * g(L3, v3, t)} \tag{5.46}$$

$$Z_n = \frac{k_1 NC}{k_{-1}} \int_{iT}^{(v+1)T} g(Z_n)dt + I_n + N_n \tag{5.47}$$

$$h_n = \frac{k_1 N}{k_{-1}} \int_{vT}^{(v+1)T} g(Z_n)dt \tag{5.48}$$

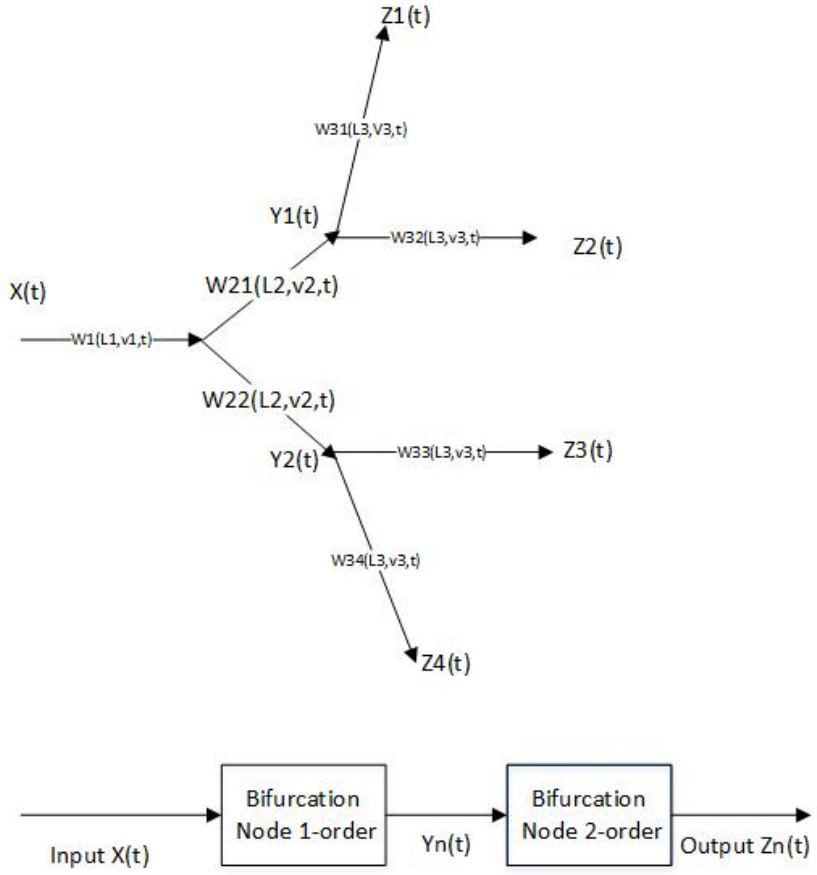

Figure 5.7: Molecular propagation model for second-order Y-shaped bifurcation blood capillaries SIMO network.

For non-symmetric branches, Maximum-ratio combining (MRC) is the spatial diversity combining technique to be applied to improve the detection performance. In each channel, Z_n in Eq.5.47 represents the received molecules concentration. N is the molecules concentration in the transmitter which represents the input X. h_n is the transmission function from Input X to Outputs Z_n, while in the symmetric branches, the channel state information of all channels are the same. Equal-Gain combiner(EGC) is the technique considered in this special case. Note that the magnitudes of the weighting factors $|a1|, |a2|, \cdots, |a_N|$ are the same and do not depend on the SNR values of all channels [139].

$$Z_{EGC} = \sum_{n}^{N} a_n Z_n = \sum_{n}^{N} e^{-j\phi n} Z_n \tag{5.49}$$

$a_n = e^{-j\phi n}$, for $n = 1, 2, \cdots, N$.

Hence, the resulting SNR at the output with the EGC technique can be given by,

$$\gamma Z_{EGC} = \frac{\left(\sum_{n=1}^{N} |h_n|\right)^2}{N{\sigma_z}^2} \tag{5.50}$$

while in the non-symmetric branches,let Z_N denote the molecular concentration received by deferent receptors N in the Nth channel. By applying the principle of MRC, we have these assumption [140]:

1. The signals from each channel are added together.

2. The gain of each channel is made proportional to signal level and inversely proportional to the mean square noise level in that channel.

3. Different proportionality constants are used for each channel.

In the non-symmetric model combined outputs following the principle of MRC at N receivers can be written as:

$$\hat{Z}_{MRC} = \frac{h_0 * Z_0 + h_1 * Z_1 + \cdots + h_n * Z_n}{|h_0|^2 + |h_1|^2 + \cdots + |h_n|^2} \tag{5.51}$$

According to [139],the SNR of SIMO system is the sum of the SNR at each channels, shown as below. In fact, one can show that the MRC scheme achieves the maximum SNR among all linear combining techniques.

$$\gamma Z_{MRC} = \gamma_n \sum_{n=1}^{N} |h_n|^2 \tag{5.52}$$

According to [141, 139], the relationship between channel capacity and SNR of a SIMO system will be:

$$C = Bp\log_2(1 + \gamma_n \sum_{n=1}^{N} |h_n|^2) \tag{5.53}$$

where the bandwidth of SIMO system is $B = \frac{1}{T_s}$.

5.5 Simulation Results

In this section, we present the simulation results of both symmetric and non-symmetric blood capillary bifurcation SIMO system. In Table 5.1, it presents the symbol meaning and parameters for following simulation results of the error probability , SNR and channel capacity performance in the SIMO channel.

Table 5.1: Symbol meaning and Parameters of SIMO blood capillary system

Parameters	Symbol	value
Transmitted molecules number	Q	$10^6 - 10^7$
Diffusion coefficient	D	$10^{-5} - 3 \times 10^{-5} m^2/s$
Boltzmann constant	k_B	$1.38 \times 10^{-23} J \cdot K^{-1}$
Viscosity	η	$2 \times 10^{-3} kg/(ms)$
Pressure differential along vessel	Δp	$8 \times 10^2 N/m^2$
Best sample time	t_{max}	
Symbol time duration	T	
Constant binding rate	k_1	
Constant release rate	k_{-1}	
ISI mean	u_I	
ISI variance	σ_I	$\sigma_I = u_I$
Channel capacity	C	
Additive Gaussian noise mean	u_N	2×10^5
Additive Gaussian noise variance	σ_N	$\sigma_N = 0.5 u_N$
Symbol error bit	p_e	
Signal-to-Noise rate	γ	dB
Decision threshold	φ	
Receive probability	P_R	
Bandwidth	B	H_z

Parameters for symmetric and non-symmetric blood capillary bifurcation SIMO system is shown in Table 5.2, which will decide the physical shape and flow velocity of blood capillaries.

Table 5.2: Parameters setting for Symmetric and Non-Symmetric SIMO system

Parameters	Symbol	value
Symmetric SIMO system		
Radius of main capillary	a_0	$4 \times 10^{-}5m$
Length of main capillary	L_0	$4 \times 10^{-}2m$
Bifurcation angle	θ	$\theta = 37.5^{\circ}$
Radius of First-level capillary	a_1	$\frac{a_0}{a_1} = 2^{\frac{1}{3}}$
Length of First-level capillary	L_1	$2 \times 10^{-}2m$
Radius of Second-level capillary	a_2	$\frac{a_1}{a_2} = 2^{\frac{1}{3}}$
Length of Second-level capillary	L_2	$2 \times 10^{-}2m$
Non-Symmetric SIMO system		
Radius of First-level capillary Y_1	a_{11}	$a_{11} = a_0/2$
Radius of First-level capillary Y_2	a_{12}	$a_{12} = a_0/4$
Radius of Second-level capillary Z_1	a_{21}	$a_{21} = a_{11}/2$
Radius of Second-level capillary Z_2	a_{22}	$a_{22} = a_{11}/4$
Radius of Second-level capillary Z_3	a_{23}	$a_{23} = a_{12}/2$
Radius of Second-level capillary Z_4	a_{24}	$a_{24} = a_{12}/4$

5.5.1 Symmetric Model

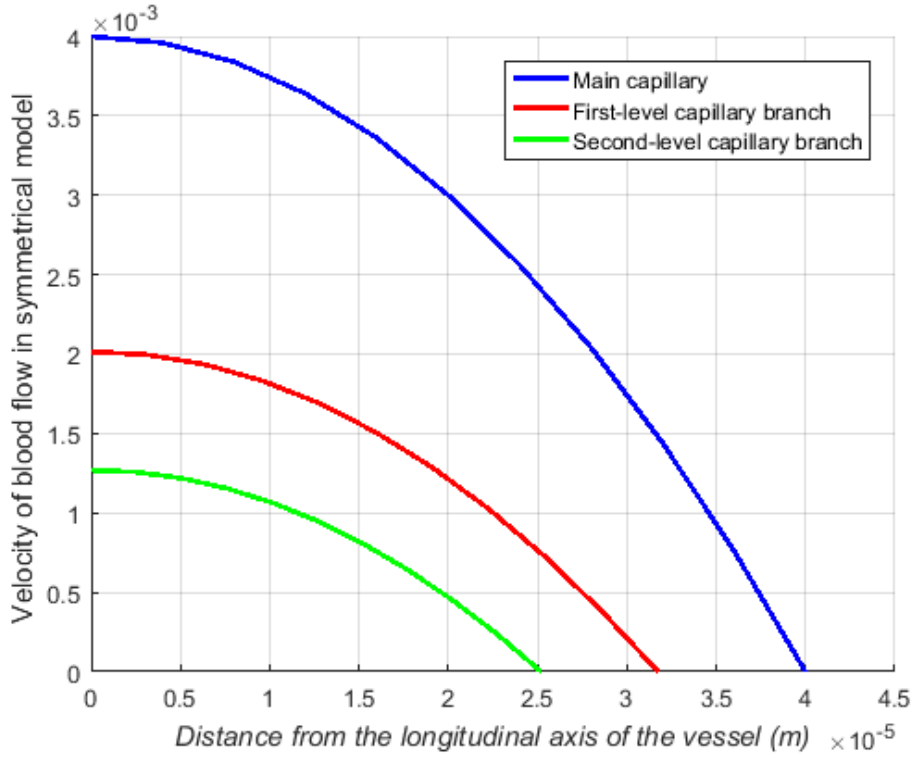

Figure 5.8: Velocity of blood flow in each level of blood capillaries(m/s)

In Figure 5.8, we plot the flow velocities of each level blood capillary branches in the symmetric model. Three curves, corresponding to the velocity of three levels of capillaries, are plotted at the site of a distance from the longitudinal axis. According to Eq.4.2, the velocity is the highest at the site of the central axis. The highest velocity in the main capillary is $4 \times 10^{-3} m/s$, which is double the value of the highest velocity in first-level capillary, whilst in the second-level capillary, the value reduces to $1.3 \times 10^{-3} m/s$. The flow velocity, has an effective impact on the propagation process, and is determined by the bifurcation angle, length and radius of secondary blood capillaries.

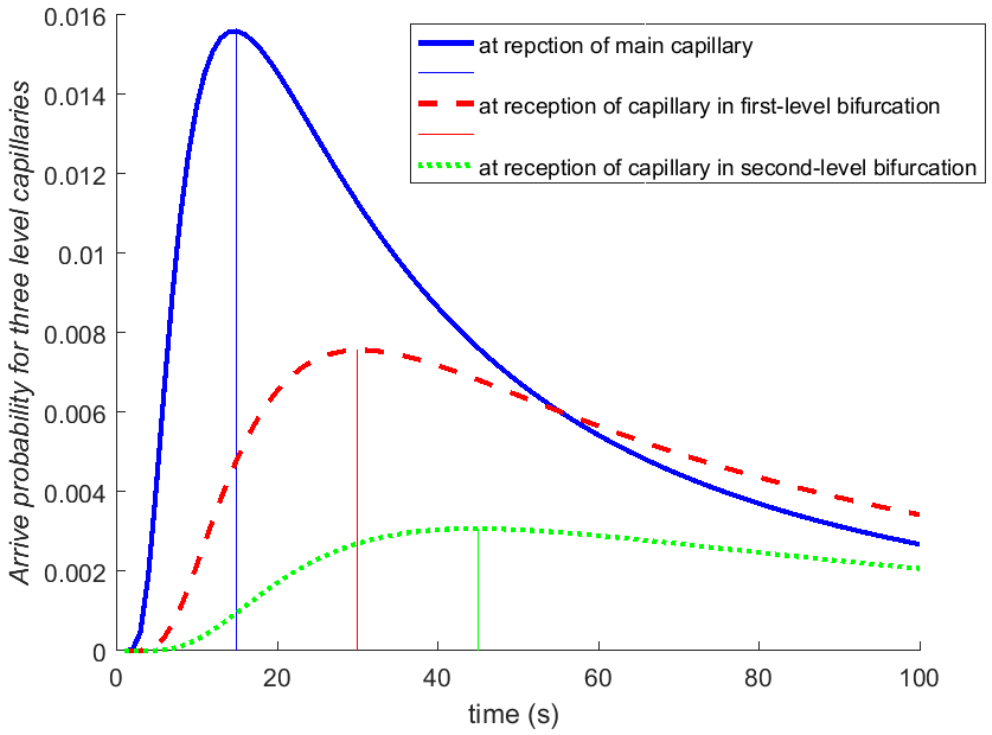

Figure 5.9: Arrival probability for each-level capillaries

In Figure 5.9, we plot the curves of $g(L1, v1, t)$, g(y_n(t)), g(Z_n(t)), which correspond to the molecules' arrival probability at the end of main capillary, first-level capillary branches and second-level capillary branches in symmetric model. We observe that the curves become flat as bifurcation level increases, thus the round trip time of one symbol increases but the maximum arrival probabilities become lower. The mathematical meanings of these curves are taken from the transfer function between transmitter and receivers along the blood capillaries through bifurcations while arrival probabilities reach the maximum at the time t_{max}.

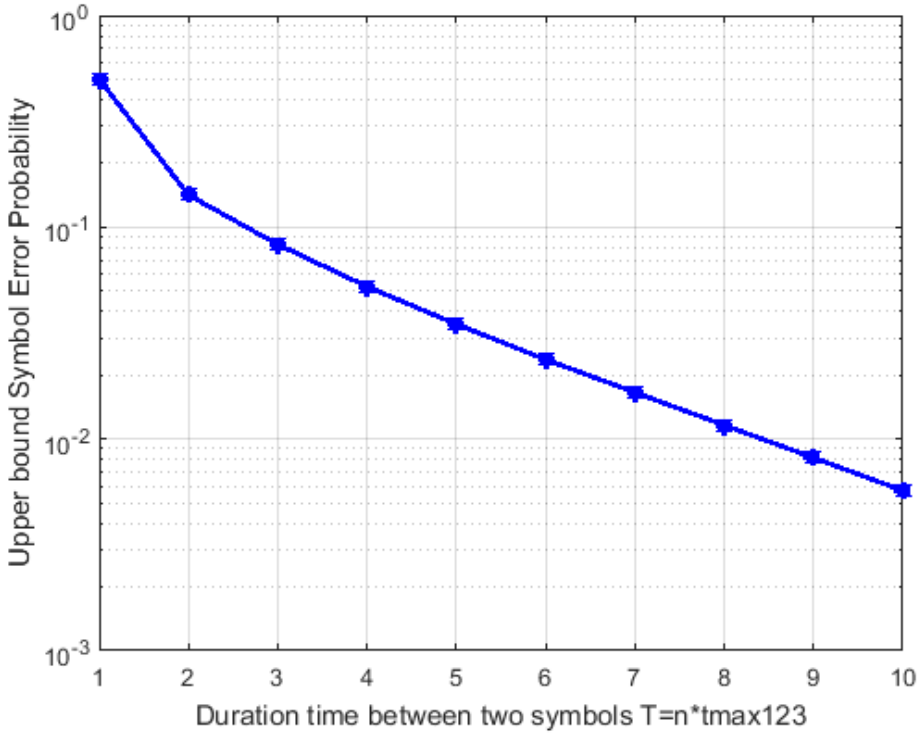

Figure 5.10: Upper bound of error probability for second-level capillary, comparing maximum symbol error probability with the time duration T.

In Figure 5.10, we plot the upper bound of error probability as a function of the time duration between two symbols. We observe that the maximum error probability meliorates with the reduced Inter-symbol Interference(ISI), when time duration increases.

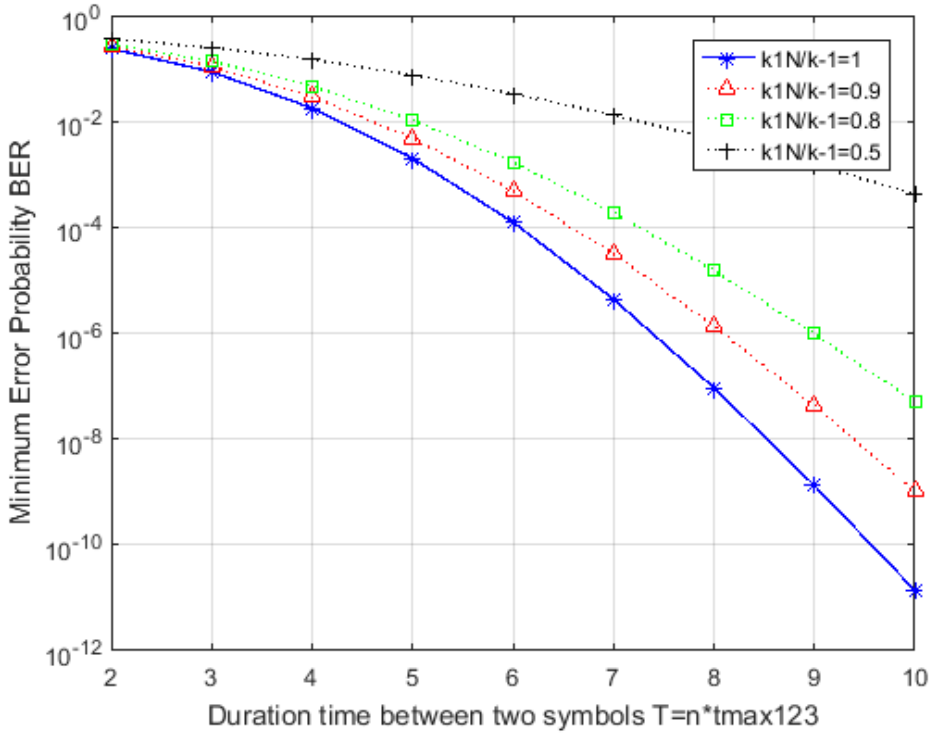

Figure 5.11: Minimum BER plot for second-level capillary in symmetric model, comparing BER with time duration T between two symbols in different receive probabilities.

In Figure 5.11, we plot the minimum error probability against the time duration for different receiving probability at the receivers, setting transmitted molecules with a number of $Q = 5 \times 10^6$. The coding mechanism is the OOK binary system, so the symbol error bit is equal to bit error rate (BER). The results show how the BER in the second-level capillary is very sensitive to different receiving probabilities $B = \frac{k_1 NA}{k_{-1}}$, whereby increasing it from 0.5 s to 1 s can meliorate the BER by several orders of magnitude.

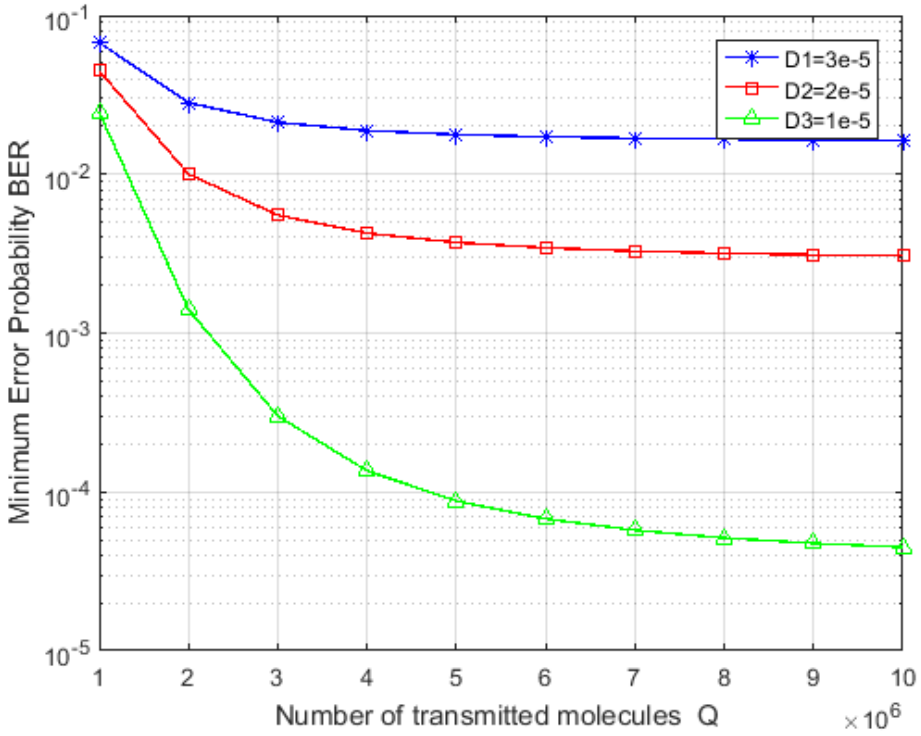

Figure 5.12: Minimum BER plot for second-level capillary in symmetric model, comparing BER with the number of transmitted molecules in different diffusion coefficient values. (time duration $T = 4 \times tmax$)

In Figure 5.12, we demonstrate the effect of the number of transmitted molecules on the minimum BER comparing with the diffusion coefficient D, setting time duration $T = 4 \times tmax$. The plot shows that increasing the number of transmitted molecules Q can improve the performance, slowly approaching the limit of BER performance. Furthermore, in the condition with a certain value of flow velocity, a minor diffusion coefficient will improve the BER performance in an effective manner.

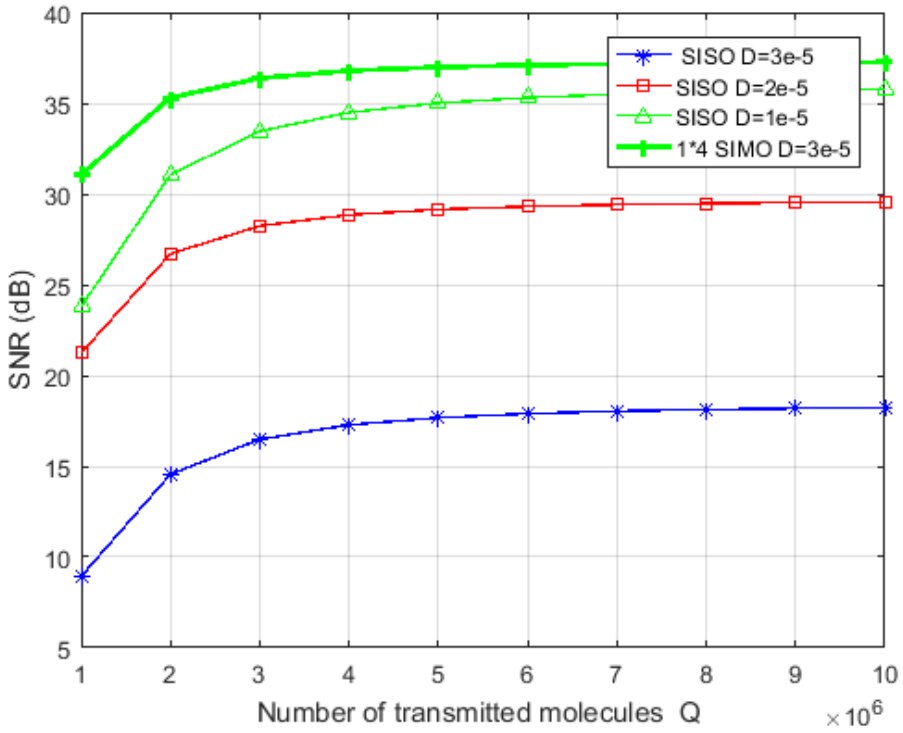

Figure 5.13: SNR plot for second-level capillary in symmetric model, comparing SNR with number of transmitted molecules in different diffusion coefficient values. (time duration $T = 4 \times tmax$)

In Figure 5.13, we plot SNR performance against the number of transmitted molecules Q for different diffusion coefficients D, setting time duration $T = 4 \times tmax$. The results show that the number of transmitted molecules Q increase from 10^6 to 10^7, which can increase SNR $15dB$, when the diffusion coefficient $D = 3 \times 10^{-5}$. Additionally, with the constant number of transmitted molecules being 4×10^6, decreasing the diffusion coefficient from $D = 3 \times 10^{-5}$ to $D = 10^{-5}$, the SNR performance gains by $12dB$.

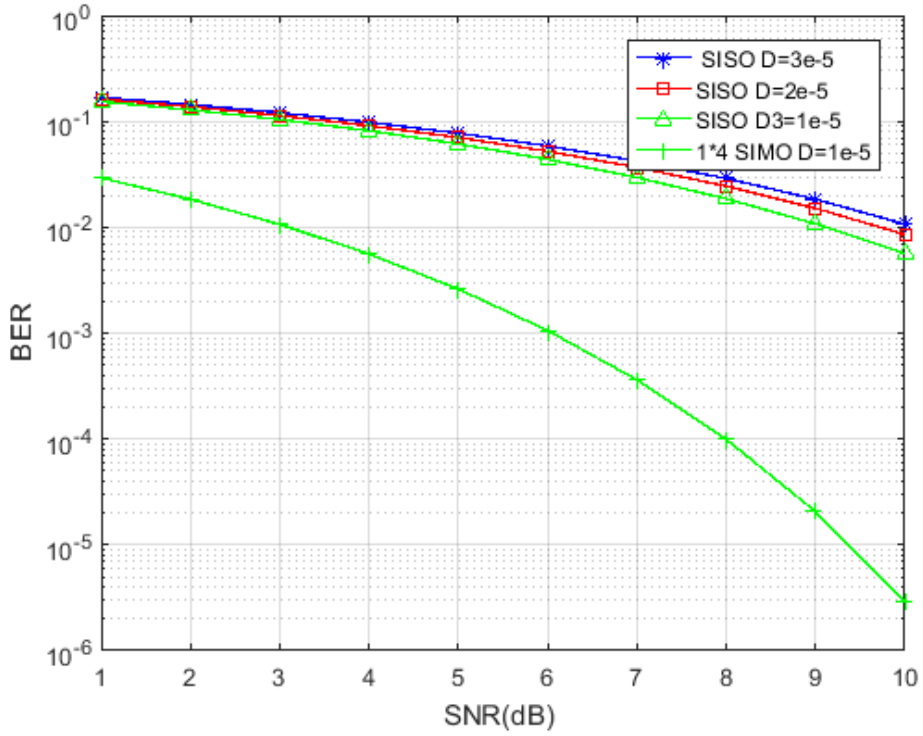

Figure 5.14: BER plot for second-level capillary in symmetric model, comparing BER with SNR in different diffusion coefficients. (time duration $T = 8 \times tmax$)

Figure 5.14 shows the relationship between BER and SNR for different diffusion coefficient D in symmetric model, setting time duration $T = 8 \times tmax$ and the number of transmitted molecules $Q = 10^6$. We can observe that in each second-level capillary, changes in the diffusion coefficient have a minor impact on the SNR to BER performance under the same velocity drift conditions. In the condition of diffusion coefficient $D = 10^{-5}$, at $BER = 10^{-2}$ the SNR performance gain of the SIMO channel with MRC combined techniques compared with the the SISO channel increase by $6dB$ (from $3dB$ to $9dB$).

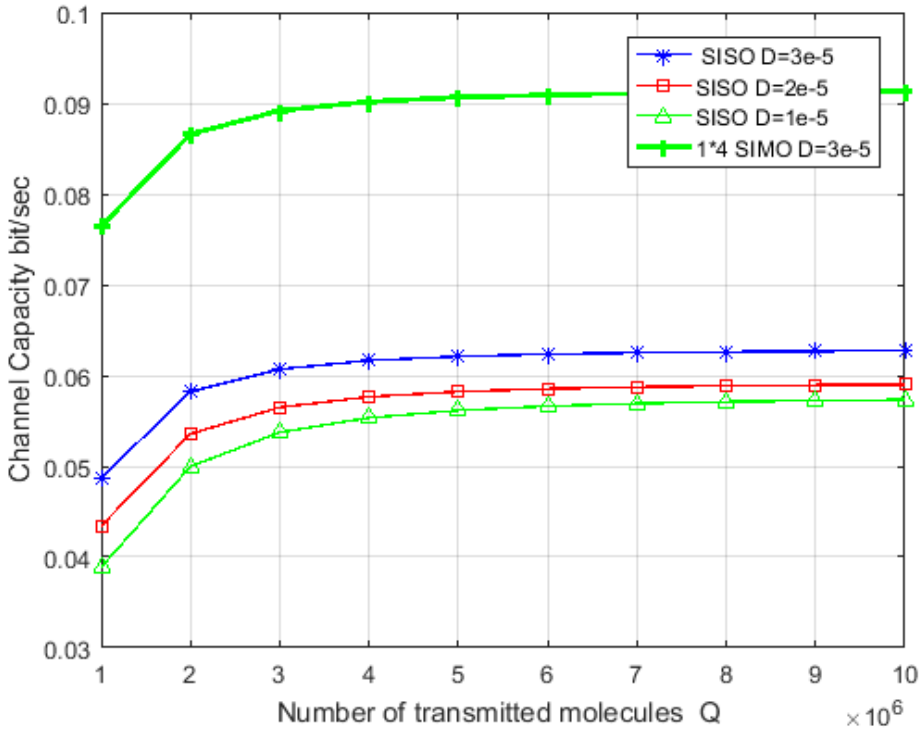

Figure 5.15: Channel capacity plot for second-level capillary in symmetric model, comparing channel capacity C with number of transmitted molecules in different diffusion coefficients. (time duration $T = 4 \times tmax$)

Figure 5.15 demonstrate the channel capacity against the number of transmitted molecules Q for different diffusion coefficient D, setting time duration $T = 4 \times tmax$. Similar to Figure 5.13, channel capacity performance has a positive correlation to SNR for fixed bit rate.

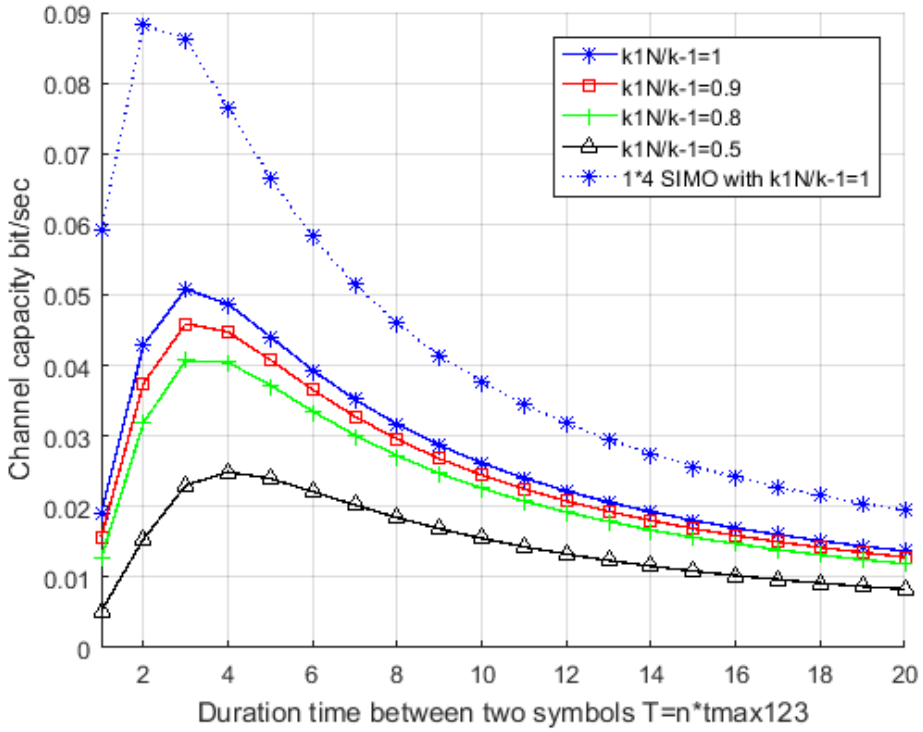

Figure 5.16: Channel capacity plot for second-level capillary in symmetric model, comparing channel capacity C with the time duration T between two symbols in different receiving probabilities.

Figure 5.16 shows the channel capacity varies with time duration T between two symbols in different receiving probabilities. We can observe that a higher receiving probability, channel capacity results in a better performance, whereby increasing it from $0.5s$ to $1s$ can meliorate the channel capacity from 0.025 to 0.05, setting time duration $T = 3 \times tmax$. Moreover, as the time duration T increases, channel capacity increases rapidly and reaches the maximum, when the time duration $T = 3 \times tmax$, then decreases gradually. On one hand, SNR increases as the as the time duration T increases, however, on the other hand, the bandwidth, as the reciprocal of time, decreases.

To obtain optimal channel capacity, we can set the as the time duration $T = 3 \times tmax$.

5.5.2 Non-symmetric Model

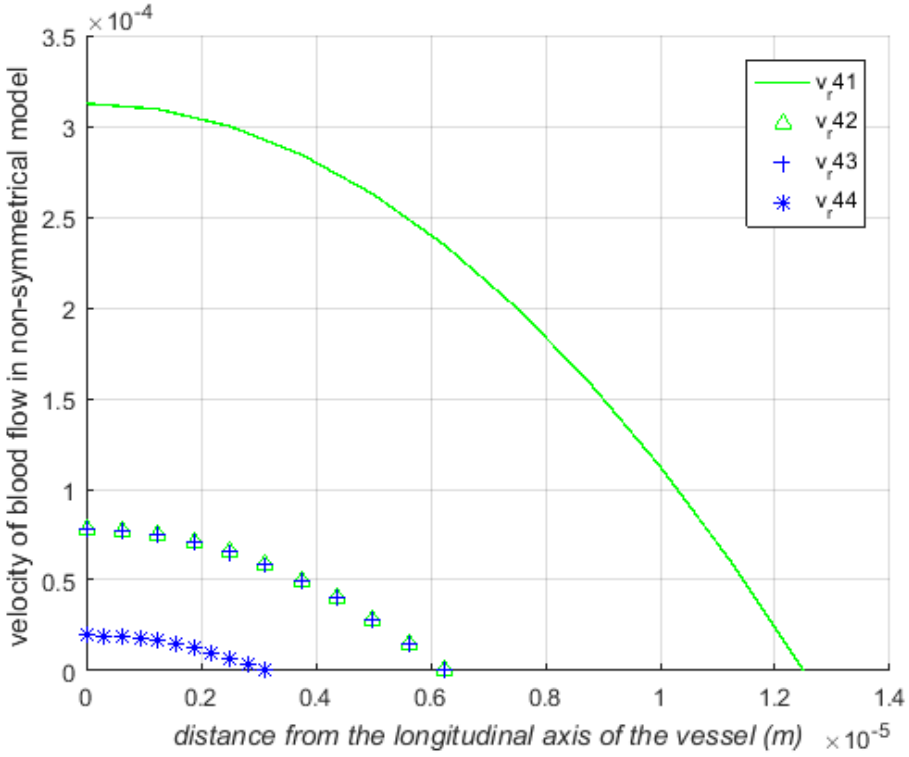

Figure 5.17: Velocity of blood flow in non-symmetric model

In Figure 5.17, we plot the flow velocities of second-level blood capillary branches in the non-symmetric model. According to the illustration in Figure5.7, Z_1 and Z_2 are the daughter capillary branches of first-level capillary Y_1, while Z_3 and Z_4 are the daughter capillary branches of first-level capillary Y_2. Because the angles of Y-shaped bifurcation are not symmetric, velocities of four second-level capillaries Z_1, Z_2, Z_3 and Z_4 are in the order of $v_{41} > v_{42} = v_{43} > v_{44}$.

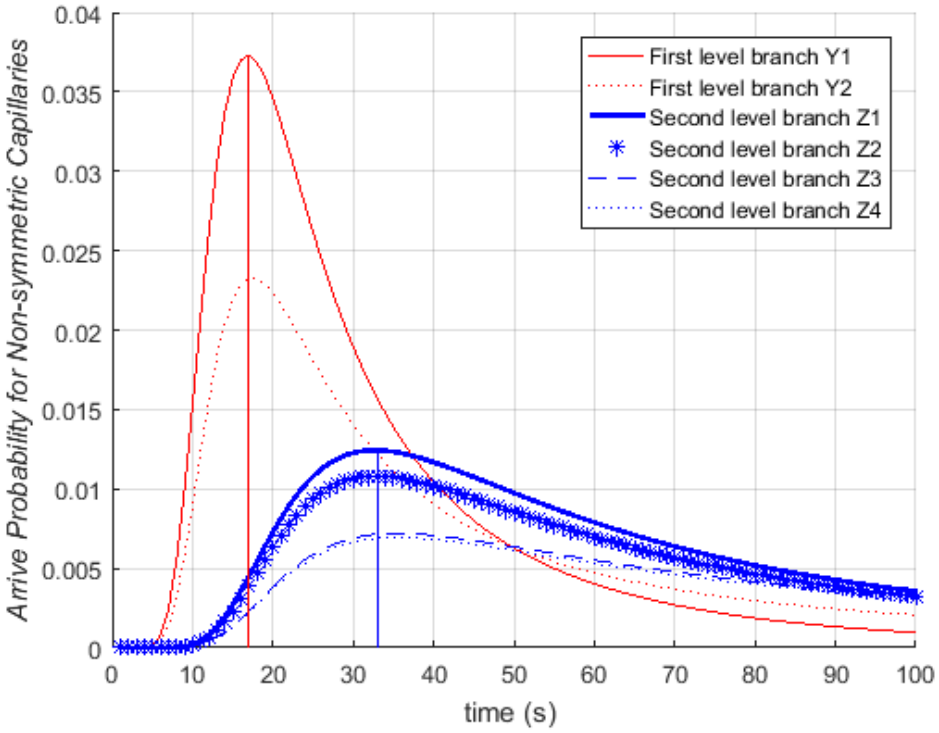

Figure 5.18: Arrival Probability for non-symmetric Capillaries

In Figure 5.18, we plot the arrival PDF for first-level capillaries Y_1 and Y_2, also the second-level capillaries Z_1, Z_2, Z_3 and Z_4 in the non-symmetric model. We can observe that the arrival probability decreases and delay for the round-trip time clearly increases, when compare the curves of second-level capillary with the ones of the first-level capillary.

Furthermore, the time to reach the peak value of arrival probability t_{max} are the same in the same level of capillaries. It is a fundamental discovery that the bifurcation angles and radius will change the velocity of flow, but the time to reach highest arrival probability is the same at the same level. Arrival probability in next level is the convolution of PDF in previous level and PDF in prorogation along this level of capillaries. Compared with the

curves at the same level Z_1,Z_2,Z_3 and Z_4, arrival probability density functions $\mathrm{g(Z_n(t))} = \mathrm{g(L1, v1, t)}*\mathrm{g(L2, v2, t)} * \mathrm{g(L3, v3, t)}$ within the same diffusion coefficient D and lower flow velocities from Z_1 to Z_4, we observe that t_{max} keep the same, while the peak of the curves from Z_1 to Z_4 gradually become broader but are not shifted with time. With this observation, we can estimate the best time duration between two symbols and the bandwidth in return only by the number of bifurcation times, without the flow velocity.

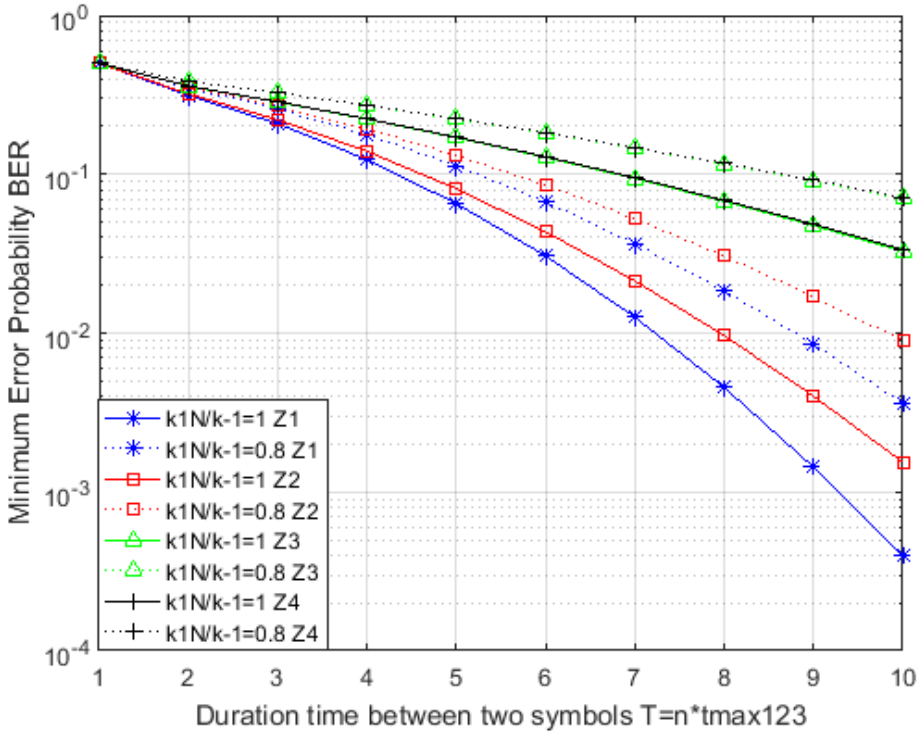

Figure 5.19: Minimum BER plot for second-level capillaries in non-symmetric model, comparing BER of each sub-channel with time duration T between two symbols in different receiving probabilities.

In Figure 5.19, we demonstrate the effect of T time duration in the condition of different receive probabilities on BER performance. Similar to sym-

metrical model in Figure 5.11, higher receive probability deserves better BER performance. In the same condition of receive probability, we observe that Z_1 with the highest flow velocity has much better BER performance than other sub-channel Z_2, Z_3, Z_4, and reached $p_e = 10^{-5}$ when we set time duration to $T = 8 \times tmax$.

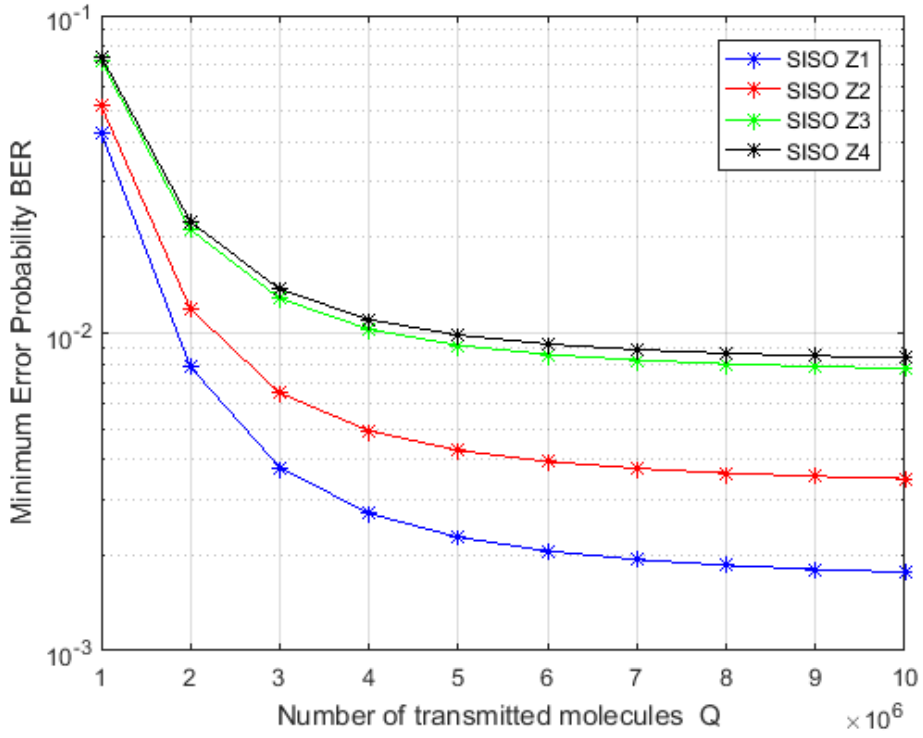

Figure 5.20: Minimum BER plot for second-level capillaries in non-symmetric model, comparing BER with number of transmitted molecules. (time duration $T = 6 \times tmax$)

In Figure 5.20, we plot the BER performance against the number of transmitted molecules Q for non-symmetric model, and set the time duration $T = 6 \times tmax$. Similar to the symmetric model in Figure 5.12, BER performance meliorates as more molecules are transmitted. Second-level cap-

illary Z_1 with the highest flow velocity has the best BER performance reach, while Z_3 BER is close to Z_4 BER.

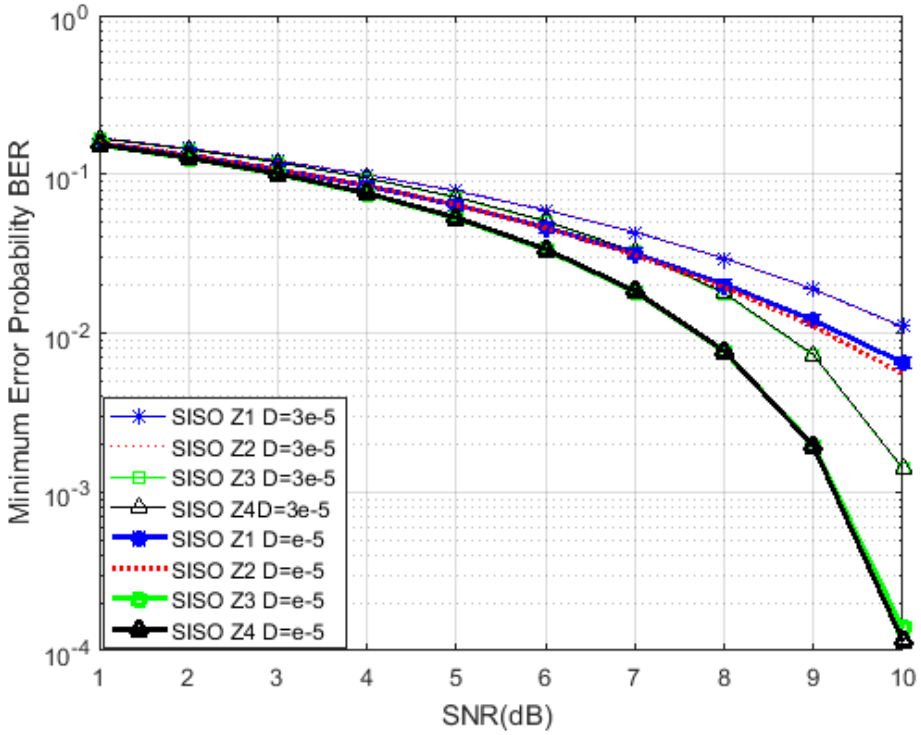

Figure 5.21: Minimum BER plot for second-level capillaries in non-symmetric model, comparing BER of each sub-channel with SNR. (time duration $T = 8 \times tmax$)

In Figure 5.21, we plot BER against SNR for non-symmetric model, compared with different diffusion coefficients D. We observe that a minor diffusion coefficient results in a better BER performance. Furthermore, for the same diffusion coefficient, Z_1 and Z_2 have close SNR to BER performance while Z_3 and Z_4 have a close SNR to BER relationship. For the Z_4 sub-channel with $D = 10^{-3}$, SNR gain from $3dB$ to $10dB$ will improve BER from 10^{-1} to 10^{-5}.

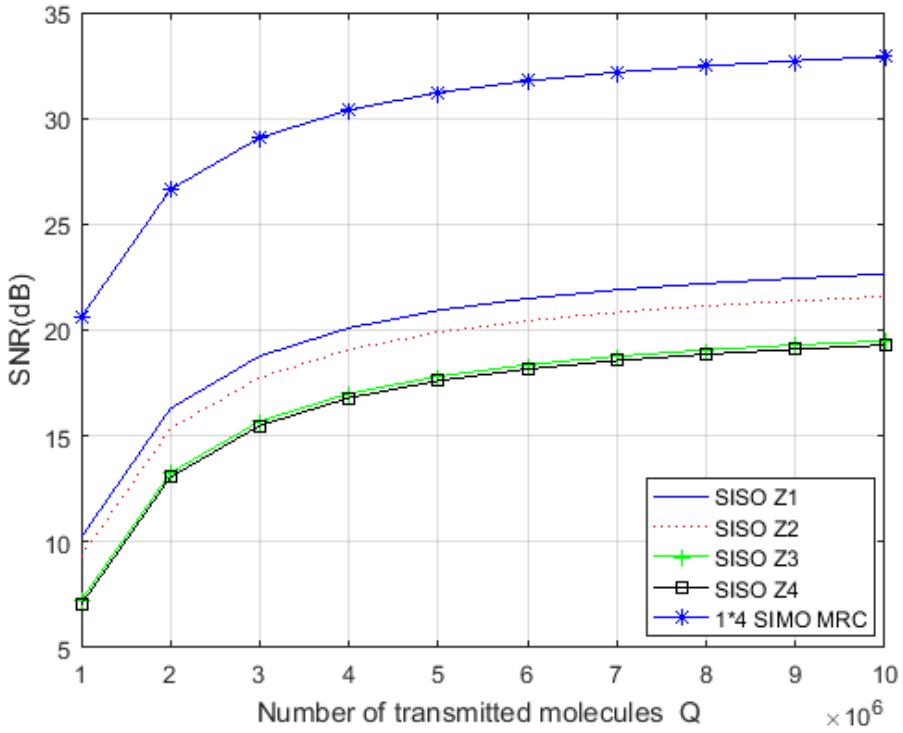

Figure 5.22: SNR plot for second-level capillaries in non-symmetric model, comparing SNR of each sub-channel with number of transmitted molecules Q. (time duration $T = 6 \times tmax$)

In Figure 5.22, we plot SNR against the number of transmitted molecules Q in a non-symmetric model. Z_1 has best SNR performance compared with all the second-level capillaries. SNR increasingly becomes flat as the number Q increases from 10^6 to 10^7, and the average SNR gain is $12dB$.

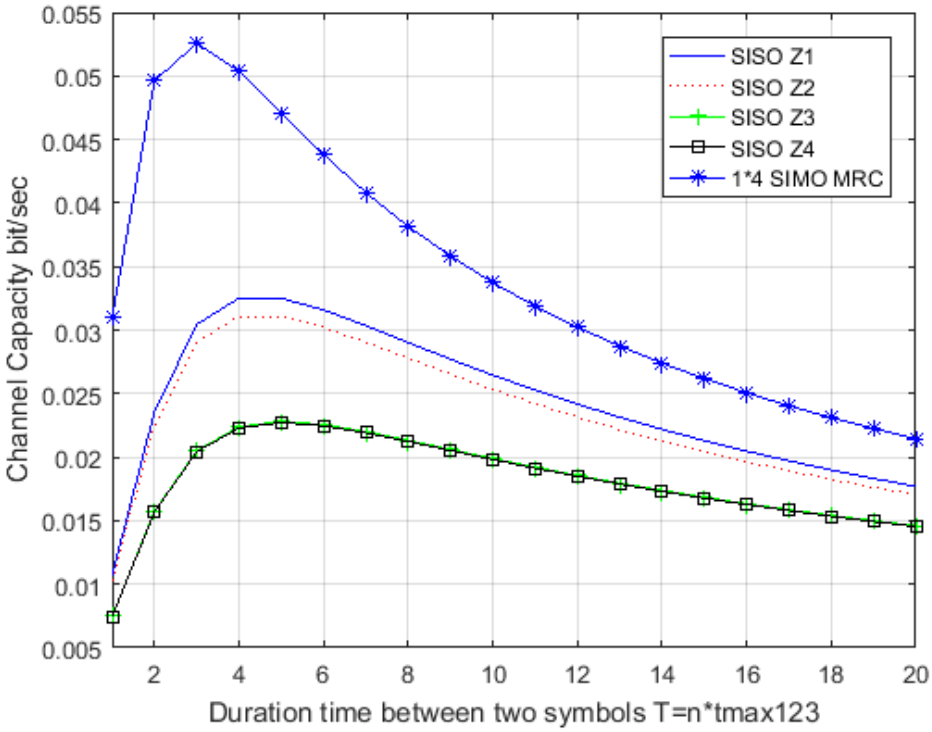

Figure 5.23: Channel capacity plot for second-level capillaries in non-symmetric model, Comparing channel capacity C with time duration T between two symbols.

In Figure 5.23, we plot channel capacity C against the time duration T for Z_1, Z_2, Z_3, Z_4 and combined these channels with MRC combination techniques. Although BER and SNR performance are improved as time duration T increases, bandwidth of the SIMO system $B = \frac{1}{T_s}$ reduces, channel capacity will reach a peak value for $T = 4 \times t_{max}$.

5.6 Chapter Summary

This chapter establishes a single input and multiple outputs (SIMO) blood capillary system with hierarchy and levels of Y-shaped bifurcations. This model provides a further research on the foundation of the blood vessels model with blood flow drift. Moreover, the bifurcation methods are divided into symmetric and non-symmetric models by the angles of the bifurcation. Possible simplification and assumption for this SIMO model have been discussed. The analysis of the interference is fundamental to the design of interference mitigation techniques and increases the performance of communication systems. The Inter Symbol Interference (ISI) and the additive noise at the receivers are jointly analysed for SIMO blood capillaries system under the assumptions of having additive Gaussian noise. The signals at each sub-channel are combined by two spatial diversity combination techniques Maximum-ratio combining (MRC) and Equal-gain combiner (EGC). Numerical results of channel capacity performance in both symmetric and non-symmetric models are analysed within the implementation of diversity combining techniques EGC and MRC. Additionally, BER and SNR performance are analysed regarding different conditions of the time duration between two symbols, the number of molecules that transmitter released and diffusion coefficient. As the bifurcation level increases; the velocity of blood flow decreases, however, it takes the same period to reach the maximum arrival probability for each sub-channel in the same level. Increasing the transmitted molecules number and decreasing the diffusion coefficient will improve the BER and SNR performance.

Due to the need for supplying the tissue demand, it is essential to distribute blood flow within organs properly. The influence of red blood cells is fundamental in the non-Newton model, which is more realistic and under future consideration for inclusion. Moreover, future work will establish a more reliable capillary microcirculation system distributed in the body under the influence of oxygen concentration.

Chapter 6

Conclusion and Future Work

6.1 Conclusion

The rising popularity of molecular communication (MC) has been accompanied by the development of intelligent bio-inspired nanotechnology-enabled devices, namely nano-machines. MC realises the exchange of molecular information through the coding, emission, propagation, reception and decoding processes, and it is proposed as a feasible solution for nano-networks. The idea behind MC is motivated by biological communication, such as intracellular and intercellular communication. Thanks to the feasibility of MC in biological environments, MC has the potential to be the enabling technology for a wide range of applications, mostly in the medical and biological engineering, but also in the industrial and environmental monitoring fields. Especially, Blood capillary-based MC, as a long-range communication in the human body, is also a potential for biomedical applications, such as the drug delivery, angiography and angiogenesis.

The focus of this PhD thesis is on the channel modelling of blood capillary-based MC, where the molecules' information is exchanged for their ubiquitous distribution network in the human body. This choice is motivated by an analysis of the literature, which identifies the blood capillary modelling,

as a fundamental and promising long-range application in MC, has not had sufficient research compared with other basic MC systems, which including diffusion and neuron-based MC. Moreover, channel modelling of blood capillary-based MC builds a complete understanding of the blood capillaries or vessels from the ground up, which is vital to drug delivery application in MC.

The objectives of the research presented in this thesis are to model the blood capillary-based MC paradigm from communication engineering and information theory and to provide analysis to the modelling and performance of this type of MC. First, a diffusion-based blood capillary model in the frequency domain is realised to investigate the processes, involving vesicle releasing, propagating, and receiving. Second, a SISO diffusion with blood flow drift model in the time domain is established, which involves the endocrine phenomenon within the blood vessels consisting of CD40 molecules emission from the platelets, propagating in the flow of blood vessels and received by the CD40L. Third, a SIMO blood capillary system with hierarchy and levels of Y-shaped bifurcations is provided, with the analysis of ISI interference as well as the BER, SNR and channel capacity performances. The main contributions included in each chapter of this PhD thesis are summarised as follows.

The main contributions in Chapter 3 are devoted to the diffusion-based blood capillary MC in the frequency domain, and are summarised as follows:

- This thesis provides an interpretation of endocrine phenomenon to blood capillary diffusion-based MC in terms of three processes: namely, vesicle release, propagation, and reception.

- Differing from previous literature in macroscopic, this thesis studies the vesicle diffusion process by microscopic Langevin equation, for which it is possible to derive the input-output transfer function in frequency domain.

- This thesis provides the derivation of the Green's function for Langevin equation and analysis Langevin diffusion with the Spectral Density of velocity dissipation as well as the displacement characteristics regarding velocity.

- This thesis provides a closed-form expression of channel capacity of the overall system then analyses the performance concerning biological and physical parameters, such as temperature and viscosity.

Through the simulation results from this diffusion-based blood capillary model, we observe that viscosity of blood fluid is sensitive to the performance. Increasing the number of vesicles in RRP, the entropy of input is increased thus channel capacity is increased. Moreover, Pure diffusion model ignores the drift is not suitable to model the blood vessels or capillaries. So in Chapter 4, this thesis provides an improved method used a generalised Langevin equation with colour noise term to model the diffusion with flow drift.

The main contributions in Chapter 4 are focused a SISO model for diffusion with blood flow drift system in the time domain, and are summarised as follows:

- This thesis provides a decomposition of the molecule diffusion with blood flow drift into two main processes; namely, the diffusion and the laminar blood flow drift; and a generalised Langevin equation with a colour noise term is used in the statistical mechanic's approach.

- This thesis presents a derivation of the relationship between the Langevin equation and its corresponding Fokker-Planck equation and the expression of the drift coefficient and the diffusion coefficient from statistical mechanics theory.

- With appropriate assumptions and boundary conditions, this thesis provides the solution of Fokker-Planck equation for the transmission

process. Then it presents a closed-form expression of channel capacity of the diffusion with drift blood vessel MC system in time domain.

- With the numerical results, this thesis provides an analysis of channel capacity regarding the physical parameters in the blood vessels, such as flow velocity, the length of blood vessels, the diffusion coefficient and pressure differential along the vessels.

Through the simulation results, we learn how the performance of a diffusion with flow drift blood vessel MC system depend on the flow velocity, the length and radius of blood vessels, the diffusion coefficient and pressure differential along the vessels. In particular, we observe that capacity reaches the maximum when prior probability $p = 0.4$, which is different from the channel capacity reaches the maximum with prior probability $P = 0.5$ in Shannon's theory.

The main contributions Chapter 5 are focused on a SIMO blood capillary system with hierarchy and levels of Y-shaped bifurcations, which also involves a joint analysis of the Inter-symbol interference and noises affection to threshold detection, BER and SNR performance. As a consequence, with diversity combination techniques, this thesis provides an analysis of the channel capacity for the overall SIMO system.

- This thesis provides two bifurcation methods: symmetric and non-symmetric models by the angles of the bifurcation. We must note that possible simplifications and assumptions for this SIMO model have been discussed.

- Joint analysis the Inter-Symbol Interference (ISI) and noises affection is presented to determine threshold detection for a SIMO blood capillary system.

- This thesis provides a derivation the probability density function for the transfer function of channels from Input-output through the first

order and second order bifurcations.

- This thesis provides BER, SNR, and channel capacity performance analysis with the implementation of diversity combining techniques EGC and MRC.

Through the numerical results, we can learn that channel capacity performance in both symmetric and non-symmetric models are analysed within the implementation of diversity combining techniques EGC and MRC. Additionally, BER and SNR performance are analysed regarding different conditions of the time duration between two symbols, the number of molecules that transmitter released and diffusion coefficient. We also observe that as the bifurcation level increases; the velocity of blood flow decreases, however, it takes the same period to reach the maximum arrival probability for each sub-channel in the same level. This fundamental discovery could be used to determine the bifurcation levels of capillary network and estimate the sites and location of bifurcations, which may have a profound implication for applications of medicine, angiography and angiogenesis.

6.2 Future Work

In the future, we plan to extend my research on molecular communication in following directions:

In the Modelling aspect:

1. Since the models of this thesis are based on the Newtonian model, non-Newtonian models, such as Casson model should be considered. Moreover, the influence of red blood cells and white blood cells should be jointly considered. Thus the comprehensive non-Newtonian model is more realistic, which involving the concentration of oxygen, red blood cells and white blood cells.

2. Expand this SIMO model with junction processes to model the blood leaves the capillaries and moves through the veins, which become larger and larger to carry the blood back to the heart. Thus the overall microcirculatory circuit can be modelled in an integrated network.

In application-specific aspect:

3. We will investigate the discovery in Chapter 5 and then implement the application in the area of image processing to self-detect the bifurcations in the capillary system.

4. We will carry on the research of intrabody molecular communication networks to the whole cardiovascular systems, for the realisation of molecular communication networks for drug-delivery systems.

5. According to the new research in last month [142], they provide a method for generating electricity from blood flow using a tiny fibre spun from carbon nanotubes. The idea is that the fibre could be implanted in a blood vessel to harvest the energy from flowing blood. We will investigate the study of other molecular communication architectures, such as carbon nano-tube (CNT)-based MC. Then we can establish a combined system with blood capillary-based MC and CNT-based MC for future applications.

Bibliography

[1] T. Nakano, M. Moore, A. Enomoto, and T. Suda, *Biological Functions for Information and Communication Technologies*, vol. 320. 2011.

[2] T. Nakano, M. J. Moore, F. Wei, A. V. Vasilakos, and J. Shuai, "Molecular communication and networking: Opportunities and challenges," *IEEE Transactions on Nanobioscience*, vol. 11, no. 2, pp. 135–148, 2012.

[3] I. F. Akyildiz, F. Brunetti, and C. Blázquez, "Nanonetworks: A new communication paradigm," *Computer Networks*, vol. 52, no. 12, pp. 2260–2279, 2008.

[4] T. Nakano, A. W. Eckford, and T. Haraguchi, *Molecular communication*. Cambridge University Press, 2013.

[5] T. Nakano, T. Suda, T. Koujin, T. Haraguchi, and Y. Hiraoka, "Molecular Communication through Gap Junction Channels," *Transactions on Computational Systems Biology X*, vol. 5410, pp. 81–99, 2008.

[6] T. Nakano, M. Moore, A. Enomoto, and T. Suda, "Molecular communication technology as a biological ICT," *Studies in Computational Intelligence*, vol. 320, pp. 49–86, 2011.

[7] D. Malak and O. B. Akan, "Molecular communication nanonetworks inside human body," *Nano Communication Networks*, vol. 3, pp. 19–35, mar 2012.

[8] C. T. Ying, J. Wang, R. J. Lamm, and D. T. Kamei, "Mathematical modeling of vesicle drug delivery systems 2: targeted vesicle interactions with cells, tumors, and the body.," *Journal of laboratory automation*, vol. 18, pp. 46–62, feb 2013.

[9] W. F. Boron and E. L. Boulpaep, *Medical physiology: a cellular and molecular approach*. 2009.

[10] D. Marino, J. Luginbuhl, S. Scola, M. Meuli, and E. Reichmann, "Bioengineering Dermo-Epidermal Skin Grafts with Blood and Lymphatic Capillaries," *Science Translational Medicine*, vol. 6, no. 221, pp. 221ra14–221ra14, 2014.

[11] R. P. Feynman, "There ' s Plenty of Room at the Bottom," *Journal of Microeleciromechanical Systems*, vol. 1, no. 1, pp. 60–66, 1992.

[12] S. Hiyama, Y. Moritani, T. Suda, R. Egashira, a. Enomoto, M. Moore, and T. Nakano, "Molecular Communication," *Journal-Institute of Electronics Information and Communication Engineers*, vol. 3, pp. 391–394, 2006.

[13] T. Nakano, T. Suda, Y. Okaie, M. J. Moore, and A. V. Vasilakos, "Molecular communication among biological nanomachines: A layered architecture and research issues," *IEEE Transactions on Nanobioscience*, vol. 13, no. 3, pp. 169–197, 2014.

[14] A. Einolghozati, M. Sardari, and F. Fekri, "Decode and Forward Relaying in Diffusion-based Molecular Communication Between Two Populations of Biological Agents," pp. 3986–3991, 2014.

[15] I. Engineering, "Politecnico di Milano Encoding and Soft Decoding in Molecular Communication based on Biological Circuits," 2016.

[16] N. Farsad, N.-r. Kim, A. W. Eckford, and C.-B. Chae, "Channel and Noise Models for Nonlinear Molecular Communication Systems," *Arxiv*, vol. 32, no. 12, p. 10, 2013.

[17] S. Hiyama, Y. Moritani, and T. Suda, "A biochemically-engineered molecular communication system," in *Lecture Notes of the Institute for Computer Sciences, Social-Informatics and Telecommunications Engineering*, vol. 3 LNICST, pp. 85–94, 2009.

[18] J. Clausen, "Man, machine and in between.," *Nature*, vol. 457, no. 7233, pp. 1080–1081, 2009.

[19] Y. Chahibi, M. Pierobon, S. O. Song, and I. F. Akyildiz, "A molecular communication system model for particulate drug delivery systems," *IEEE Transactions on Biomedical Engineering*, vol. 60, no. 12, pp. 3468–3483, 2013.

[20] Y. Chahibi and I. F. Akyildiz, "Molecular communication noise and capacity analysis for particulate drug delivery systems," *IEEE Transactions on Communications*, vol. 62, no. 11, pp. 3891–3903, 2014.

[21] L. Parcerisa Giné and I. F. Akyildiz, "Molecular communication options for long range nanonetworks," *Computer Networks*, vol. 53, pp. 2753–2766, nov 2009.

[22] M. Pierobon and I. F. Akyildiz, "Capacity of a diffusion-based molecular communication system with channel memory and molecular noise," *IEEE Transactions on Information Theory*, vol. 59, no. 2, pp. 942–954, 2013.

[23] Q. Liu and K. Yang, "Multiple-access channel capacity of diffusion and ligand-based molecular communication," *Proceedings of the 16th ACM international conference on Modeling, analysis & simulation of wireless and mobile systems - MSWiM '13*, pp. 151–158, 2013.

[24] M. Pierobon and I. F. Akyildiz, "A statistical-physical model of interference in diffusion-based molecular nanonetworks," *IEEE Transactions on Communications*, vol. 62, no. 6, pp. 2085–2095, 2014.

[25] B. Atakan and O. B. Akan, "Single and multiple-access channel capacity in molecular nanonetworks," in *Lecture Notes of the Institute for Computer Sciences, Social-Informatics and Telecommunications Engineering*, vol. 20 LNICST, pp. 14–23, 2009.

[26] M. Moore, A. Enomoto, T. Nakano, R. Egashira, T. Suda, A. Kayasuga, H. Kojima, H. Sakakibara, and K. Oiwa, "A Design of a Molecular Communication System for Nanomachines Using Molecular Motors," *Fourth Annual IEEE International Conference on Pervasive Computing and Communications Workshops (PERCOMW'06)*, pp. 554–559, 2006.

[27] M. Gregori and I. F. Akyildiz, "A new NanoNetwork architecture using flagellated bacteria and catalytic nanomotors," *IEEE Journal on Selected Areas in Communications*, vol. 28, no. 4, pp. 612–619, 2010.

[28] S. Hiyama and Y. Moritani, "Molecular communication: Harnessing biochemical materials to engineer biomimetic communication systems," *Nano Communication Networks*, vol. 1, no. 1, pp. 20–30, 2010.

[29] K. Darchini and A. S. Alfa, "Molecular communication via microtubules and physical contact in nanonetworks: A survey," 2013.

[30] S. Balasubramaniam, S. Ben-Yehuda, S. Pautot, A. Jesorka, P. Lio', and Y. Koucheryavy, "A review of experimental opportunities for molecular communication," *Nano Communication Networks*, vol. 4, no. 2, pp. 43–52, 2013.

[31] T. Nakano, T. Suda, Y. Okaie, M. J. Moore, and A. V. Vasilakos, "Molecular communication among biological nanomachines: A lay-

ered architecture and research issues," *IEEE Transactions on Nanobioscience*, vol. 13, no. 3, pp. 169–197, 2014.

[32] N. Farsad, H. B. Yilmaz, A. Eckford, C.-B. Chae, and W. Guo, "A Comprehensive Survey of Recent Advancements in Molecular Communication," *IEEE Communications Surveys & Tutorials*, vol. 18, no. 3, pp. 1887–1919, 2016.

[33] D. Malak and O. B. Akan, "Synaptic interference channel," *2013 IEEE International Conference on Communications Workshops, ICC 2013*, pp. 771–775, 2013.

[34] B. Alberts, A. Johnson, J. Lewis, M. Raff, K. Roberts, and P. Walter, *Molecular Biology of the Cell*. 2002.

[35] T. Nakano and J.-q. Liu, "Information Transfer through Calcium Signaling," *Nano-Net*, pp. 29–33, 2009.

[36] M. J. Berridge, M. D. Bootman, and H. L. Roderick, "Calcium: Calcium signalling: dynamics, homeostasis and remodelling," *Nature Reviews Molecular Cell Biology*, vol. 4, no. 7, pp. 517–529, 2003.

[37] A. Enomoto, M. Moore, T. Nakano, R. Egashira, and T. Suda, "A molecular communication system using a network of cytoskeletal filaments .," *Communication*, vol. 1, pp. 725–728, 2006.

[38] S. Hiyama, Y. Isogawa, T. Suda, Y. Moritani, and K. Sutoh, "A Design of an Autonomous Molecule Loading/Transporting/Unloading System Using DNA Hybridization and Biomolecular Linear Motors," *Dans European Nano Systems Worshop*, pp. 3–5, 2007.

[39] Y. Hiratsuka, T. Tada, K. Oiwa, T. Kanayama, and T. Q. Uyeda, "Controlling the direction of kinesin-driven microtubule movements along microlithographic tracks.," *Biophysical journal*, vol. 81, no. 3, pp. 1555–1561, 2001.

[40] T. Nakagaki, H. Yamada, and A. Tóth, "Maze-solving by an amoeboid organism.," *Nature*, vol. 407, no. 6803, p. 470, 2000.

[41] S. Song, K. D. Miller, and L. F. Abbott, "Competitive Hebbian learning through spike-timing-dependent synaptic plasticity.," *Nature neuroscience*, vol. 3, no. 9, pp. 919–926, 2000.

[42] P. P. Ray, "Nano computer design based on intra body nanoscale neuro-spike communication: A nanonetwork paradigm," in *Proceedings of the 2012 International Conference on Communications, Devices and Intelligent Systems, CODIS 2012*, pp. 306–309, 2012.

[43] M. Bear, M; Connors, B; Paradiso, "NEUROSCIENCE Exploring the Brain," *Lippincott Williams & Wilkins*, no. 1, pp. 1–5, 2014.

[44] E. Purves D, Augustine GJ, Fitzpatrick D, et al., "Neuroscience," *Sunderland (MA): Sinauer Associates*, 2001.

[45] R. Llinás, I. Z. Steinberg, and K. Walton, "Relationship between presynaptic calcium current and postsynaptic potential in squid giant synapse," *Biophysical Journal*, vol. 33, no. 3, pp. 323–351, 1981.

[46] E. Balevi and O. B. Akan, "A physical channel model for nanoscale neuro-spike communications," *IEEE Transactions on Communications*, vol. 61, no. 3, pp. 1178–1187, 2013.

[47] A. Guney, B. Atakan, and O. B. Akan, "Mobile ad hoc nanonetworks with collision-based molecular communication," *IEEE Transactions on Mobile Computing*, vol. 11, no. 3, pp. 353–366, 2012.

[48] D. Malak, M. Kocaoglu, and O. B. Akan, "Communication theoretic analysis of the synaptic channel for cortical neurons," *Nano Communication Networks*, vol. 4, no. 3, pp. 131–141, 2013.

[49] J. Lee and D. H. Cho, "Capacity analysis of neuro-spike communication system for nanonetworks," in *Procedia Computer Science*, vol. 37, pp. 428–433, 2014.

[50] K. Aghababaiyan and B. Maham, "Error probability analysis of neuro-spike communication channel," *2017 IEEE Symposium on Computers and Communications (ISCC)*, pp. 932–937, 2017.

[51] A. Fallis, *Harrison's Principles of Internal Medicine*, vol. II. 2015.

[52] N. Pottier, "Chapter 10 Brownian motion: the Langevin Model," *Nonequilibrium statistical physics: linear irreversible processes*, 2009.

[53] E. Nelson, "Dynamical Theories of Brownian Motion," *Mathematical Notes*, vol. 131, no. 6, pp. 2381–2396, 1967.

[54] S. Berghout, "The Einstein Smoluchowski Equation in the One Dimensional Exclusion Process," 2013.

[55] J. Philibert, "One and a half century of diffusion: Fick, Einstein, before and beyond," *Diffusion Fundamentals*, vol. 4, pp. 1–19, 2005.

[56] K. Sekimoto, " Langevin Equation and Thermodynamics ," 1998.

[57] J. W. Westwater and H. G. Drickamer, "The Mathematics of Diffusion," *Journal of the American Chemical Society*, vol. 79, no. 5, pp. 1267–1268, 1957.

[58] Q. Liu, K. Yang, and S. Leng, "Channel Capacity Analysis for Molecular Communication with Different Emission Schemes,"

[59] B. Atakan and O. B. Akan, "On Channel Capacity and Error Compensation in Molecular Communication," *Transactions on Computational Systems Biology X*, pp. 59–80, 2008.

[60] M. Pierobon, "A systems-theoretic model of a biological circuit for molecular communication in nanonetworks," *Nano Communication Networks*, vol. 5, no. 1-2, pp. 25–34, 2014.

[61] M. Pierobon and I. F. Akyildiz, "Fundamentals of Diffusion-Based Molecular Communication in Nanonetworks," *Foundations and Trends® in Networking*, vol. 8, no. 1-2, pp. 1–147, 2012.

[62] K. V. Srinivas, A. W. Eckford, and R. S. Adve, "Molecular communication in fluid media: The additive inverse gaussian noise channel," *IEEE Transactions on Information Theory*, vol. 58, no. 7, pp. 4678–4692, 2012.

[63] B. Tepekule, A. E. Pusane, H. B. Yilmaz, C. Chae, and T. Tugcu, "ISI Mitigation Techniques in Molecular Communication," *Arxiv*, vol. 7804, no. c, pp. 1–30, 2015.

[64] A. Singhal, R. K. Mallik, and B. Lall, "Effect of Molecular Noise in Diffusion-Based Molecular Communication," vol. 3, no. 5, pp. 489–492, 2014.

[65] R. Barry and D. Ivanov, "Microfluidics in biotechnology," *Journal of nanobiotechnology*, vol. 2, no. 1, p. 2, 2004.

[66] T. Nitta, A. Tanahashi, M. Hirano, and H. Hess, "Simulating molecular shuttle movements: towards computer-aided design of nanoscale transport systems.," *Lab on a chip*, vol. 6, no. 7, pp. 881–885, 2006.

[67] F. Gentile, M. Ferrari, and P. Decuzzi, "The transport of nanoparticles in blood vessels: The effect of vessel permeability and blood rheology," *Annals of Biomedical Engineering*, vol. 36, no. 2, pp. 254–261, 2008.

[68] A. Mernone, J. Mazumdar, and S. Lucas, "A mathematical study of peristaltic transport of a casson fluid," *Mathematical and Computer Modelling*, vol. 35, pp. 895–912, apr 2002.

[69] J. Venkatesan, D. S. Sankar, K. Hemalatha, and Y. Yatim, "Mathematical Analysis of Casson Fluid Model for Blood Rheology in Stenosed Narrow Arteries," *Journal of Applied Mathematics*, vol. 2013, pp. 1–11, 2013.

[70] R. Bali, "A Casson Fluid Model for Multiple Stenosed Artery in the Presence of Magnetic Field," *Applied Mathematics*, vol. 03, no. 05, pp. 436–441, 2012.

[71] L. Felicetti, M. Femminella, and G. Reali, "Establishing digital molecular communications in blood vessels," *2013 First International Black Sea Conference on Communications and Networking (BlackSeaCom)*, pp. 54–58, jul 2013.

[72] L. Felicetti, M. Femminella, and G. Reali, "Simulation of molecular signaling in blood vessels: Software design and application to atherogenesis," *Nano Communication Networks*, vol. 4, pp. 98–119, sep 2013.

[73] L. Felicetti, M. Femminella, G. Reali, P. Gresele, M. Malvestiti, and J. N. Daigle, "Modeling CD40-based molecular communications in blood vessels," *IEEE Transactions on Nanobioscience*, vol. 13, no. 3, pp. 230–243, 2014.

[74] L. Felicetti, M. Femminella, V. G. Duranti, and P. Liò, "A Molecular Communication System in Blood Vessels for Tumor Detection," 2014.

[75] W. Hundsdorfer, "Numerical Solution of Advection-Diffusion-Reaction Equations," *Lecture*, pp. 1–122, 2000.

[76] E. L. Cussler, "Diffusion: Mass Transfer in Fluid Systems," *Engineering*, vol. Second, p. 580, 1997.

[77] F. Mainardi and P. Pironi, "The Fractal Brownian Motions.pdf," 1996.

[78] S. Wang, W. Guo, S. Qiu, and M. D. McDonnell, "Performance of macro-scale molecular communications with sensor cleanse time," *2014 21st International Conference on Telecommunications, ICT 2014*, pp. 363–368, 2014.

[79] H. Mahdavifar and A. Beirami, "Diffusion Channel with Poisson Reception Process : Capacity Results and Applications," no. 2, pp. 1956–1960, 2015.

[80] J. Ahlqvist, "Atherosclerosis, and Newton, Poiseuille, Reynolds and Prandtl.," *Medical hypotheses*, vol. 57, no. 4, pp. 446–52, 2001.

[81] N. J. Quinlan and P. N. Dooley, "Models of flow-induced loading on blood cells in laminar and turbulent flow, with application to cardiovascular device flow," *Annals of Biomedical Engineering*, vol. 35, no. 8, pp. 1347–1356, 2007.

[82] W. T. Coffey, Y. P. Kalmykov, and J. T. Waldron, "The Langevin Equation With Applications to Stochastic Problems in Physics, Chemistry and Electrical Engineering," *Chemical Physics*, vol. 14, no. SEPTEMBER, p. 678, 2004.

[83] X. Xing, "Dynamic statistical information theory," *Science in China Series G*, vol. 49, no. 1, pp. 1–37, 2006.

[84] K. S. Fa, "Solution of Fokker-Planck equation for a broad class of drift and diffusion coefficients," *Physical Review E - Statistical, Nonlinear, and Soft Matter Physics*, vol. 84, no. 1, 2011.

[85] B. Atakan and O. B. Akan, "Single and multiple-access channel capacity in molecular nanonetworks," in *Lecture Notes of the Institute for Computer Sciences, Social-Informatics and Telecommunications Engineering*, vol. 20 LNICST, pp. 14–23, 2009.

[86] S. Kadloor, R. S. Adve, and A. W. Eckford, "Molecular Communication Using Brownian Motion with Drift," pp. 1–19, 2011.

[87] P. Charoenphol, R. B. Huang, and O. Eniola-Adefeso, "Potential role of size and hemodynamics in the efficacy of vascular-targeted spherical drug carriers," *Biomaterials*, vol. 31, no. 6, pp. 1392–1402, 2010.

[88] M. Pierobon and I. F. Akyildiz, "A physical end-to-end model for molecular communication in nanonetworks," *IEEE Journal on Selected Areas in Communications*, vol. 28, no. 4, pp. 602–611, 2010.

[89] J. W. Piper, R. a. Swerlick, and C. Zhu, "Determining force dependence of two-dimensional receptor-ligand binding affinity by centrifugation.," *Biophysical Journal*, vol. 74, no. 1, pp. 492–513, 1998.

[90] J. Tan, T. Antony, and Y. Liu, "Influence of Red Blood Cells on Nanoparticle Targeted Delivery," pp. 1934–1946, 2012.

[91] B. C. Fry, T. K. Roy, and T. W. Secomb, "Capillary recruitment in a theoretical model for blood flow regulation in heterogeneous microvessel networks.," *Physiological reports*, vol. 1, no. 3, p. e00050, 2013.

[92] Y. Yun, Y. W. Cho, and K. Park, "Nanoparticles for oral delivery: Targeted nanoparticles with peptidic ligands for oral protein delivery," 2013.

[93] A. K. Gupta, C. Berry, M. Gupta, and A. Curtis, "Receptor-mediated targeting of magnetic nanoparticles using insulin as a surface ligand to prevent endocytosis," *IEEE Transactions on Nanobioscience*, vol. 2, no. 4, pp. 255–261, 2003.

[94] V. Hartenstein, "The neuroendocrine system of invertebrates: A developmental and evolutionary perspective," 2006.

[95] S. O. Rizzoli and W. J. Betz, "Synaptic vesicle pools.," *Nature reviews. Neuroscience*, vol. 6, pp. 57–69, jan 2005.

[96] V. Matveev and X. Wang, "Implications of all-or-none synaptic transmission and short-term depression beyond vesicle depletion: a computational study," *The Journal of Neuroscience*, vol. 20, no. 4, pp. 1575–1588, 2000.

[97] L. E. Dobrunz, "Release probability is regulated by the size of the readily releasable vesicle pool at excitatory synapses in hippocampus," *International Journal of Developmental Neuroscience*, vol. 20, pp. 225–236, jun 2002.

[98] W. Van, der Kloot, J. Molgó, R. Cameron, and C. Colasante, "Vesicle size and transmitter release at the frog neuromuscular junction when quantal acetylcholine content is increased or decreased," *The Journal of Physiology*, vol. 541, pp. 385–393, jun 2002.

[99] G. Deco, V. K. Jirsa, P. A. Robinson, M. Breakspear, and K. Friston, "The Dynamic Brain : From Spiking Neurons to Neural Masses and Cortical Fields," vol. 4, no. 8, 2008.

[100] L. E. Dobrunz and C. F. Stevens, "Heterogeneity of Release Probability, Facilitation, and Depletion at Central Synapses," *Neuron*, vol. 18, pp. 995–1008, jun 1997.

[101] R. Brown and A. Einstein, "Brownian Motion : Langevin Equation,"

[102] D. Hofmann, S. Tenzer, M. B. Bannwarth, and C. Messerschmidt, "Mass Spectrometry and Imaging Analysis of Nanoparticle-Containing Vesicles Provide a Mechanistic Insight into Cellular Tra ffi cking," no. 10, pp. 10077–10088, 2014.

[103] G. R. Kneller, "Stochastic dynamics and relaxation in molecular systems,"

[104] G. L. Mosley, C. D. Yamanishi, and D. T. Kamei, "Mathematical modeling of vesicle drug delivery systems 1: vesicle formation and stability along with drug loading and release.," *Journal of laboratory automation*, vol. 18, pp. 34–45, feb 2013.

[105] C. Shannon, "A mathematical theory of communication," *ACM SIGMOBILE Mobile Computing and ...*, vol. 27, no. July 1928, pp. 379–423, 2001.

[106] M.H.E., "Molecular thermodynamics," *Journal of Molecular Structure*, vol. 63, no. 2, p. 309, 1980.

[107] T. M. Cover and J. A. Thomas, *Elements of Information Theory*. 2005.

[108] A. H. Wagner, M. Gebauer, B. Pollok-Kopp, and M. Hecker, "Cytokine-inducible CD40 expression in human endothelial cells is mediated by interferon regulatory factor-1," *Blood*, vol. 99, no. 2, pp. 520–525, 2002.

[109] K. Ghoshal and M. Bhattacharyya, "Overview of platelet physiology: Its hemostatic and nonhemostatic role in disease pathogenesis," 2014.

[110] F. White, "Fluid Mechanics," *McGraw-Hill,New York*, p. 862, 2010.

[111] G. K. Batchelor, *An Introduction to Fluid Dynamics*. 2000.

[112] S. Pramanik, "Casson fluid flow and heat transfer past an exponentially porous stretching surface in presence of thermal radiation," *Ain Shams Engineering Journal*, vol. 5, no. 1, pp. 205–212, 2014.

[113] H. J. V. Tyrrell and K. Harris, *Diffusion in liquids: a theoretical and experimental study*. Butterworth-Heinemann, 2013.

[114] R. Zwanzig, *Nonequilibrium statistical mechanics*, vol. 54. 2001.

[115] H. G. E. Hentschel and I. Procaccia, "Relative diffusion in turbulent media: The fractal dimension of clouds," *Physical Review A*, vol. 29, no. 3, pp. 1461–1470, 1984.

[116] M. Pierobon and I. F. Akyildiz, "Noise analysis in ligand-binding reception for molecular communication in nanonetworks," *IEEE Transactions on Signal Processing*, vol. 59, no. 9, pp. 4168–4182, 2011.

[117] A. J. Lemonte and G. M. Cordeiro, "The exponentiated generalized inverse Gaussian distribution," *Statistics and Probability Letters*, vol. 81, no. 4, pp. 506–517, 2011.

[118] J. Safari and Z. Zarnegar, "Advanced drug delivery systems: Nanotechnology of health design A review," 2014.

[119] R. Rosen and W. Roux, "Blood Vessel Branching: Beyond the Standard Calculus Problem," *Mathematics Magazine*, vol. 84, no. 3, pp. 196–207, 2011.

[120] Y. Sun, K. Yang, and Q. Liu, "Channel Capacity Analysis of Blood Capillary-Based Molecular Communication," *2015 IEEE International Conference on Computer and Information Technology; Ubiquitous Computing and Communications; Dependable, Autonomic and Secure Computing; Pervasive Intelligence and Computing*, pp. 1209–1215, 2015.

[121] Y. Sun, K. Yang, and Q. Liu, "Channel Capacity Modelling of Blood Capillary-based Molecular Communication With Blood Flow Drift," *In Proceedings of September27-29, 2017, DC,USA, Washington D.C (NANOCOM'2017)*, pp. 1209–1215, 2017.

[122] H. Kurz, K. Sandau, and B. Christ, "On the bifurcation of blood vessels - Wilhelm Roux's Doctoral Thesis (Jena 1878) - A seminal work for

biophysical modelling in developmental biology," *Annals of Anatomy*, vol. 179, no. 1, pp. 33–36, 1997.

[123] A. Bhuiyan, B. Nath, and K. Ramamohanarao, "Detection and classification of bifurcation and branch points on retinal vascular network," *2012 International Conference on Digital Image Computing Techniques and Applications, DICTA 2012*, 2012.

[124] J. Zhou, S. Chang, D. Metaxas, and L. Axel, "Vascular structure segmentation and bifurcation detection," *2007 4th IEEE International Symposium on Biomedical Imaging: From Nano to Macro - Proceedings*, pp. 872–875, 2007.

[125] D. M. Baboiu and G. Hamarneh, "Vascular bifurcation detection in scale-space," *Proceedings of the Workshop on Mathematical Methods in Biomedical Image Analysis*, pp. 41–46, 2012.

[126] A. Jafari, S. M. Mousavi, and P. Kolari, "Numerical investigation of blood flow. Part I: In microvessel bifurcations," *Communications in Nonlinear Science and Numerical Simulation*, vol. 13, no. 8, pp. 1615–1626, 2008.

[127] X. Li, A. S. Popel, and G. E. Karniadakis, "Bloodplasma separation in Y-shaped bifurcating microfluidic channels: a dissipative particle dynamics simulation study," *Physical Biology*, vol. 9, no. 2, p. 026010, 2012.

[128] E. Gabryś, M. Rybaczuk, and A. Kdzia, "Blood flow simulation through fractal models of circulatory system," *Chaos, Solitons and Fractals*, vol. 27, no. 1, pp. 1–7, 2006.

[129] H. C. Bauer, I. A. Krizbai, H. Bauer, and A. Traweger, ""You shall not pass"-tight junctions of the blood brain barrier," 2014.

[130] M. Pavelka and J. Roth, *Functional Ultrastructure: Atlas of Tissue Biology and Pathology*, vol. 53. 2010.

[131] R. E. Serda, B. Godin, E. Blanco, C. Chiappini, and M. Ferrari, "Multi-stage delivery nano-particle systems for therapeutic applications," *Biochimica et Biophysica Acta - General Subjects*, vol. 1810, no. 3, pp. 317–329, 2011.

[132] M. S. Leeson and M. D. Higgins, "Forward error correction for molecular communications," *Nano Communication Networks*, vol. 3, pp. 161–167, sep 2012.

[133] H. ShahMohammadian, G. G. Messier, and S. Magierowski, "Optimum receiver for molecule shift keying modulation in diffusion-based molecular communication channels," *Nano Communication Networks*, vol. 3, pp. 183–195, sep 2012.

[134] L. S. Meng, P. C. Yeh, K. C. Chen, and I. F. Akyildiz, "MIMO communications based on molecular diffusion," *GLOBECOM - IEEE Global Telecommunications Conference*, pp. 5380–5385, 2012.

[135] R. S. Chhikara and J. L. Folks, *The Inverse Gaussian Distribution: Theory, Methodology, and Applications*. New York, NY, USA: Marcel Dekker, Inc., 1989.

[136] C. D. Murray, "the Physiological Principle of Minimum Work : a Reply.," *The Journal of general physiology*, vol. 14, no. 4, p. 445, 1931.

[137] R. Malaka, T. Ragg, and M. Hammer, "Kinetic models of odor transduction implemented as artificial neural networks - Simulations of complex response properties of honeybee olfactory neurons," *Biological Cybernetics*, vol. 73, no. 3, pp. 195–207, 1995.

[138] J. G. Proakis and M. Salehi, *Digital Communications*. 2008.

[139] C.-C. J. Hong, Y-W Peter and Huang, Wan-Jen and Kuo, *Cooperative communications and networking: technologies and system design.* Springer Science, 2010.

[140] M. R. McKay, A. J. Grant, and I. B. Collings, "Performance analysis of MIMO-MRC in double-correlated Rayleigh environments," *IEEE Transactions on Communications*, vol. 55, no. 3, pp. 497–507, 2007.

[141] E. Ghayoula, A. Bouallegue, and R. Ghayoula, "Capacity and Performance of MIMO systems for Wireless Communications," vol. 7, no. 3, pp. 108–111, 2014.

[142] Y. Xu, P. Chen, J. Zhang, S. Xie, F. Wan, J. Deng, X. Cheng, Y. Hu, M. Liao, B. Wang, *et al.*, "A one-dimensional fluidic nanogenerator with a high power conversion efficiency," *Angewandte Chemie International Edition*, 2017.